

Multicomponent Adsorption of Volatile Organic Compounds in the Liquid Phase

**Predictive Engineering Models, Molecular Simulations,
and Experiments**

Cristian Constantin BRUNCHI

Multicomponent Adsorption of Volatile Organic Compounds in the Liquid Phase

**Predictive Engineering Models, Molecular Simulations,
and Experiments**

Proefschrift

ter verkrijging van de graad van doctor
aan de Technische Universiteit Delft,
op gezag van de Rector Magnificus prof. ir. K.C.A.M. Luyben,
voorzitter van het College voor Promoties,
in het openbaar te verdedigen op
donderdag 10 December 2015 om 12:30 uur

door

Cristian Constantin BRUNCHI

Chemical Engineer, University Politehnica of Bucharest
geboren te Boekarest, Roemenië

Dit proefschrift is goedgekeurd door de
promotor: Prof. Dr. Ir. T. J. H. Vlugt
copromotor: Dr.Ir. H. J. M. Kramer

Samenstelling promotiecommissie bestaat uit:

| | |
|------------------------------|------------|
| Rector Magnificus, | voorzitter |
| Prof. Dr. Ir. T. J. H. Vlugt | promotor |
| Dr.Ir. H. J. M. Kramer | copromotor |

Onafhankelijke leden:

| | |
|--------------------------------|---------------|
| Prof. Dr. Ir. A.I. Stankiewicz | 3mE, TU Delft |
| Prof. Dr. Ir. B.J. Boersma | 3mE, TU Delft |
| Prof. Dr. Ir. J. Gascon | TNW, TU Delft |
| Prof. Dr. Ir. R. Tuinier | TU Eindhoven |
| Dr. Ir. B. Schuur | U Twente |

This thesis was performed as part of the “Trace Removal” project (BC-00-06) funded by the Institute for Sustainable Process Technology (ISPT). This thesis was also sponsored by the Stichting Nationale Computerfaciliteiten (National Computing Facilities Foundation, NCF) for the use of supercomputing facilities.

ISBN 978-94-6186-545-8

Copyright © 2015 by Cristian Constantin Brunchi

All rights reserved. No part of the material protected by this copyright notice may be reproduced or utilized in any form or by any means, electronic or mechanical, including photocopying, recording or by any information storage and retrieval system, without written prior permission from the author.

Printed in The Netherlands by Ipskamp Drukkers

Contents

| | |
|---|----------|
| 1 Introduction | 1 |
| 1.1 Adsorption | 2 |
| 1.2 Multicomponent adsorption equilibrium | 2 |
| 1.3 Adsorbed phase activity coefficients | 4 |
| 1.4 Outline and scope of this thesis | 5 |
| | |
| 2 Adsorption of volatile organic compounds. Experimental and theoretical study | 7 |
| 2.1 Introduction | 8 |
| 2.2 Experimental | 9 |
| 2.2.1 Chemicals | 9 |
| 2.2.2 Adsorbents | 10 |
| 2.2.3 Experimental procedure | 10 |
| 2.3 Simulations | 11 |
| 2.3.1 Monte Carlo simulations | 11 |
| 2.3.2 Ideal adsorbed solution theory (IAST) | 14 |
| 2.4 Results and discussion | 16 |
| 2.4.1 Experimental testing of commercial adsorbents | 16 |
| 2.4.2 Experimental adsorption isotherms in NaY zeolite | 22 |
| 2.4.3 Pure component adsorption isotherms in NaY zeolite computed using Monte Carlo simulations | 26 |
| 2.4.4 Prediction of multicomponent adsorption data using a combined molecular simulation-IAST technique | 26 |
| 2.5 Conclusions | 34 |

| | |
|--|-----------|
| 3 Evaluating adsorbed-phase activity coefficient models using a 2D-lattice model | 37 |
| 3.1 Introduction | 38 |
| 3.2 Monte Carlo simulations on a 2D-lattice | 41 |
| 3.3 Simulations | 41 |
| 3.3.1 Constant spreading pressure simulations | 41 |
| 3.3.2 Segregated 2D-lattice model | 45 |
| 3.4 Results and discussion | 47 |
| 3.4.1 Testing of adsorbed-phase activity coefficient models using a 2D-lattice model | 47 |
| 3.4.2 Testing the spreading pressure dependency of adsorbed-phase activity coefficients using a 2D-lattice model | 50 |
| 3.4.3 Predicting adsorption of mixtures using a segregated 2D-lattice model | 51 |
| 3.5 Conclusions | 57 |
| 4 Multicomponent equilibrium and breakthrough adsorption of volatile organic compounds | 59 |
| 4.1 Introduction | 60 |
| 4.2 Experimental section | 61 |
| 4.2.1 Chemicals and adsorbents | 61 |
| 4.2.2 Equilibrium experiments | 62 |
| 4.2.3 Breakthrough experiments | 63 |
| 4.3 Mathematical models | 63 |
| 4.3.1 Equilibrium models | 63 |
| 4.3.2 Breakthrough model | 65 |
| 4.4 Results and discussion | 68 |
| 4.4.1 Performance of equilibrium models | 68 |
| 4.4.2 Multicomponent breakthrough curves | 69 |
| 4.5 Conclusions | 70 |

| | |
|-------------------------|-----|
| Appendix A | 79 |
| Appendix B | 91 |
| Appendix C | 105 |
| Bibliography | 127 |
| Summary | 139 |
| Samenvatting | 143 |
| Curriculum Vitae | 147 |
| Published Work | 149 |
| Acknowledgements | 151 |

Chapter 1

Introduction

1.1 Adsorption

In the past years, the release of volatile organic compounds (VOCs) into the environment has become a worldwide threat of growing concern [1-4]. One of the main issues in the chemical industry is the removal of VOCs from air streams, wastewater or other intermediary streams [5-9]. Distillation is the most commonly used unit operation in the separation technology, but it becomes unpractical when the boiling points of the fluid components are close [10]. Adsorption is a proven, reliable and one of the most interesting alternative technologies in separation [11]. However, many of the technologically important adsorption from solution phenomena are exceedingly complex. Although most of the experimental data reported in the literature were determined from relatively dilute binary solutions, even these are generally difficult to interpret [11]. Part of the difficulty comes from the lack of models that can describe the non-ideal behavior of adsorbed phase mixtures. The developing and testing of new models requires more than just binary adsorption experiments. Therefore, adsorption of multicomponent systems, containing three or more components, is of great importance in many engineering applications such as certain separations for removing impurities from fluid streams (e.g. removal of VOCs from airstreams, dehydration of natural gas), chromatography as well as design of heterogeneous chemical reactors [12-17]. In addition, multicomponent adsorption data are considerably more difficult to measure than pure component data [13]. Research should be directed towards measuring and modelling of more complex multicomponent adsorption systems.

The primary requirement for an economic adsorption process is an adsorbent with high selectivity and capacity [10]. The selectivity depends on either adsorption kinetics or adsorption equilibrium but most of the industrial adsorption processes depend on equilibrium selectivity [2,10,18]. The adsorbent performance is determined by the competitive adsorption of the different compounds simultaneously present in the liquid solution [19]. Therefore, the assessment of the adsorption capacity of a compound in the presence of other solutes as well as the definition of appropriate theoretical models is imperative for a proper design of adsorption processes.

1.2 Multicomponent adsorption equilibrium

Prediction of mixture adsorption equilibrium from pure component information remains one of the most challenging problems in adsorption [20]. Many efforts have been carried out in developing predictive models for calculating the adsorption equilibrium of multicomponent mixtures using only pure component data [21-29]. The most commonly used approach for predicting equilibrium competitive adsorption,

using only pure component data is the adsorbed solution theory, of which an excellent overview is given by Murthi and Snurr [22]. The Ideal Adsorbed Solution Theory (IAST) was derived by Myers and Prausnitz [21] for a two-dimensional homogenous adsorbed phase. The adsorbed phase is considered as a temperature-invariant area equally accessible to all compounds. The main assumption of IAST is that the adsorbed mixture forms an ideal solution in equilibrium with the bulk (gas or liquid) phase at a constant spreading pressure for each solute [21]. The spreading pressure is an intensive thermodynamic variable for adsorption equilibria; it is defined as the difference in surface tension between a clean surface and a surface covered with adsorbate [10,19]. In the Real Adsorbed Solution Theory (RAST) [25], the non-ideal behavior of the adsorbed phase is accounted for by the use of activity coefficients.

Successful application of IAST in the liquid phase are reported by Li and co-workers [30] who studied the adsorption of trichloroethylene and tetrachloroethylene from aqueous solutions in zeolites. The same compounds were later studied by Erto and co-workers [19]. Noroozi and co-workers [31] obtained reasonable predictions when applying IAST to describe the adsorption of binary mixtures of cationic textile dyes from aqueous solutions in granular activated carbon. However, for ternary mixtures of hydrocarbons, the IAST model does not provide accurate predictions [13, 32].

The attraction of IAST is that it allows the calculation of multicomponent adsorption equilibrium from pure component data. For screening adsorbents, one can use IAST to calculate the multicomponent adsorption equilibrium of the desired mixture if pure component data for each component present in the mixture is available for the tested adsorbents. However, the screening of adsorbent for multicomponent mixtures of five or more compounds still requires considerable experimental effort which is, in most cases, undesirable. Nowadays, most adsorbent materials can be modelled and pure component adsorption data can be obtained using molecular simulations. Molecular simulations provide a useful insight to molecular behavior within channels and pores. The well-known Configurational-bias Monte Carlo (CBMC) technique [33, 34] in the grand-canonical ensemble enables the calculation of the adsorption characteristics of a wide variety of molecules in a large number of adsorbents with reasonable accuracy and reliability [35-39]. Snurr and co-workers successfully predicted the adsorption behavior of benzene and p-xylene in MFI [40] and later the adsorption of binary liquid mixtures of m-xylene, p-xylene and toluene [41]. Smit and co-workers [33, 34] proved that CBMC can be used to predict the adsorption behavior of long-chain alkanes in zeolites.

The questions and challenges that arise when trying to calculate multicomponent adsorption equilibria can be summarized as follows:

1. Can pure component isotherms be predicted with enough accuracy using molecular simulation?
2. Can multicomponent adsorption equilibria (five or more compounds) be predicted using models such as IAST/RAST combined with molecular simulation?
3. What is the minimum experimental data required for such methodologies to work?

In chapter 2 of this thesis, we provide answers to these questions.

1.3 Adsorbed phase activity coefficients

Throughout the years, various activity coefficient models were used with RAST. Due to the lack of models to describe activity coefficients for the adsorbed phase, most of the authors used activity coefficient models valid for vapor-liquid equilibrium. Sochard and co-workers [26] used RAST together with the UNIQUAC [42] and NRTL [43] models for calculating activity coefficients in the adsorbed phase but did not take into account the spreading pressure-dependency of activity coefficients. Erto and co-workers [44] used the Wilson model [45] for calculating adsorbed phase activity coefficients and accounted for the spreading pressure dependency by using an empirical equation proposed by Kopatsis and Myers [46]. The same model is used in the work published recently by Jadhav and co-workers [47]. However, there is no solid theoretical basis for using activity coefficient models from liquid systems for calculating adsorbed phase equilibria.

The activity coefficient models valid for vapor-liquid equilibria are function of temperature and composition. Adsorbed-phase activity coefficients are also dependent on spreading pressure. Often, the failure of vapor-liquid activity coefficient models in describing adsorption data is attributed to the non-dependency on spreading pressure [44,47]. Therefore, testing the validity of such models for the adsorbed phase requires adsorption data obtained at constant spreading pressure.

Three questions arise when trying to account for adsorbed phase non-ideality using models taken from the vapor-liquid theory:

1. Is it possible to obtain adsorption data at constant spreading pressure?
2. Are the activity coefficient models valid for vapor-liquid equilibrium also valid for describing adsorbed-phase non-ideality?

3. Can the spreading pressure dependency of activity coefficients be described using the equation proposed by Kopatsis and Myers [46]?

These questions are answered in chapter 3 of this thesis.

1.4 Objectives and outline of this thesis

The objectives of this thesis are:

1. Develop and validate experimentally a consistent methodology for the prediction of multicomponent (six-component system) adsorption equilibrium for screening purposes.
2. Check if the activity coefficient models taken from the gas-liquid theory are valid for adsorbed phase.
3. Check if a simple 2D-lattice model can be used, with the segregated sites approach [27], to predict binary adsorption equilibria.

In chapter 2 of this thesis, the adsorption of traces of five volatile organic compounds (VOCs) comprising butanal, 2-ethyl-2-hexenal, 2,6-dimethylcyclohexanone, 2,4,6-trimethylphenol and 2,4,6-trimethylanisole from liquid toluene was investigated. Twenty-one commercial adsorbents of different classes were tested in batch adsorption experiments using the six-component mixture. The sodium form of FAU zeolite (NaY) performed by far the best for the overall removal of these compounds from toluene. A force field was developed for these compounds that allows the computation of pure component adsorption isotherms in zeolites using Monte Carlo simulations. The pure component isotherms are used as input in an IAST model to predict multicomponent adsorption behavior in zeolites. Simulations of binary and six-component mixture are compared to experimentally obtained adsorption isotherms. We show that (1) NaY zeolite performs best for the overall adsorption of the selected compounds from liquid toluene, and (2) a combined molecular simulation-IAST approach can be used for this system to predict the adsorption behavior in NaY reasonably well.

In chapter 3 of this thesis, molecular simulations performed on a 2D-lattice are used to generate adsorption data. The generated data is used to check the suitability of the Wilson [45] and NRTL [43] activity coefficient models. The advantage of using a 2D-lattice model is that it allows the generation of multicomponent adsorption data at constant spreading pressure (or, if needed, constant adsorbed-phase composition). It is difficult to achieve these conditions using experimental techniques. The results show that the commonly used Wilson and NRTL models cannot describe the adsorbed phase activity coefficients for slightly non-ideal to strong non-ideal mixtures. In the

second part of chapter 3, the use of Monte Carlo simulations for a segregated 2D-lattice model, for predicting adsorption of mixtures is investigated. The segregated model assumes that the competition for adsorption occurs at isolated adsorption sites, and that the molecules from each adsorption site interact with the bulk phase independently [27]. Two binary mixtures in two adsorbent materials were used as case studies for testing the predictions of the segregated 2D-lattice model: the binary system $\text{CO}_2\text{-N}_2$ in the hypothetical pure silica zeolite PCOD8200029, with isolated adsorption sites and normal preference for adsorption, and the binary system $\text{CO}_2\text{-C}_3\text{H}_8$ in pure silica MOR, with isolated adsorption sites and inverse site preference. The segregated 2D-lattice model provides accurate predictions for the system $\text{CO}_2\text{-N}_2$ in PCOD8200029, but fails in predicting the adsorption behavior of $\text{CO}_2\text{-C}_3\text{H}_8$ in pure silica MOR. The predictions of the segregated IAST model are superior to those of the 2D-lattice model.

In chapter 4, experimental adsorption data for the binary mixtures toluene - butanal, toluene - 2-ethyl-2-hexenal, toluene - 2,6-dimethylcyclohexanone, toluene - 2,4,6-trimethylphenol and toluene - 2,4,6-trimethylanisole on an ammonium form of Y zeolite are presented. The binary experimental data are used for the parameterization of four multicomponent equilibrium models: the multicomponent Langmuir model, the multicomponent dual-site Langmuir model, the coupled IAST - dual-site Langmuir model and the coupled SIAST (segregated ideal adsorbed solution theory) - Langmuir model. The prediction accuracy of the four equilibrium models is compared to experimental multicomponent equilibrium adsorption data. We show that the multicomponent dual-site Langmuir and the coupled SIAST-Langmuir equilibrium models outperformed the other equilibrium models. For the studied system, the prediction accuracy of the multicomponent dual-site Langmuir model proves to be superior to that of the coupled SIAST-Langmuir model. A multicomponent breakthrough model is introduced and compared to experimentally obtained multicomponent breakthrough curves. We show that the breakthrough model, together with the multicomponent dual-site Langmuir model (used to calculate the equilibrium isotherms), can provide a rough qualitative estimation of the breakthrough behavior for the chosen system.

Chapter 2

Adsorption of volatile organic compounds. Experimental and theoretical study

This chapter is based on:

C.C. Brunchi, J.M. Castillo Sanchez, A.I. Stankiewicz, H.J.M. Kramer, T.J.H. Vlugt, Adsorption of Volatile Organic Compounds. Experimental and Theoretical Study, Industrial & Engineering Chemistry Research, 51, 2012, 16697-16708.

2.1 Introduction

One of the main concerns in the chemical industry is related to removal of traces of VOCs [5-9]. The largest fraction of production costs in the chemical industry is related to separation processes [10]. Distillation is the most commonly used unit operation in the separation technology but becomes unpractical when the boiling points of the fluid components are close [10]. Adsorption is one of the most interesting alternative technologies in separation and can be applied in both liquid and gas phases.

The design of adsorption separation units depends mainly on the adsorbent capacity in equilibrium conditions. Their performance is determined by the competitive adsorption of the different compounds simultaneously present in the liquid solution [19]. Therefore, the assessment of the adsorption capacity of a compound in the presence of other solutes as well as the definition of appropriate theoretical models is imperative for a proper design of adsorption processes.

A successful application of zeolite adsorbents to fluid separation requires knowledge and understanding of sorption and diffusion behavior of the fluid components. Molecular simulations give a useful insight to molecular behavior within zeolite channels and pores. The well-known Configurational-bias Monte Carlo (CBMC) technique [33, 34] in the grand-canonical ensemble enables the calculation of the adsorption characteristics of a wide variety of molecules in a wide variety of materials with reasonable accuracy and reliability [35-39]. Snurr and co-workers successfully predicted the adsorption behavior of benzene and p-xylene in MFI [40] and later the adsorption of binary liquid mixtures of m-xylene, p-xylene and toluene [41]. Smit and co-workers [33, 34] proved that CBMC can be used to predict the adsorption behavior of long-chain alkanes in zeolites.

Grand-canonical Monte Carlo simulations usually consist of four types of trial moves: displacement, rotation, (partial) regrowth and swap moves. The move that the MC algorithm is using in a certain step is randomly chosen from these four trial moves. The swap move implies either (1) deletion of a randomly selected molecule from the system or (2) insertion of a molecule in a randomly selected place in the system. The proposed system comprises large, quite rigid molecules that have different shapes and strong specific interaction sites. The liquid-phase adsorption leads to high loadings. Because of the high loadings and molecule characteristics, very few insertions and deletions are successful and the simulations of the multicomponent mixture do not converge easily [41]. Therefore, for the multicomponent mixture, this Monte Carlo simulations should be avoided, as the resulting simulation would be computationally

demanding [41]. As an alternative for predicting multicomponent adsorption isotherms the Ideal Adsorbed Solution Theory (IAST) can be used. IAST is a thermodynamically consistent method used for predicting multicomponent adsorption isotherms using single-compound isotherm data. It was proposed by Myers and Prausnitz [21] for gas mixture adsorption and extended for liquid phase adsorption by Radke and Prausnitz [48]. Successful application of IAST in the liquid phase are reported by Li and co-workers [30] who studied the adsorption of trichloroethylene and tetrachloroethylene from aqueous solutions in zeolites. The same compounds were later studied by Erto and co-workers [19]. Noroozi and co-workers [31] obtained reasonable predictions when applying IAST to study the adsorption of mixtures of cationic textile dyes from aqueous solutions in granular activated carbon.

The first goal of this study is to determine which class of adsorbents performs best for the selected VOCs mixture. For this purpose, twenty-one different adsorbents were tested using batch adsorption experiments. The experimental procedure is explained in Section 2.2 of this chapter. Zeolites seem to perform best. The second goal of this chapter was to test if the adsorption behavior of the selected compounds in NaY zeolite can be predicted using Monte Carlo simulations combined with an Ideal Adsorbed Solution Theory. A force field for the selected compounds was defined and used to compute pure component adsorption isotherms in NaY zeolite. The computed pure component isotherms were used as input for an IAST model. The molecule and zeolite models along with the IAST are explained in Section 2.3 of this chapter.

The adsorption behavior of the binary and six-component mixture in NaY zeolite was investigated. The simulation results are compared to experimental isotherms. In Section 2.4 the results are discussed. We show that if a proper force field is available, the adsorption behavior of the six-component mixture in NaY zeolite can be predicted using a combined molecular simulation and IAST approach. To the best of our knowledge, there is no data on adsorption measurements for the removal of VOCs from liquid toluene in the literature. Our findings are summarized in Section 2.5.

2.2 Experimental

2.2.1 Chemicals.

Toluene (99.99 % anhydrous), 2,6-dimethylcyclohexanone (mixture of isomers, 98 %) and 2,4,6-trimethylphenol (99 %) were obtained from Sigma-Aldrich Chemie B.V., Netherlands; 2-ethyl-2-hexenal (95 %) was purchased from Frinton Laboratories (USA) and 2,4,6-trimethylanisole (>99 %) was purchased from SIA MolPort (Latvia).

2.2.2 Adsorbents

A total of 21 commercial adsorbents were tested in batch adsorption experiments using the six-component mixture. The adsorbents can be divided into six main classes; activated aluminas, polymeric resins, graphitized carbon black, carbon molecular sieves, zeolites and other. Three activated alumina type of adsorbents were tested: the basic, acidic and neutral form. The polymeric resins tested are: Levatit AF5, Dowex L-493 and XAD2. Carbotrap X, Carbotrap F, Carbotrap Y and Carbotrap C are graphitized carbon black type of adsorbents. The carbon molecular sieves used are: Carboxen 569, Carboxen 1000, Carboxen 1003, Carboxen 1012, Carboxen 1016, Carboxen 1018, Carboxen 1021, Carbosieve G and Carbosieve SIII. From the zeolite class, NaY, the Na form of FAU type zeolites was tested. In the “other” category we tested Florisil (activated magnesium silicalite). The list of suppliers for the adsorbents used is provided in Appendix A (Table A1).

2.2.3 Experimental procedure

Except for NaY, all the adsorbent samples were added, as received from the supplier, to 20 ml vials. The vials were immediately sealed to avoid water uptake and weighted. The solution comprising traces of butanal, 2-ethyl-2-hexenal, 2,6-dimethylcyclohexanone, 2,4,6-trimethylphenol and 2,4,6-trimethylanisole in liquid toluene (Appendix A, Table A2), was injected through the septum into the vials and part of the solution was analyzed as a blank. The test vials were stirred continuously at room temperature (24 °C) and samples were collected after 1, 2 and 3 days to ensure that the equilibrium was reached. The samples and blanks were analyzed using a Varian 430 gas chromatograph (GC). A CPSIL8 CB column was used to determine the composition of all blanks and samples.

In the case of NaY zeolite, regeneration of the sample was conducted before the adsorption process. The technical data for the sample, provided by the supplier, reported a 20% weight loss upon drying. This means that the zeolite samples are highly hydrophilic and any water or volatile compounds present in the samples need to be removed before the adsorption experiment.

The NaY samples (Si/Al = 2.556) were added to 20 ml vials and heated overnight in an oven at 500 °C, under nitrogen flow, in order to remove any water and impurities present in the pores. The vials were cooled to around 70 °C and, while keeping the nitrogen flow running, the stirrers were added to the bottles and the caps were placed on the bottles to avoid water adsorption on the samples. Measurements indicated an average weight loss of 21% of the samples during regeneration. The measured weight loss is in agreement with the technical data provided by the supplier (20%). After regeneration the vials were immediately sealed to avoid water uptake and weighted.

The solution was injected through the septum into the vials and part of the solution was analyzed as a blank. The rest of the experiment was conducted like explained above. The amount adsorbed at equilibrium was calculated using the mass balance equation:

$$q_i = \frac{wt_{\text{blank},i} \cdot M_{L,0} - wt_{\text{sample},i} \cdot M_{L,A}}{m_{\text{adsorbent}}} \quad (2.1)$$

where $wt_{\text{blank},i}$ is the mass fraction of the i -th component in the blank, $wt_{\text{sample},i}$ is the mass fraction of the i -th component in the solution after adsorption, $m_{\text{adsorbent}}$ is the mass of adsorbent (grams) and $M_{L,0}$ is the mass of fresh solution (grams). The mass of solution after adsorption is calculated as:

$$M_{L,A} = M_{L,0} - 0.29 \cdot m_{\text{adsorbent}} \cdot \rho_{\text{ad.phase}} \quad (2.2)$$

Eq. 2.2 is used to correct for the change of mass in the external liquid phase due to the adsorbent uptake. There is no accurate experimental procedure for measuring the adsorbed phase mass of solution. A common practice is to assume that the density of the adsorbed phase ($\rho_{\text{ad.phase}}$) is equal to the density of the solution (which approximately equals the density of the solvent) [49]. Van Assche and co-workers [50] report a void fraction of 0.29 l/g for the NaY zeolite used in this work. Therefore, this void fraction was assumed for all the adsorbents. The loading of the impurity compounds is not sensitive to the void fraction. By varying the void fraction of the adsorbents from 0.2 to 0.4, deviations below 1% in the impurity loadings are obtained. These assumptions allow for the calculation of the mass of liquid in the adsorbed phase.

2.3 Simulations

2.3.1 Monte Carlo simulations

Molecular Models. The molecules were modeled as rigid and/or flexible structures using the united atom approach as described by Ryckaert and Bellemans [51]. For the flexible molecular structures, the pseudoatoms are connected through harmonic bonding potentials, harmonic bending potentials and the cosine series torsion potential described by Siepmann and co-workers [52]. The parameters for bond lengths, bend angles and torsion are given in Appendix A (Tables A3-A5).

Butanal (Bt) was modeled as a flexible molecule using the united-atom approach as explained by Ryckaert and co-workers [51]. The parameters for bond lengths, bend angles and torsion were taken from the TraPPE force-field for aldehydes of Siepmann and co-workers [52].

2-Ethyl-2-hexenal (2E2H) was modeled as a flexible molecule using the united-atom approach. The 2E2H molecule is more complex than the others, it contains a double bond, a branch at the sp^2 carbon atom of the double bond and an aldehyde carbon connected to the same sp^2 carbon atom of the double bond. To the best of our knowledge there is no force field available that can provide all the required information for a complete description of the interactions of this molecule inside a zeolite. The parameters from the TraPPE force field for aldehydes [52] and the TraPPE force field for branched alkenes [53] were used to describe this molecule and approximations were made where data was lacking. The parameters for bond lengths and bend angles were taken from the TraPPE force-field for aldehydes, alkenes and alkanes [52-54]. The torsion parameters for the configuration: $\text{CH} = \text{C}_a - \text{CH}_{\text{ald}} = \text{O}_{\text{ald}}$ and $\text{CH}_2 - \text{C}_a - \text{CH}_{\text{ald}} = \text{O}_{\text{ald}}$ are not available in any force field and were taken equal to the torsion for aldehydes [52]. The torsion for the configuration: $\text{CH}_3 - \text{CH}_2 - \text{C}_a - \text{CH}_{\text{ald}}$ were also approximated by the torsion of normal alkanes [54]. In this study we only consider the cis-form of 2-ethyl-2-hexenal. The difference between the cis- and trans-form of the molecule can be described by a harmonic torsional potential as described by Siepmann and co-workers [53].

Toluene (Tol), **2,4,6-trimethylphenol** (3Mp) and **2,4,6-trimethylanisole** (3Ma) were modeled as rigid molecules. The aromatic ring was modeled using the explicit hydrogen force field for benzene of Siepmann and co-workers [55]. The substituting alkyl groups are modeled using the united-atom approach. The parameters for the phenolic groups were taken from the TraPPE force field for alcohols [56] and the parameters for the ether groups in 3Ma were taken from the TraPPE force field for ethers [52]. The atomic coordinates for the cycloalkane part of **2,6-dimethylcyclohexanone** (dMc) were obtained using a DFT geometry optimization simulation with the B3LYP functional and the 6-31G* basis set. Using the obtained coordinates, the dMc molecule was modeled as semi-rigid; the cyclohexane ring is rigid while the alkyl and ketone groups are flexible.

Zeolite model. A zeolite mineral is a crystalline substance with a structure characterized by a framework of linked tetrahedral each consisting of four oxygen atoms surrounding a cation. This framework contains open cavities in the form of channels and cages [57]. The charges introduced by the aluminum atoms are compensated by non-framework cations (Na^+ , K^+ , Ba^{2+} , for example). The Faujasite type zeolite used in this study had a composition with $\text{Si}/\text{Al} = 2.56$ corresponding to 54 aluminum atoms per unit cell. The negative charges introduced by the Al atoms are compensated by Na^+ cations. The atomic charges used for the FAU framework are chosen as $q_{\text{Na}} = +1$ [e], $q_{\text{Al}} = +1.75$ [e] and $q_{\text{Si}} = +2.05$ [e] [58]. The charges for the oxygen atoms were -1.2 [e] for the oxygen atoms connected to aluminum and -1.025 [e] for the oxygen atoms connected to silica [58]. The FAU framework was assumed

to be rigid as described by Kiselev and co-workers [59]. Vlugt and Schenk [60] showed that only small variations in the adsorption isotherms are obtained by using a flexible zeolite framework. One unit cell of FAU with periodic boundary conditions was used in all simulations.

Guest – guest interactions. The non-bonded interactions are described by a pairwise additive Lennard-Jones (LJ) and Coulombic potentials. The LJ guest-guest parameters of the pseudo-atoms used in this work are given in Appendix A. The LJ size parameters for the guest-guest interactions, σ_i , and the charges of the pseudo-atoms were taken from the corresponding TraPPE force-fields of Siepmann and co-workers [52-56, 61] and used without further modifications. The partial charges of the pseudo-atoms used to describe the molecules were taken from the corresponding TraPPE force field [52-56, 61] and are given in Appendix A (Table A6).

The LJ well depth parameters for guest-guest interactions, ε_i , for all the molecules, were fitted to liquid densities using simulations in the *NPT ensemble*. The absolute relative difference between the predicted liquid density and the experimental one had a maximum of 4.9 % in the case of dMc, as can be seen in Appendix A (Table A7). The internal structure of the guest and the guest-guest interactions is of less importance because the properties are dominated by the strong interactions with the force field exerted by the host [62]. Therefore, for the purpose of this work we consider this relative difference of 4.9 % for the impurities to be acceptable.

Guest – host interactions. The zeolite and the guest molecules interact through a pairwise additive Lennard-Jones potential between atoms of the guest molecule and atoms of the zeolite and through electrostatic interactions. Following the work of Kiselev et al. and June et al. [63, 64] the dispersive interactions with the silicon atoms of the zeolite were neglected. Where data about these interactions was not found, the well-known Lorentz-Berthelot mixing rules were used [65, 66].

The LJ guest-host parameters for the aromatic ring and for the substituting methyl groups were taken from the work of Snurr and co-workers [40]. For the interactions between the phenolic oxygen and hydrogen and the zeolite oxygen, geometric and arithmetic mean combining rules between the TraPPE force field parameters [56] and the parameters given by Snurr and co-workers for the oxygen zeolite atoms [40] were used. The interaction between the anisole oxygen and the oxygen zeolite atoms were obtained from mixing rules between the parameters given by Thompson [67] and Snurr [40] respectively.

The guest-host interaction parameters for the methyl pseudo-atoms in dMc, Bt and 2E2H were taken from the work of Dubbeldam and co-workers [62], the guest-host parameters for the sp^2 carbon atom in 2E2H was taken from the work of Liu and co-

workers [68] and the guest-host parameters for the sp^2 carbon atom adjacent to the aldehyde carbon in 2E2H was obtained from mixing rules between the parameters obtained in this work and the parameters for the zeolite oxygen provided by Snurr and co-workers [40]. The guest-host interaction parameters for the aldehyde oxygen, aldehyde carbon, ketone oxygen, ketone carbon and carbon atoms adjacent to the aldehyde carbon were obtained from mixing rules between the parameters for guest-guest defined in this work and the parameters for the zeolite oxygen provided by Snurr and co-workers [40].

The Lennard-Jones potentials are truncated and shifted at 12 Å and the Coulombic interactions in the system were calculated using the Ewald summation [35] with a relative precision of 10^{-6} . All the guest-host LJ interaction parameters used in this work, along with the corresponding references are listed in Appendix A (Table A8).

Simulation Technique. The pure component adsorption isotherms were obtained from grand-canonical simulations (μVT ensemble). The simulations are performed in cycles. In each cycle an attempt is made to perform one of the following trial moves: displacement, rotation, (partial) regrowth and swap trial moves performed with the Configurational-bias Monte Carlo technique [33, 34], were used to equilibrate the system. The number of equilibration cycles used in our simulations was $2 \cdot 10^5$ and the number of production cycles used in our simulations was $2.5 \cdot 10^5$. More details about the simulation technique can be found in the work of Vlugt and co-workers [39, 69].

2.3.2 Ideal Adsorbed Solution Theory (IAST)

The IAST was derived by Myers and Prausnitz [21] for a two-dimensional homogenous adsorbed phase. The adsorbed phase is considered as a temperature-invariant area equally accessible to all compounds (the so-called spreading pressure). The theory was later extended to treat a three-dimensional adsorbed phase [23, 24]. The interpretation of the thermodynamics of adsorption for the three-dimensional approach is different than the interpretation of Myers and Prausnitz [21]. However the two approaches are computationally and thermodynamically identical. An excellent explanation of the IAST is given by Murthi and Snurr [22]. A summary of the equations used in the IAST model is given bellow.

At equilibrium the fugacity of the liquid phase should be equal to the fugacity of the adsorbed phase:

$$y_i \hat{\phi}_i P = x_i f_i^0(T, \pi) \quad (2.3)$$

where y_i is the molar fraction of compound i in the bulk liquid phase in equilibrium with the adsorbed phase, P is the system pressure, x_i is the adsorbed phase molar

fraction of compound i , f_i^0 is the fugacity of pure i adsorbed at the same temperature (T) and spreading pressure (π) as the (adsorbed) mixture (Pa).

The condition of equal spreading pressure for all components is written as:

$$\frac{\pi_i A}{RT} = \frac{\pi_j A}{RT} = \int_0^{f_i^0} n_i^0(t) d \ln t = \int_0^{f_j^0} n_j^0(t) d \ln t \quad i \neq j \quad (2.4)$$

where n_i^0 is the loading of component i . The total loading can be calculated from:

$$\frac{1}{n_T} = \sum_{i=1}^{NC} \left[\frac{x_i}{n_i^0(f_i^0)} \right] \quad (2.5)$$

where NC is the number of components.

The individual loadings can be calculated from:

$$n_i = x_i n_T \quad (2.6)$$

The non-ideality of the liquid phase is expressed through fugacity coefficients of the compounds in the liquid phase mixture, $\hat{\varphi}_i$. The fugacity coefficients were computed using the Peng-Robinson equation of state (Appendix C). The quality of the data provided by the Peng-Robinson EOS was tested for toluene, butanal and 2,4,6-trimethylphenol. The vapor pressures calculated using the Peng-Robinson EOS for this three compounds were in good agreement with available literature data [70]. For 2-ethyl-2-hexenal, 2,6-dimethylcyclohexanone and 2,4,6-trimethylanisole no literature data was found for the vapor pressure. However, the non-ideality of the liquid phase can also be expressed through activity coefficients. The UNIFAC method [71-77] was used to compute the activity coefficients of the six compounds in the liquid mixture. The precision of IAST was the same using both the activity coefficient and the Peng-Robinson EOS approach. Therefore, the Peng-Robinson EOS was used further in this study. The critical data needed for computing the fugacity coefficients along with the specific references are given in Appendix A (Table A9).

For a binary system, Eqs. 2.3 and 2.4 provide a system of three equations for the five unknowns (P , y_i , x_i , f_1^0 , f_2^0). Therefore, the specification of any two variables allows the calculation of the other three. The Matlab commercial software was used for solving the system of equations.

2.4 Results and discussion

2.4.1 Experimental testing of commercial adsorbents

The first goal of this study was to determine which class of adsorbents has the highest capacity for the removal of all the impurities simultaneously. Batch adsorption experiments were performed using the six-component mixture and the adsorption capacities of the studied compounds were measured in 21 commercial adsorbents as explained in the experimental section. The six-component mixture contained butanal (Bt), 2-ethyl-2-hexenal (2E2H), 2,6-dimethylcyclohexanone (dMc), 2,4,6-trimethylphenol (3Mp), 2,4,6-trimethylanisole (3Ma) and toluene as solvent.

In Figs. 2.1-2.5, the results of the experimental tests performed on the 21 adsorbents are presented. Each figure represents the adsorption on 21 different adsorbents of one of the impurity compounds in a multicomponent mixture. Note that the amount of adsorbent that was added in the experiments and also the void fraction was not exactly the same for each adsorbent. In the calculation of the loading, the measured amount of adsorbent was used while a constant void fraction of 0.29 was assumed for all the adsorbents. The concentration of the compounds in the initial solution used for the testing of the 21 adsorbents is listed in Table A2 (Appendix A).

Amongst the alumina-type of adsorbents, the basic form of activated alumina performs best. Noticeable amount of butanal is adsorbed using the basic activated alumina adsorbent (Fig. 2.1). The adsorption capacity of all types of activated alumina for the other compounds is negligible. The adsorption capacity of the resin-type of adsorbents is very small for the selected compounds. Adsorption capacities below 15 mg/g are obtained for all five compounds. Also, none of the graphitized carbon black-type of adsorbents has noticeable adsorption capacities (Figs. 2.1-2.5). Amongst the carbon molecular sieves, Carboxen 1012 and Carbosieve G perform best and have noticeable adsorption capacities for butanal and 2,4,6-trimethylphenol (Fig. 2.1 and Fig. 2.4). As can be seen in Figs. 2.1-2.5, NaY zeolite (red circle) is the best adsorbent. It can remove the highest amounts of impurities simultaneously from the six-component mixture. The adsorption capacity of NaY towards the impurity compounds is far superior to that of the other adsorbents tested. Therefore, the adsorption behavior of the chosen compounds in this zeolite is analyzed in more detail.

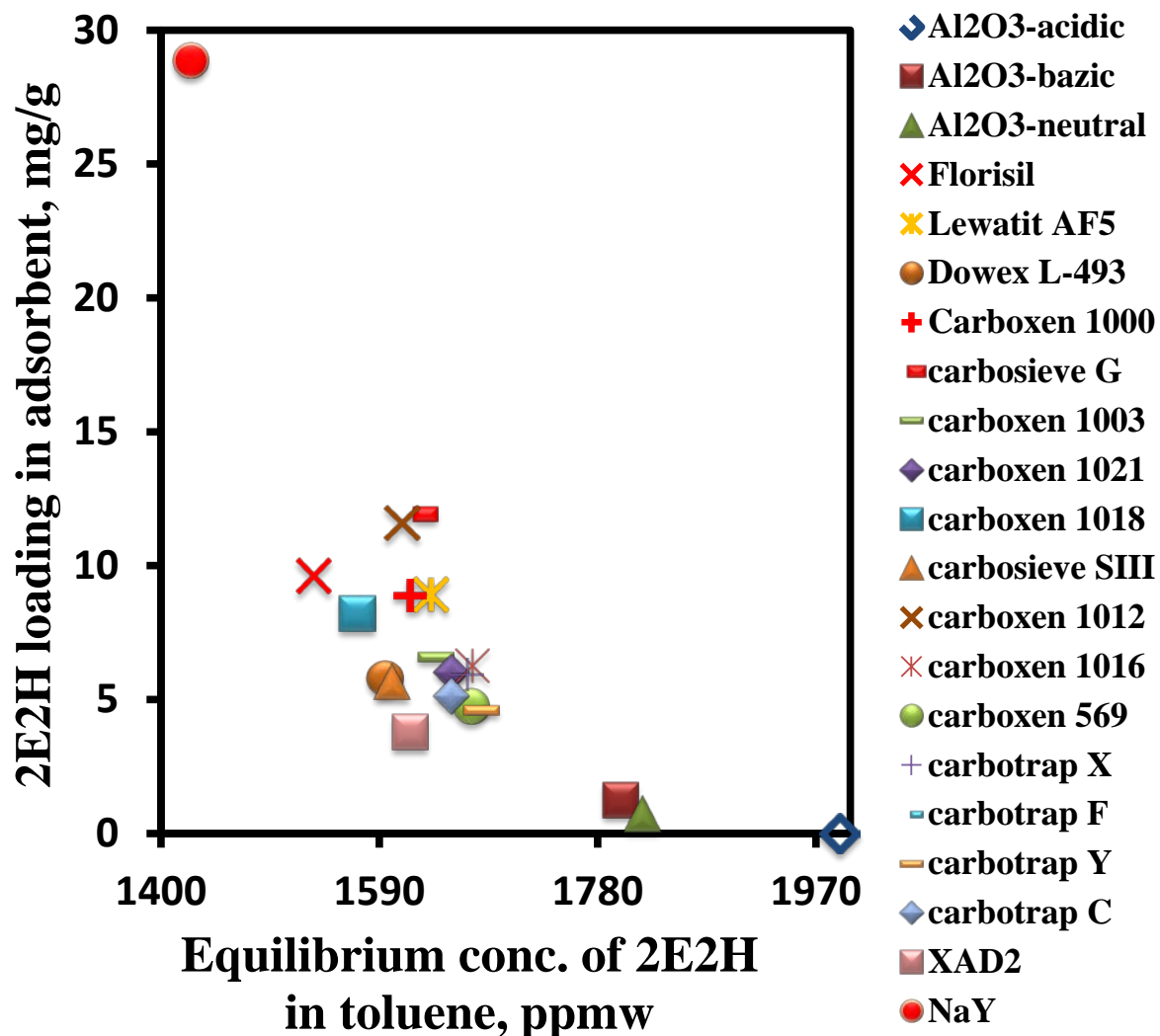


Figure 2.2. The loading of 2-ethyl-2-hexenal as measured in the experiments. The bulk liquid phase consists of a six-component mixture and only 2-ethyl-2-hexenal is showed here. The adsorbents are listed on the right of the figure. The complete name of the adsorbents along with the suppliers are listed in Table A1 (Appendix A).

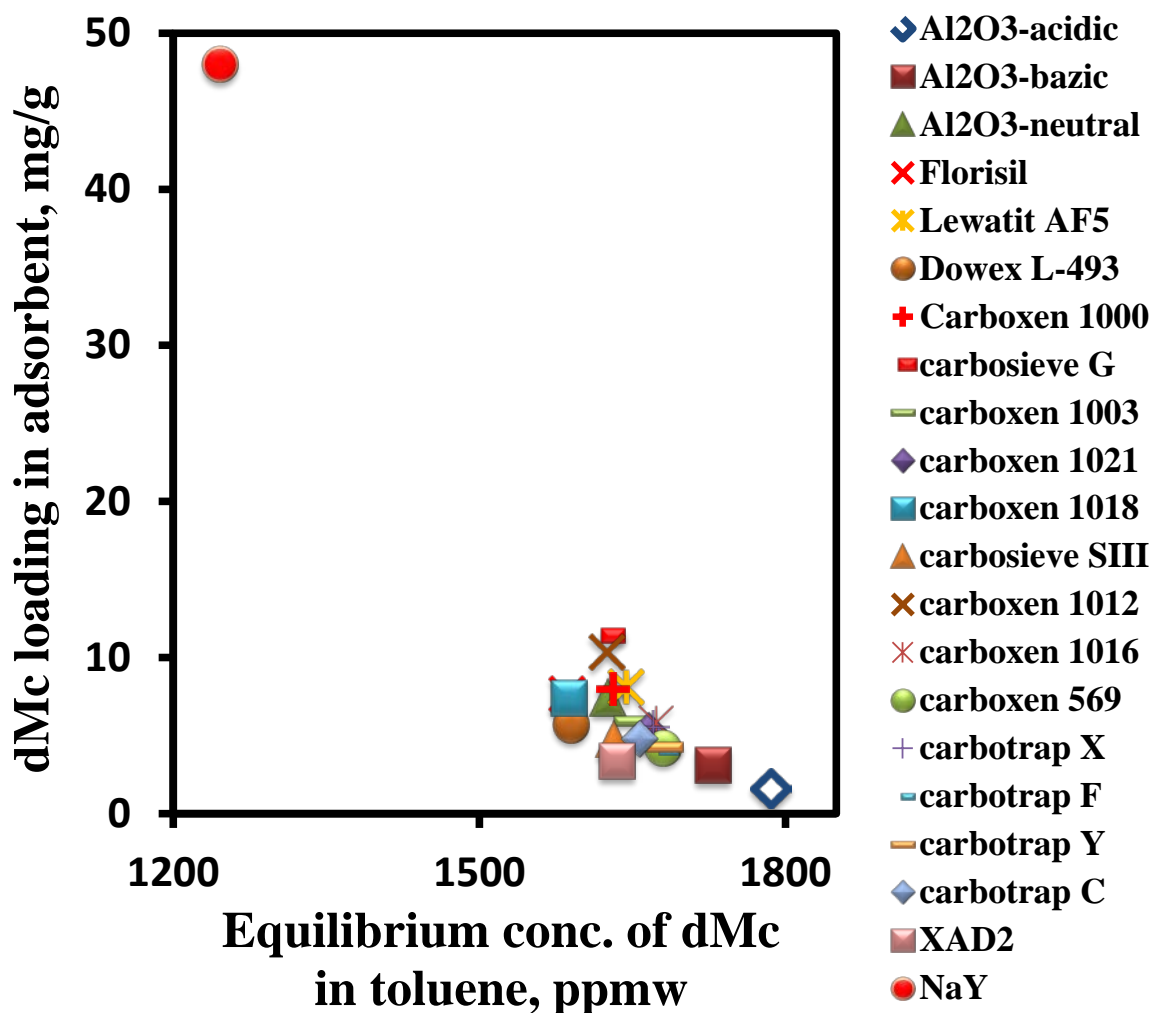


Figure 2.3. The loading of 2,6-dimethylcyclohexanone as measured in the experiments. The bulk liquid phase consists of a six-component mixture and only 2,6-dimethylcyclohexanone is showed here. The adsorbents are listed on the right of the figure. The complete name of the adsorbents along with the suppliers are listed in Table A1 (Appendix A).

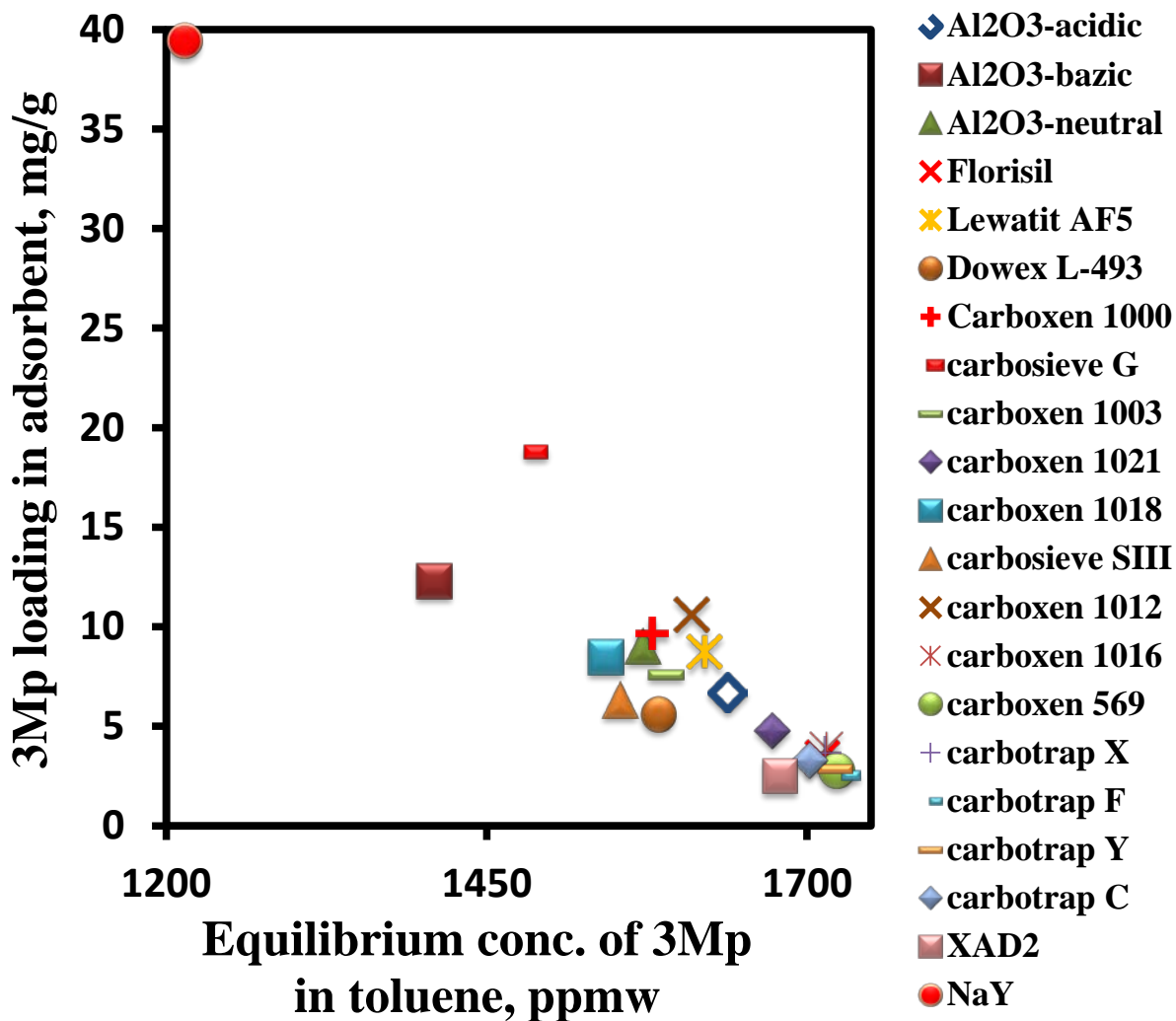


Figure 2.4. The loading of 2,4,6-trimethylphenol as measured in the experiments. The bulk liquid phase consists of a six-component mixture and only 2,4,6-trimethylphenol is showed here. The adsorbents are listed on the right of the figure. The complete name of the adsorbents along with the suppliers are listed in Table A1 (Appendix A).

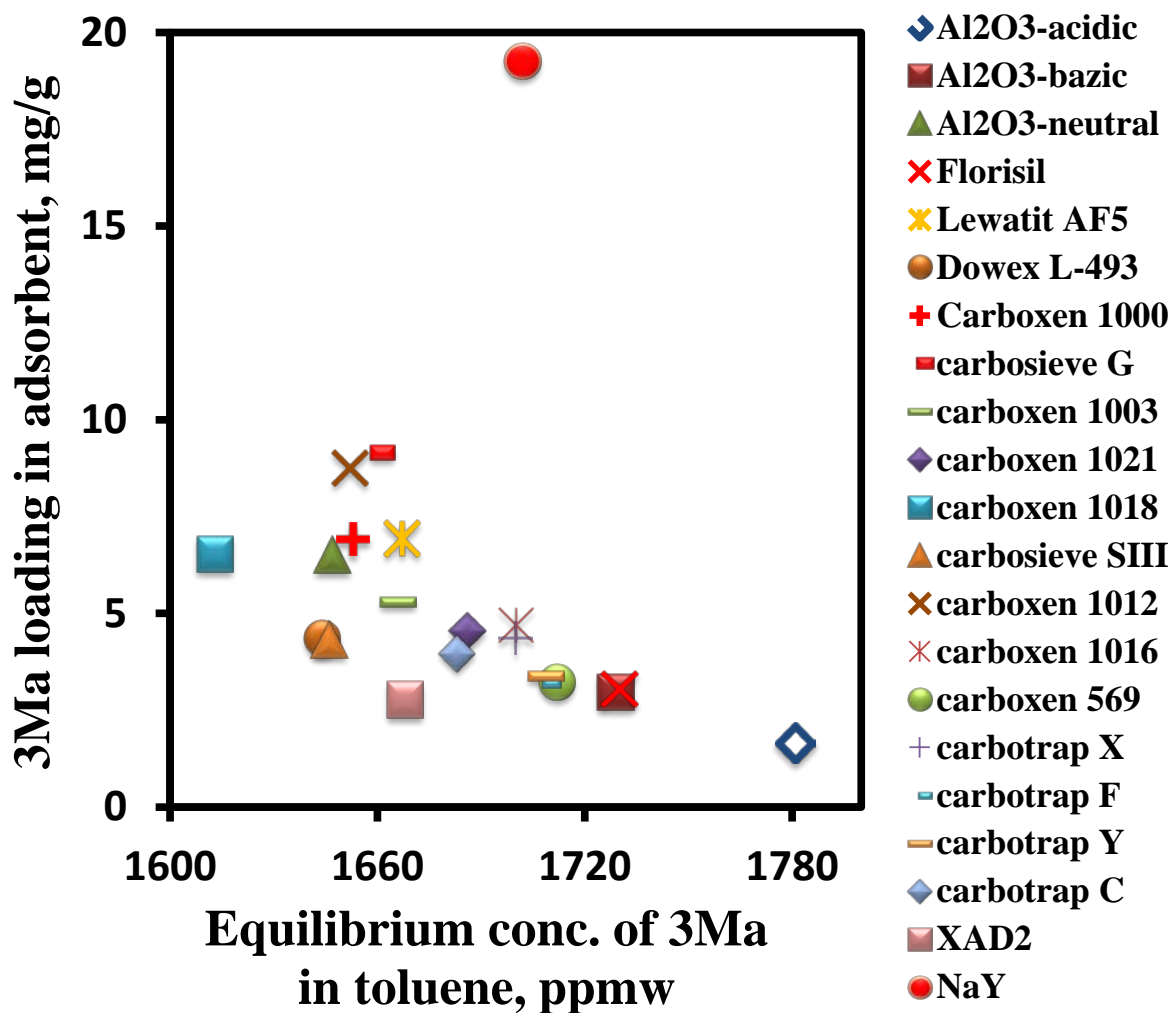


Figure 2.5. The loading of 2,4,6-trimethylanisole as measured in the experiments. The bulk liquid phase consists of a six-component mixture and only 2,4,6-trimethylanisole is showed here. The adsorbents are listed on the right of the figure. The complete name of the adsorbents along with the suppliers are listed in Table A1 (Appendix A).

2.4.2 Experimental adsorption isotherms in NaY zeolite.

The Na form of zeolite Y performs best. However, the capacity and selectivity of the NaY zeolite can be altered by modifying the cation type and the number of cations (Si/Al ratio) present in the zeolite framework [78]. Therefore, a thorough study of Y-type zeolites with different Si/Al ratio and cation types might reveal a better adsorbent than the used NaY zeolite. An attractive technique for this study is using molecular simulations combined with an Ideal Adsorbed Solution Theory. We intend to use pure-component adsorption isotherms obtained from molecular simulations as input in an IAST model. The IAST model should predict the multicomponent adsorption behavior of the selected compounds in NaY zeolite. To check the reliability of this approach, experimental adsorption data is required. The binary adsorption isotherms of the impurities in toluene along with the adsorption isotherm of the 6-component mixture will be presented in the following sub-chapter.

Fig. 2.6 shows the adsorption isotherms of the binary system toluene-butanal in NaY zeolite at room temperature. It can be seen that significant values for the adsorption capacity of butanal are obtained even at concentrations of butanal as low as 1000 ppm. At butanal concentrations above 10000 ppm, the adsorption capacity is inversed and butanal is the preferred specie for adsorption in NaY zeolite. Therefore, NaY zeolite is a suitable adsorbent for separating butanal from liquid toluene.

For the binary system toluene-2-ethyl-2-hexenal (2E2H), toluene is preferential adsorbed up to ketone concentrations of above 50000 ppm (Fig. 2.7). However, for high concentrations of 2E2H, NaY zeolite is a suitable adsorbent for removing this ketone from liquid toluene. A similar behavior can be observed for the binary system toluene-2,6-dimethylcyclohexanone (dMc, Fig. 2.8). Toluene is preferentially adsorbed up to high concentrations of dMc of above 50000 ppm.

Fig. 2.9 shows the adsorption isotherm of the binary system toluene – 2,4,6-trimethylphenol (3Mp) in NaY zeolite at room temperature. Experiments at concentrations of 3Mp higher than 10000 ppm were not performed. It can be seen that toluene is preferentially adsorbed for the whole range of 3Mp concentrations investigated. However a shift in the adsorption capacity is expected for higher concentrations. A loading of around 50 mg/g for 3Mp can be observed at 3Mp concentrations above 10000 ppm, making NaY zeolite a suitable adsorbent for this binary system.

The adsorption isotherms for the binary system toluene-2,4,6-trimethylanisole (3Ma) is shown in Fig. 2.10. Experiments at concentrations of 3Ma higher than 10000 ppm were not performed. It can be seen that there is no appreciable adsorption of 3Ma for the whole range of concentrations studied. It appears that the NaY zeolite is not a

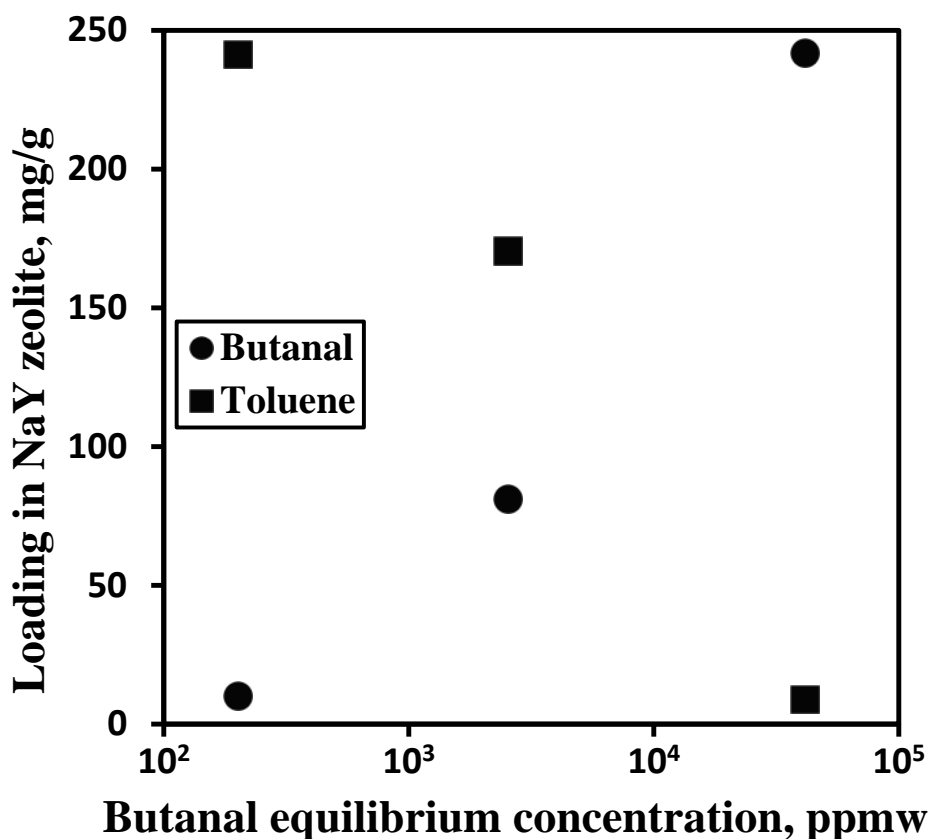


Figure 2.6. Experimental adsorption isotherms for the binary system toluene - butanal in NaY zeolite. Circles - butanal data, squares - toluene data.

suitable adsorbent for this binary system, although in the multicomponent mixture higher loadings were found. This will be discussed in the next section.

The experimental adsorption isotherms for the six-component mixture in NaY zeolite at room temperature are presented in Fig. 2.11. The three sets of experimental data are marked with different colors in the graph. It can be seen that even at impurity concentrations below 500 ppm, there is reasonable adsorption for three of the compounds studied. 2,4,6-trimethylanisole has higher adsorption capacities in the six-component mixture than in the binary mixture with toluene. It appears that this class of zeolites is a good candidate for an adsorption of the studied compounds from toluene. The used NaY zeolite however, might not be able to reduce the concentration of some of the impurities below desired values (50 ppm) in an industrial process (in a single step). Our strategy is to check if the adsorption behavior of this system in NaY can be predicted using a combined IAST-molecular modeling approach.

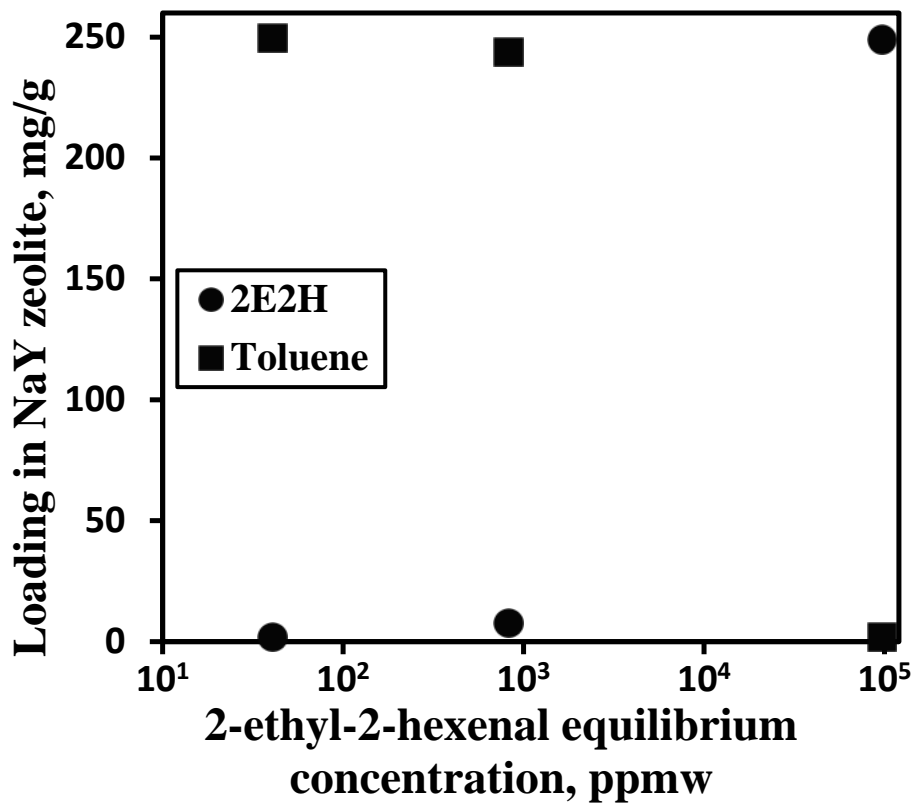


Figure 2.7. Experimental adsorption isotherms for the binary system toluene - 2E2H in NaY zeolite. Circles - 2E2H data, squares - toluene data.

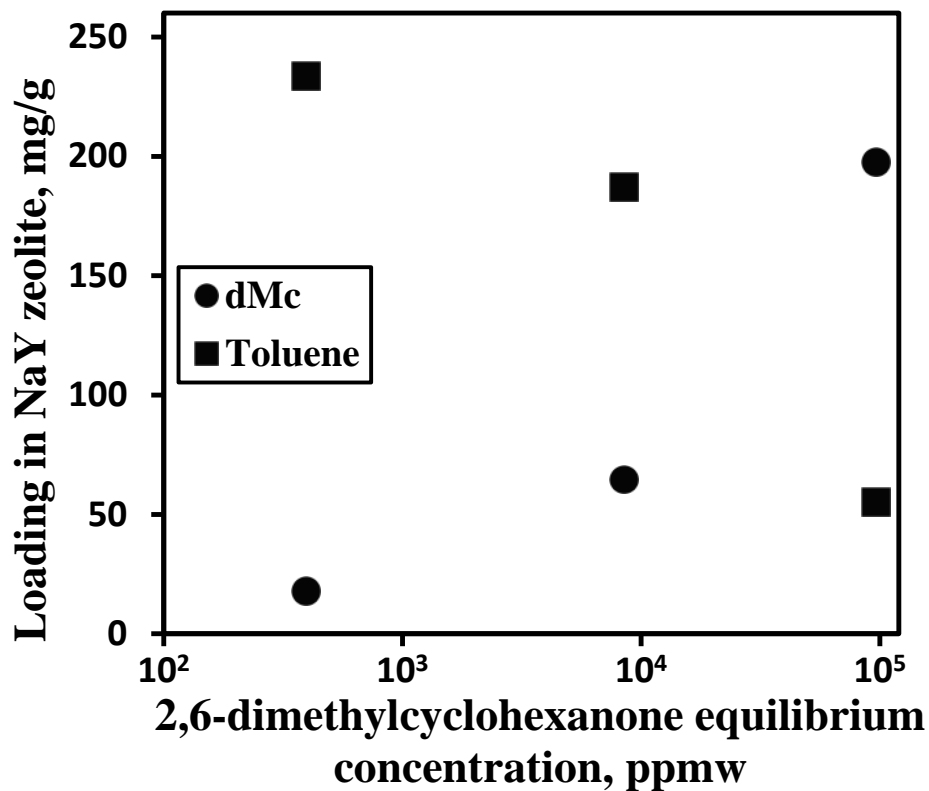


Figure 2.8. Experimental adsorption isotherms for the binary system toluene - dMc in NaY zeolite. Circles - dMc data, squares - toluene data.

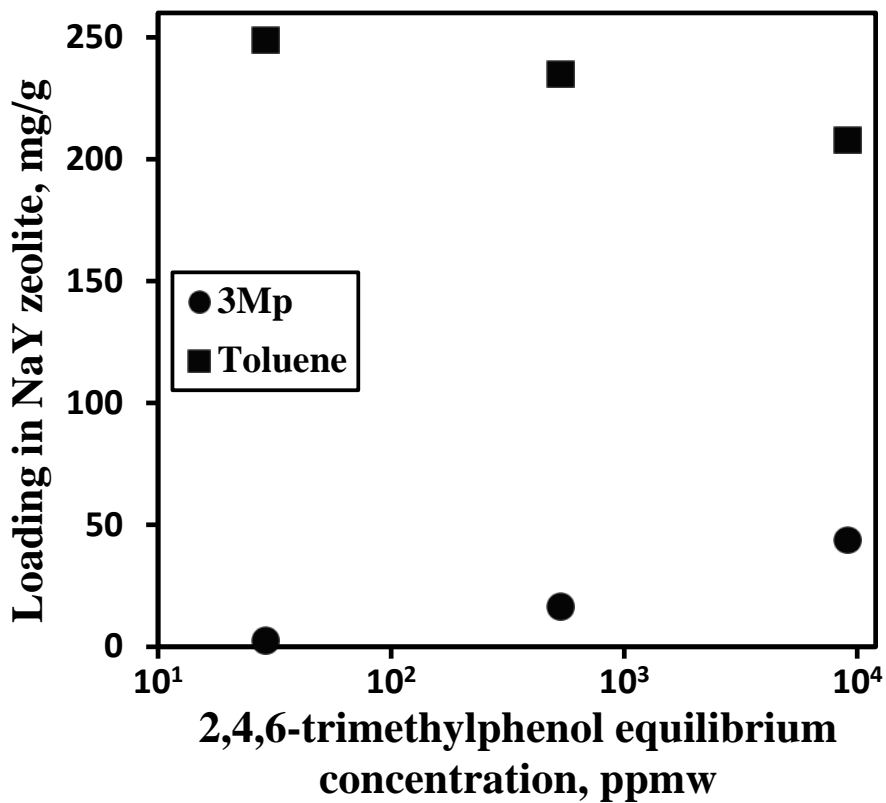


Figure 2.9. Experimental adsorption isotherms for the binary system toluene - 3Mp in NaY zeolite. Circles - 3Mp data, squares - toluene data.

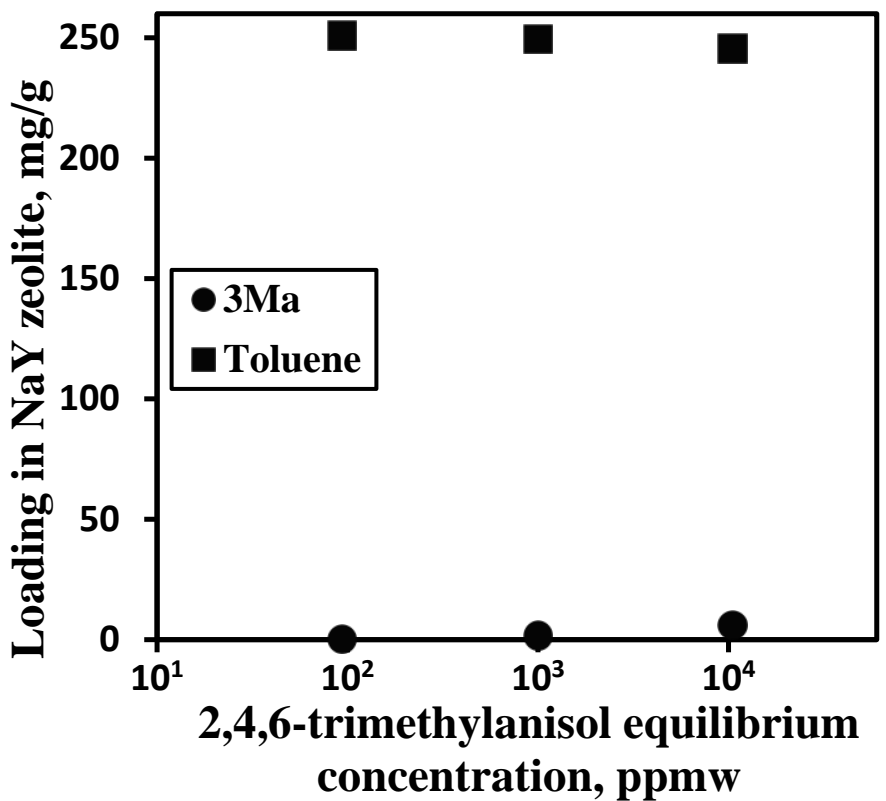


Figure 2.10. Experimental adsorption isotherms for the binary system toluene - 3Ma in NaY zeolite. Circles - 3Ma data, squares - toluene data.

2.4.3 Pure component adsorption isotherms in NaY zeolite computed using Monte Carlo simulations.

The pure component adsorption isotherms in NaY zeolite, at 300 K were obtained using molecular simulations as explained in the simulation section. The obtained isotherms are used in an Ideal Adsorbed Solution Theory model and the multicomponent adsorption isotherms can be predicted.

In Fig. 2.12, the pure component adsorption isotherm of butanal in NaY zeolite, computed using Monte Carlo simulations is depicted. The dual-site Langmuir equation was used to fit the simulated data. It can be seen that the dual-site Langmuir equation does not provide a perfect fit for the whole range of fugacities. However, the purpose of this work is to study trace removal (low concentration/fugacity region) and for the low fugacity region, the dual-site Langmuir equation provides a more than reasonable fit. The pure component adsorption isotherms of the other compounds, together with the dual-site Langmuir fit, are listed in Appendix A (Figs. A1-A6).

2.4.4 Prediction of multicomponent adsorption data using a combined molecular simulation-IAST technique

As stated earlier in this chapter, it is difficult to calculate mixture adsorption isotherms using molecular simulations for the chosen system [41]. The Ideal Adsorbed Solution Theory was used instead to predict the multicomponent behavior in NaY zeolite. The pure component adsorption isotherms in NaY zeolite, computed by molecular simulations were used as input for the IAST model. The dual-site Langmuir equation was used to fit the pure-component data.

A comparison between data predicted by simulations and the three experimental data sets presented in Fig. 2.11 was made. The result of the IAST predictions compared with experimental values is given in Table 2.1. As can be seen in Table 2.1, IAST strongly overestimates the adsorption of butanal for all three data sets. The toluene loading is also strongly underestimated by IAST predictions.

As experimental adsorption isotherms for our compounds in NaY zeolite are not available, they were obtained using molecular simulations. The IAST predictions critically rely on the accuracy of the pure-component isotherms, and therefore on the accuracy of the guest-host interactions defined in the force field. Since the guest-host interactions used in the force field are estimated on the basis of very limited thermodynamic data that was available for the studied system, it is expected that the predicted pure-component isotherms are not quantitatively accurate. However, the force field interaction parameters for toluene were previously used successfully by Snurr and co-workers [40]. Therefore, by studying the adsorption competition using

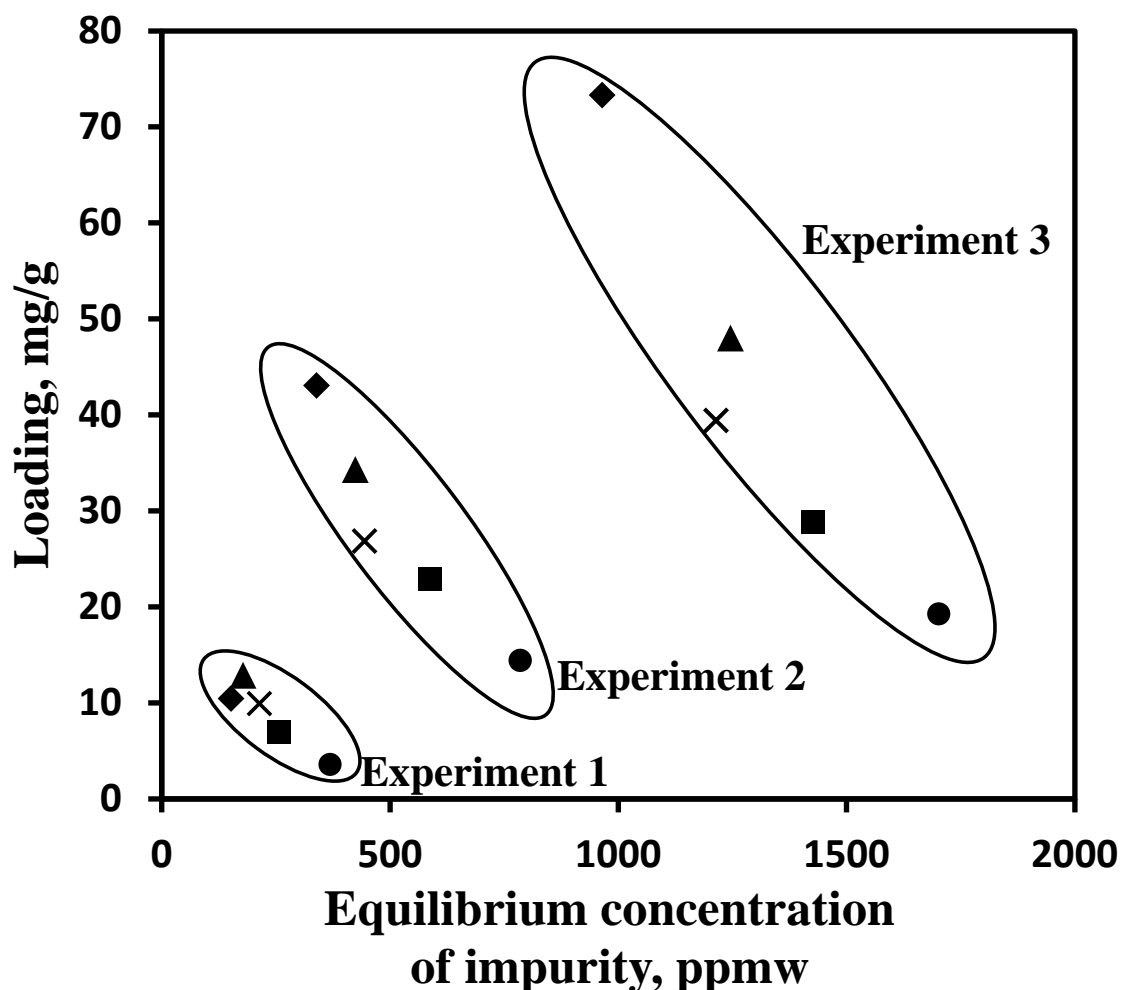


Figure 2.11. Experimental multicomponent adsorption isotherms in NaY zeolite for impurities in liquid toluene. Three experimental datasets are presented. Each compound has a geometric figure assigned: ◆ butanal, ■ 2-ethyl-2-hexenal, ▲ 2,6-dimethylcyclohexanone, × 2,4,6-trimethylphenol, ● 2,4,6-trimethylanisole. The equilibrium concentration of toluene (solvent) does not fit in the scale. The loading of toluene for each data set in the order blue, orange, red is: 216 mg/g, 109 mg/g and 37 mg/g respectively, clearly showing that the amount of adsorbed toluene is highly dependent on the impurity concentration of the liquid phase.

binary solutions with toluene, the accuracy of the predicted pure component isotherms for the impurity compounds can be checked. The comparison between experimental results and IAST predictions for the binary system toluene-butanal are shown in Fig. 2.13.

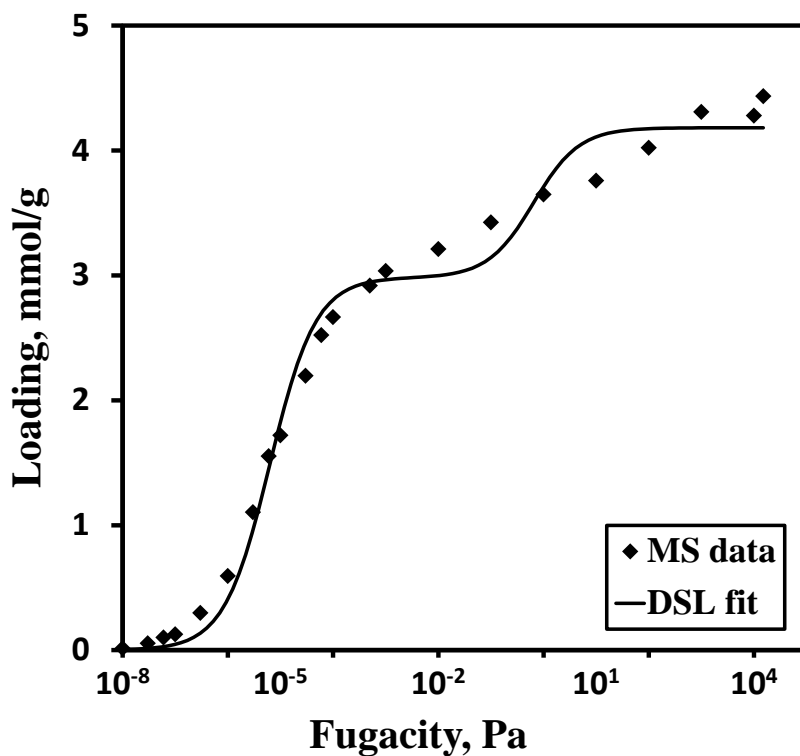


Figure 2.12. Adsorption isotherm of butanal in NaY zeolite; symbols - molecular simulation (MS) results, line - dual-site Langmuir (DSL) fit.

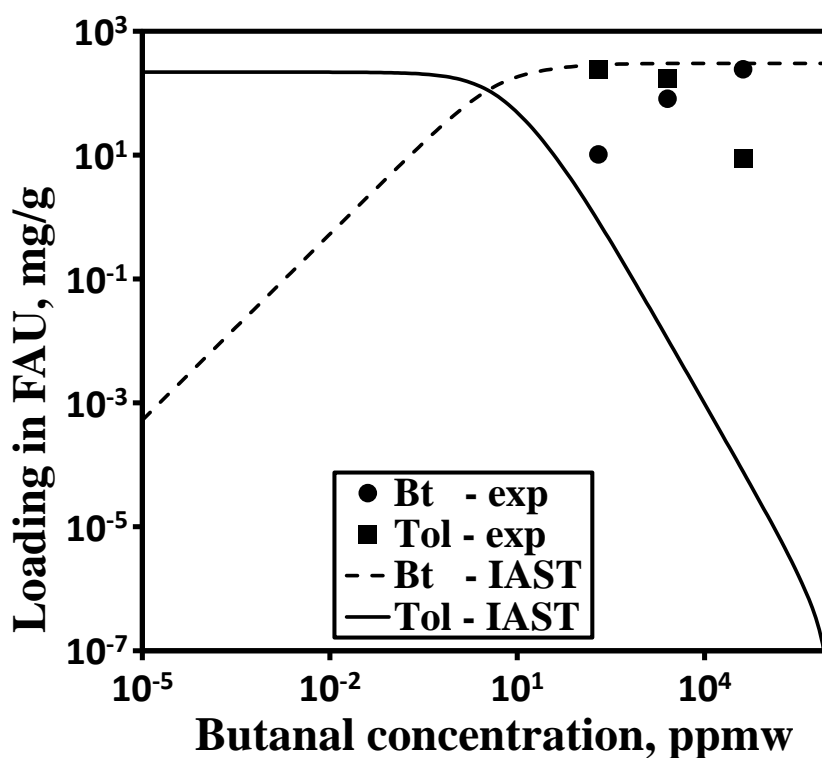


Figure 2.13. Adsorption isotherms for the binary system toluene-butanal in NaY zeolite. Lines - IAST predictions, circles - experimental results for butanal, squares - experimental results for toluene.

As can be seen in Fig. 2.13, the IAST predictions for the binary system toluene-butanol are also far from the experimental results. However, the trend of the competition between butanol and toluene in both IAST and experimental results is the same. Butanol is preferentially adsorbed starting with low concentrations but IAST overestimates this competition. The large difference between the predicted isotherms and the experimental ones can be explained by either *i*) non-ideal behavior of the adsorbed phase, in other words IAST cannot be used for this system or *ii*) inaccurate values of the parameters describing the guest-host interactions in the force field. The second variant is investigated in more detail.

Assuming that the force field parameters for butanol are off, the maximum loading of 4.2 mmol/g (see Fig. 2.12) would still be valid because it is determined by the pore volume of the NaY zeolite and the volume of the butanol molecule which are precisely known. In other words, the force field parameters describing the size of the butanol molecule and the size of the zeolite pore is precisely known. However, the uncertainty comes from the parameters describing the interaction between the zeolite structure and the fluid phase (which will determine the fugacity range where the loading of the pure component increases steeply). Castillo and co-workers [79] showed that for water and other strongly polar molecules, a small variation in the force field parameters can result in a shift in the fugacity range of the isotherms of several orders of magnitude. Therefore, a very small variation of the strength of the guest-host interaction parameters can lead to a shift of the pure component isotherm in the fugacity range.

To calculate the shift in the pure component isotherm of butanol, a shifting parameter K was introduced in the dual-site Langmuir equation (Eq. 2.7). The intention is to check how much the fugacity range (horizontal axis) is shifted. The shifted isotherm equals:

$$q = \frac{q_{m1} \cdot b_1 \cdot F}{1 + b_1 \cdot F} + \frac{q_{m2} \cdot b_2 \cdot F}{1 + b_2 \cdot F} \quad (2.7)$$

in which

$$b_1' = b_1 \cdot K \quad (2.8)$$

$$b_2' = b_2 \cdot K \quad (2.9)$$

The condition that the IAST result satisfies (only) the butanol experimental data point with the lowest concentration (see Fig. 2.13) was imposed and the K parameter was computed. A value for the shifting parameter of $8.6 \cdot 10^{-4}$ was found. The shift of the butanol isotherm is 4 orders of magnitude. However, according to the work of Castillo and co-workers [79], this shifting parameter would correspond to a very small error in the force-field parameters.

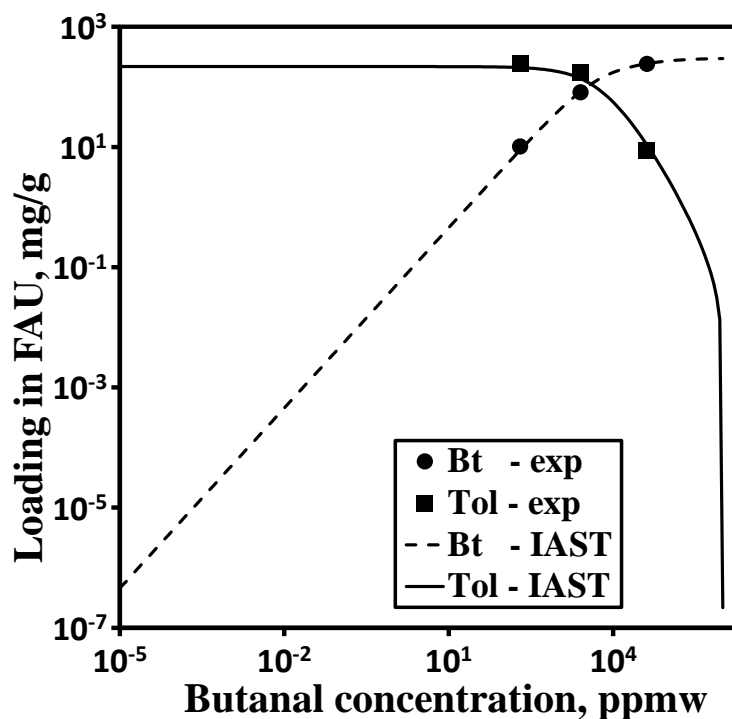


Figure 2.14. Adsorption isotherms for the binary system toluene - butanal in NaY zeolite. Lines - IAST predictions, circles - experimental results for butanal, squares - experimental results for toluene. The pure component isotherm of butanal was shifted in the horizontal axis (fugacity) by a factor of $8.6 \cdot 10^{-4}$.

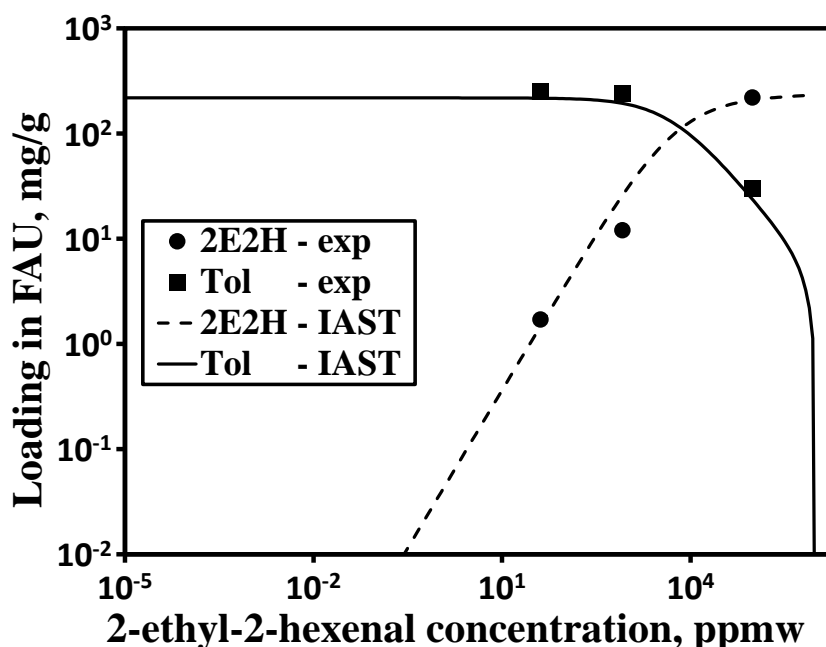


Figure 2.15. Adsorption isotherms for the binary system toluene - 2-ethyl-2-hexenal in NaY zeolite. Lines - IAST predictions, circles - experimental results for 2-ethyl-2-hexenal, squares - experimental results for toluene. The pure component isotherm of 2-ethyl-2-hexenal was shifted in the horizontal axis (fugacity) by a factor of $6.3 \cdot 10^{-3}$.

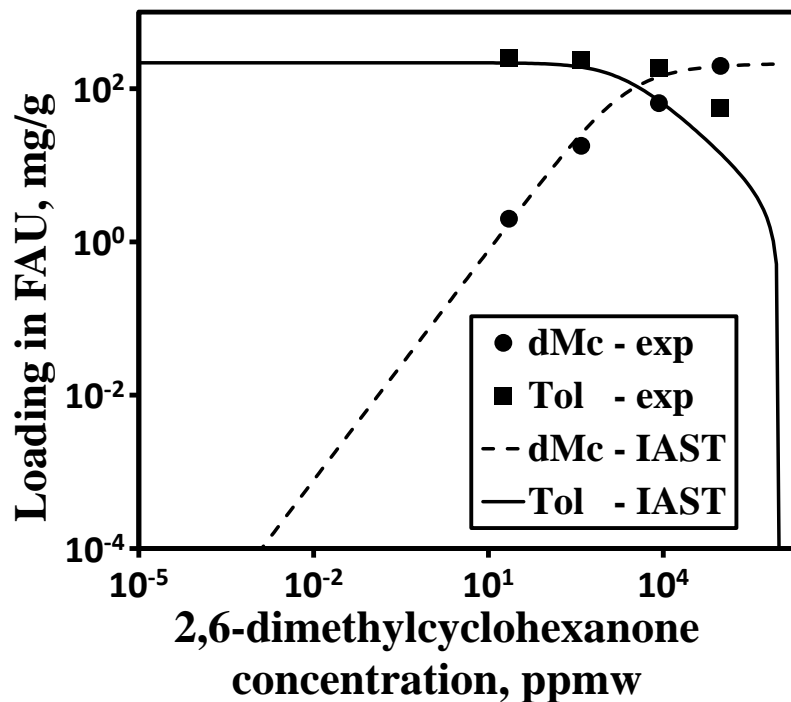


Figure 2.16. Adsorption isotherms for the binary system toluene - 2,6-dimethylcyclohexanone in NaY zeolite. Lines - IAST predictions, circles - experimental results for 2,6-dimethylcyclohexanone, squares - experimental results for toluene. The pure component isotherm of 2,6-dimethylcyclohexanone was shifted in the horizontal axis (fugacity) by a factor of 35.5.

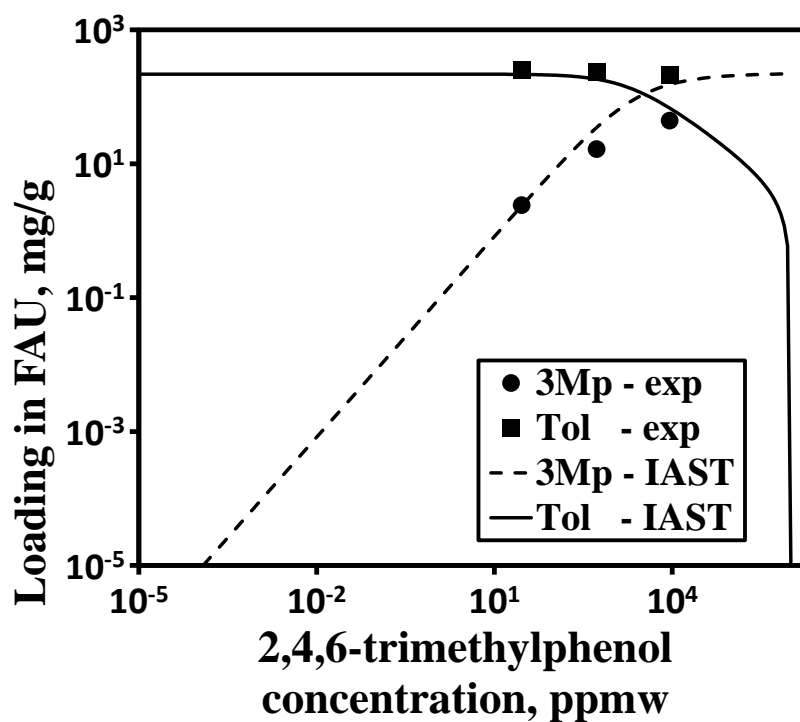


Figure 2.17. Adsorption isotherms for the binary system toluene - 2,4,6-trimethylphenol in NaY zeolite. Lines - IAST predictions, circles - experimental results for 2,4,6-trimethylphenol, squares - experimental results for toluene.

Table 2.1. Comparison of IAST with experimental adsorption results for the 6-component mixture comprising toluene (Tol), butanal (Bt), 2-ethyl-2-hexenal (2E2H), 2,6-dimethylcyclohexanone (dMc), 2,4,6-trimethylphenol (3Mp) and 2,4,6-trimethylanisole (3Ma) in NaY zeolite. Three data sets are presented corresponding to the three data sets of Fig. 2.11.

| Comp. | Data set 1 | | | Data set 2 | | | Data set 3 | | |
|-------|----------------|---------------------|-------------|----------------|---------------------|-------------|----------------|---------------------|-------------|
| | Eq. conc., ppm | q IAST, mg/g | q exp, mg/g | Eq. conc., ppm | q IAST, mg/g | q exp, mg/g | Eq. conc., ppm | q IAST, mg/g | q exp, mg/g |
| Tol | 999199 | 1.2 | 215.7 | 997420 | 0.3 | 108.8 | 993447 | 0.05 | 37.5 |
| Bt | 152 | 282.4 | 10.5 | 339 | 292.5 | 43 | 965 | 298.4 | 73.3 |
| 2E2H | 257 | 1.6 | 7 | 588 | 0.7 | 22.9 | 1426 | 0.2 | 28.9 |
| dMc | 178 | $1.9 \cdot 10^{-4}$ | 12.9 | 424 | $6.7 \cdot 10^{-5}$ | 34.3 | 1246 | $1.5 \cdot 10^{-5}$ | 48 |
| 3Mp | 214 | 0.007 | 9.9 | 444 | 0.002 | 26.9 | 1214 | $4.2 \cdot 10^{-4}$ | 39.4 |
| 3Ma | 369 | $7.9 \cdot 10^{-5}$ | 3.6 | 785 | $1.8 \cdot 10^{-5}$ | 14.4 | 1702 | $1.8 \cdot 10^{-6}$ | 19.3 |

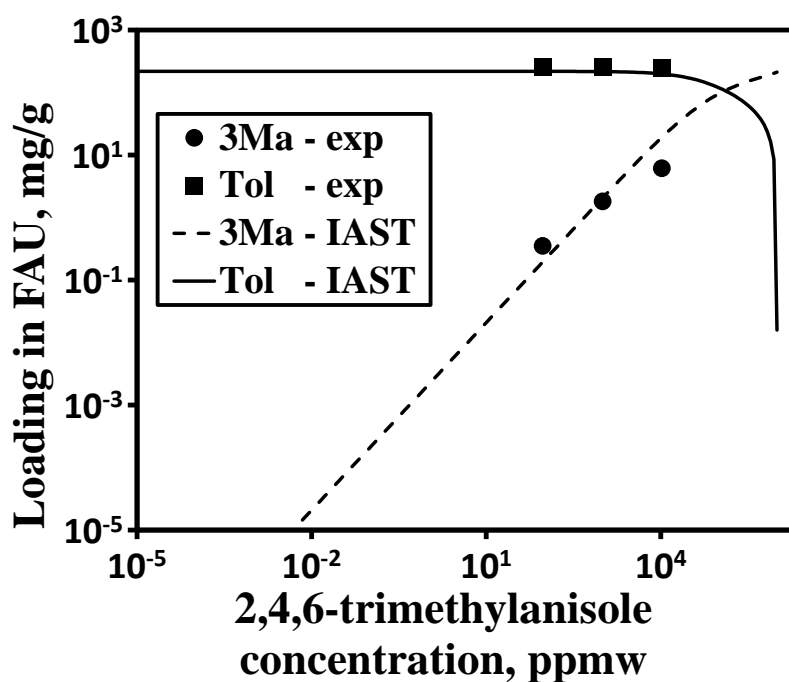


Figure 2.18. Adsorption isotherms for the binary system toluene - 2,4,6-trimethylanisole in NaY zeolite. Lines - IAST predictions, circles - experimental results for 2,4,6-trimethylanisole, squares - experimental results for toluene.

Using the shifted pure component isotherm of butanal, the IAST was recalculated and the comparison between experimental results and IAST predictions for the binary mixture toluene-butanal is depicted in Fig. 2.14. By shifting the adsorption isotherm of pure butanal in NaY, IAST is able to accurately describe the behavior of the toluene-butanal system for all the available experimental data points. This is a clear indication that (1) the adsorption isotherm of pure toluene is well predicted by molecular simulations and (2) the adsorption behavior of the system toluene-butanal can be predicted by IAST.

Table 2.2. Comparison of IAST with experimental adsorption results for the 6-component mixture comprising toluene (Tol), butanal (Bt), 2-ethyl-2-hexenal (2E2H), 2,6-dimethylcyclohexanone (dMc), 2,4,6-trimethylphenol (3Mp) and 2,4,6-trimethylanisole (3Ma) in NaY zeolite. Three data sets are presented corresponding to the three data sets of Fig. 2.11. The pure component adsorption isotherms of butanal, 2-ethyl-2-hexenal and 2,6-dimethylcyclohexanone, used in the IAST calculations, were shifted in the fugacity scale with the shifting parameters $8.6 \cdot 10^{-4}$, $6.3 \cdot 10^{-3}$ and 35.5 respectively (as explained in the main text).

| Comp. | Data set 1 | | | Data set 2 | | | Data set 3 | | |
|-------|----------------|--------------|-------------|----------------|--------------|-------------|----------------|--------------|-------------|
| | Eq. conc., ppm | q IAST, mg/g | q exp, mg/g | Eq. conc., ppm | q IAST, mg/g | q exp, mg/g | Eq. conc., ppm | q IAST, mg/g | q exp, mg/g |
| Tol | 999199 | 180.1 | 215.7 | 997420 | 150.7 | 108.8 | 993447 | 103.2 | 37.5 |
| Bt | 152 | 6.1 | 10.4 | 339 | 11.8 | 43.1 | 965 | 25 | 73.3 |
| 2E2H | 257 | 7.2 | 6.7 | 588 | 13.2 | 22.9 | 1426 | 19.8 | 28.9 |
| dMc | 178 | 10.4 | 12.9 | 424 | 19.5 | 34.3 | 1246 | 34 | 48 |
| 3Mp | 214 | 14 | 9.9 | 444 | 22.7 | 26.9 | 1214 | 36.3 | 39.4 |
| 3Ma | 369 | 0.5 | 3.6 | 785 | 0.9 | 14.4 | 1702 | 1 | 19.3 |

Following the same approach, the pure component adsorption isotherm of 2-ethyl-2-hexenal and 2,6-dimethylcyclohexanone were shifted with shifting factors of $6.3 \cdot 10^{-3}$ and 35.5 respectively. The comparison between experimental results and IAST predictions for the binary systems toluene-2-ethyl-2-hexenal and toluene-2,6-dimethylcyclohexanone are showed in Figs. 2.15 and 2.16 respectively. As can be seen in Fig. 2.16, the IAST does not accurately describe the system toluene-2,6-dimethylcyclohexanone for high concentrations of the ketone. This is probably an indication that this binary system behaves as non-ideal in the adsorbed phase. For the binary systems toluene-2,4,6-trimethylphenol and toluene-2,4,6-trimethylanisole no shifting of the isotherms was required. As can be seen in Figs. 2.17 and 2.18, IAST accurately describes the adsorption behavior of these mixtures in the range of low impurity concentration. In the range of high impurity concentration, deviations from IAST predictions can be observed, which are probably due to non-ideal behavior of the adsorbed phase.

Using the shifted isotherms for butanal, 2-ethyl-2-hexenal and 2,6-dimethylcyclohexanone, the IAST for the six component mixture was re-calculated. The comparison with experimental results is given in Table 2.2. As can be seen in Table 2.2, the first experimental data set is predicted well by IAST. This is a clear indication that for the low concentration region of the impurities, the system behaves as ideal in the adsorbed phase and therefore IAST is applicable. For the second and third experimental data set, corresponding to higher concentration range of the impurities, large deviations are observed. These deviations are expected due to the

deviations found in the binary toluene-2,6-dimethylcyclohexanone, toluene-2,4,6-trimethylphenol and toluene-2,4,6-trimethylanisole systems.

The results presented in this work indicate that if appropriate force fields describing the interaction parameters with the zeolite framework would be available for this system, the adsorption behaviour in zeolites could be predicted. There is also an indication of non-ideal behaviour of this system in the adsorbed phase for high concentrations, as can be seen in Table 2.2 for the data set 2 and 3.

2.5 Conclusions

Twenty-one commercial adsorbents of different classes were tested in batch adsorption experiments with respect to the adsorption capacity towards a six-component mixture comprising butanal, 2-ethyl-2-hexenal, 2,6-dimethylcyclohexanone, 2,4,6-trimethylphenol and 2,4,6-trimethylanisole as impurities and toluene as solvent. The Na form of FAU-type zeolite performed best.

The research was further extended to check if the adsorption behaviour of the chosen mixture can be predicted in zeolites. A force field was defined and used to compute the pure component adsorption isotherms of the selected compounds in NaY zeolite using molecular simulations. The pure component adsorption isotherms were used as input for an IAST model and the adsorption isotherm of the six-component mixture was computed. Because the IAST predictions were far from the experimentally obtained isotherm, the binary systems with toluene were investigated.

IAST was able to accurately describe the trend for the competition of all the binary toluene/impurity systems. Only the adsorption of the binary toluene-2,4,6-trimethylphenol and toluene-2,4,6-trimethylanisole mixtures in NaY zeolite were accurately predicted by IAST. For the toluene-butanal, toluene-2-ethyl-2-hexenal and toluene-2,6-dimethylcyclohexanone systems, a shift of the pure component isotherm of butanal, 2-ethyl-2-hexenal and 2,6-dimethylcyclohexanone along the fugacity axis was applied in order for IAST to accurately predict the experimental adsorption behaviour.

Using the shifted isotherms for butanal, 2-ethyl-2-hexenal and 2,6-dimethylcyclohexanone, IAST is able to predict the adsorption behaviour of the six-component mixture in NaY in the range of low concentrations. At high concentrations, deviations are observed. There are two possible reasons for this behaviour: *i*) the deviation is due to non-ideal behaviour of the adsorbed phase or, *ii*) deviations are due to inappropriate fitting of the pure component adsorption data for the range of high concentrations as depicted in Figs. A1-A6 (Appendix A).

However, this work proves that in principle, the adsorption behaviour of the studied six-component mixture can be predicted using simulations if an appropriate force field is available.

Chapter 3

Evaluating Adsorbed-Phase Activity Coefficient Models Using a 2D-lattice Model

This chapter is for a large part based on:

C.C. Brunchi, P. Englebienne, H.J.M. Kramer, S.K. Schnell, T.J.H. Vlugt, Evaluating adsorbed-phase activity coefficient models using a 2D-lattice model, *Molecular Simulation*, 2015, in press, DOI: [10.1080/08927022.2014.972394](https://doi.org/10.1080/08927022.2014.972394).

3.1 Introduction

Adsorption of multicomponent systems is of great importance in many natural and engineering applications such as certain separations for removing impurities from fluid streams (e.g. removal of volatile organic compounds from airstreams, dehydration of natural gas), chromatography as well as design of heterogeneous chemical reactors [12-17]. The design of adsorption separation units depends mainly on the adsorbent capacity at equilibrium conditions [80]. The performance of such units is determined by the competitive adsorption of the different compounds simultaneously present in the bulk (gas or liquid) solution [19]. Therefore, the assessment of the adsorption capacity of a compound in the presence of other solutes as well as the definition of appropriate theoretical models for predicting the adsorption behavior of multicomponent mixtures is imperative for a proper design of adsorption processes [19].

Multicomponent adsorption data is considerably more difficult to measure than pure component data [13]. Therefore, models that can predict multicomponent adsorption equilibrium using only pure component data have become very attractive. The most commonly used approach for predicting equilibrium competitive adsorption, using only pure component data is the adsorbed solution theory, of which an excellent overview is given by Murthi and Snurr [22]. The Ideal Adsorbed Solution Theory (IAST) was derived by Myers and Prausnitz [21] for a two-dimensional homogenous adsorbed phase. The adsorbed phase is considered as a temperature-invariant area equally accessible to all compounds (the so-called spreading pressure). The main assumption of IAST is that the adsorbed mixture forms an ideal solution in equilibrium with the bulk (gas or liquid) phase at a constant spreading pressure for each solute [21]. The spreading pressure of a solute is an intensive thermodynamic variable for adsorption equilibria; it is defined as the difference between the interfacial tension of the pure solvent-solid interface and that of the solution-solid interface [10]. The IAST was later extended to treat a three-dimensional adsorbed phase [23, 24]. In the Real Adsorbed Solution Theory (RAST) [25], the non-ideal behavior of the adsorbed phase is accounted for by the use of activity coefficients. Myers and Prausnitz [21] showed that the activity coefficients are a function of temperature, adsorption capacity (mole fractions of adsorbed species), and spreading pressure.

Throughout the years, various activity coefficient models were used with RAST. Due to the lack of models to describe activity coefficients for the adsorbed phase, most of the authors used vapour-liquid activity coefficient models. Sochard and co-workers [26] used RAST together with the UNIQUAC [42] and NRTL [43] models for calculating activity coefficients in the adsorbed phase but did not take into account the

spreading pressure-dependency of activity coefficients. Erto and co-workers [44] used the Wilson model [45] for calculating adsorbed phase activity coefficients and accounted for the spreading pressure dependency by using an empirical equation proposed by Kopatsis and Myers [46]. The same model is used in the work published recently by Jadhav and co-workers [47].

The most common approach used by authors when studying the RAST is to relate the theory to experimental adsorption data [26, 44]. Swisher and co-workers [27] used molecular simulations to obtain adsorption data in zeolites. The generated data was used to test the accuracy of IAST with the segregated sites approach. The segregated model assumes that the competition for adsorption occurs at isolated adsorption sites and that molecules from each adsorption site interact with the bulk phase independently. In this chapter, we use molecular simulations performed on a 2D-lattice to generate adsorption data. The generated data is used, in the first part of this chapter, to check the suitability of the Wilson [45] and NRTL [43] activity coefficient models. The simulation technique for the 2D-lattice is explained in section 3.2 of this chapter. The advantage of using a 2D-lattice model is that we can generate multicomponent adsorption data at constant spreading pressure (or, if needed, constant adsorbed-phase composition). It is difficult to achieve these conditions using experimental techniques. By generating multicomponent adsorption data at constant spreading pressure, we can evaluate the Wilson [45] and NRTL [43] models which are only composition dependent (at constant temperature). The methodology for generating multicomponent adsorption data at constant spreading pressure using the 2D-lattice model is explained in section 3.3.1. Using multicomponent adsorption data generated at different spreading pressures and constant composition, we can also evaluate the empirical equation proposed by Kopatsis and Myers [46] describing the spreading pressure dependency of the adsorbed phase activity coefficients. This will be done in section 3.4.2 of this chapter.

From a purely conceptual point of view, any adsorbed-phase activity coefficient model should describe multicomponent activity coefficient data for the adsorbed phase regardless of how the data was obtained (experiments, molecular simulations in zeolites or Monte Carlo simulations performed on a simple 2D-lattice model). The lattice model provides a very simplified model for adsorption and any adsorbed-phase activity coefficient model should be able to describe such data. In section 3.4.1 of this chapter, we show that the Wilson and NRTL models do not provide an accurate description of adsorbed phase activity coefficients for slightly non-ideal ($\gamma \cong 0.3$) to strong non-ideal systems ($\gamma \cong 0.01$).

As shown by Swisher and co-workers [27], by assuming that competition for adsorption occurs at isolated adsorption sites and molecules from each adsorption site

interact with the bulk phase independently, one can apply IAST to each adsorption site to calculate the adsorption equilibrium. The overall total loading for each compound present in the mixture is simply the sum of the loading obtained for each individual adsorption site. This approach is called the Segregated Ideal Adsorbed Solution Theory, SIAST. For a complete description of the SIAST model we refer the reader to the work of Swisher and co-workers [27]. The SIAST model provides a significant improvement of IAST predictions with just a few simple assumptions. Therefore, it is of great interest to check if such improvements can be achieved with similar theories used for predicting multicomponent adsorption data. One such theory is the use of Monte Carlo simulations on 2D-lattice models, for predicting multicomponent adsorption equilibrium. This approach has been applied in the literature by several authors [28, 81-83] with different degrees of success. In the second part of this chapter we use Monte Carlo simulations on a simple 2D-lattice model together with the segregated sites approach, to predict multicomponent adsorption data from pure component data.

For a better understanding of the concept, we emphasize a clear difference between the following terminologies: lattice, lattice point and adsorption site. A lattice is a two-dimensional representation of the adsorbed phase containing multiple lattice points. Throughout the text, the term adsorption site refers to the distinct sites available for adsorption; e.g. Swisher and co-workers [27] showed that the system $\text{CO}_2\text{-C}_3\text{H}_8$ in MOR has two distinct adsorption sites and therefore the pure component adsorption isotherms of CO_2 and C_3H_8 can be fitted using a dual-site Langmuir equation. Similar to the SIAST model [27] of Swisher and co-workers, in our 2D-lattice simulations, we assume that each adsorption site can be represented by a lattice, and molecules adsorbed on each lattice only interact with the bulk fluid. By performing Monte Carlo simulations on each lattice, corresponding to an adsorption site, we can measure the individual loading of each species (pure or multicomponent mixture) in each adsorption site. The total loading of each species is the sum over all the lattices (adsorption sites) of each species. The technique used for predicting multicomponent adsorption data from single component isotherms using the segregated sites approach is presented in section 3.3.2 of this chapter.

In section 3.4.2, two binary mixtures in two adsorbent materials are used as case studies for testing the predictions of the segregated 2D-lattice model: the binary system $\text{CO}_2\text{-N}_2$ in pure silica hypothetical zeolite PCOD8200029, with isolated adsorption sites and normal preference for adsorption and the binary system $\text{CO}_2\text{-C}_3\text{H}_8$ in pure silica MOR, with isolated adsorption sites and inverse site preference. The segregated 2D-lattice provides accurate predictions for the system $\text{CO}_2\text{-N}_2$ in PCOD8200029 but fails in predicting the adsorption behavior of $\text{CO}_2\text{-C}_3\text{H}_8$ in pure silica MOR. Our findings are summarized in section 3.5.

3.2 Monte Carlo simulations on a 2D-lattice

The Monte Carlo technique in the grand-canonical ensemble (μVT) [33-35] is used to simulate the adsorption of molecules on a homogeneous 2D-lattice surface. The lattice model is used such that each molecule, modelled as a lattice point, can occupy a specific site on the surface and each site can only be occupied by one molecule. Each molecule on a specific site can interact with 4 neighboring sites (coordination number 4). Periodic boundary conditions are used.

As an example, the parameters for simulating the adsorption of a binary mixture (compounds X and Y) using the 2D-lattice model, are: the total number of sites, the interaction energy between like molecules (w_{XX} , w_{YY}), the interaction energy between unlike molecules (w_{XY}) and the interaction energy between the molecules and the surface (w_{XS} , w_{YS}). Fig. 3.1 shows a schematic representation of a grand-canonical Monte Carlo simulation (GCMC) used to equilibrate an infinitely-large reservoir containing a binary mixture (black circles - compound X, grey circles - compound Y) with a square 2D-lattice. The simulations are performed in cycles, in each cycle an attempt is made to perform one of the following trial moves: displacement - a molecule is selected at random and given a random displacement, insertion - it is attempted at random to insert a molecule into a random lattice point, removal - it is attempted at random to remove a molecule from a random lattice point, identity change - one of the components is selected at random and an attempt is made to change a random molecule of this type to the other type. All trial moves are performed with the grand-canonical Monte Carlo technique [33, 34]. We have allowed 10^6 cycles for equilibration, and subsequent production runs were 10^7 cycles. The solid surface is modelled as a square (2D) lattice of dimensions 40 x 40. More details about the Monte Carlo simulation technique can be found in the literature [35, 39, 62, 69, 84].

3.3 Simulations

3.3.1 Constant spreading pressure simulations

Kopatsis and Myers [46] proposed an empirical equation for the excess free energy for adsorption, using the ISAC (isoactive solvent) theory and based on similarities between solution thermodynamics and adsorption thermodynamics:

$$\psi^e = g^e \cdot (1 - e^{C \cdot (\pi \cdot A / RT)}) \quad (3.1)$$

where g^e is the excess Gibbs free energy (dependent only on composition and temperature), C is a constant specific to each adsorbent, π is the spreading pressure of the mixture, A is the surface area of the adsorbent, R is the gas constant and T is the absolute temperature.

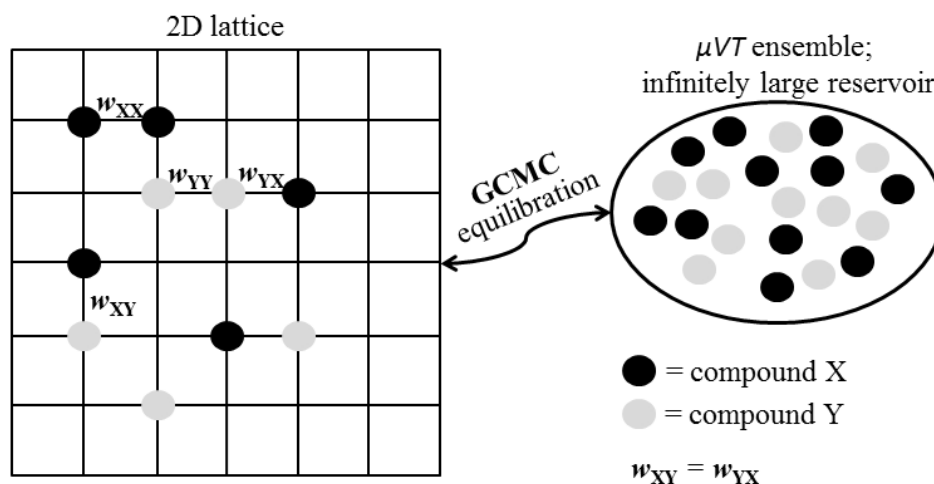


Figure 3.1. Schematic representation of a grand-canonical Monte Carlo simulation (GCMC) used to equilibrate an infinitely-large reservoir containing a binary mixture of molecules, X+Y (black circles – compound X, grey circles – compound Y), with a 2D-lattice. The lattice sites are situated at the line intersections. w_{XX} – interaction energy between two type X molecules, w_{YY} – interaction energy between two type Y molecules, w_{XY} ($= w_{YX}$) – interaction energy between one type X molecule and one type Y molecule.

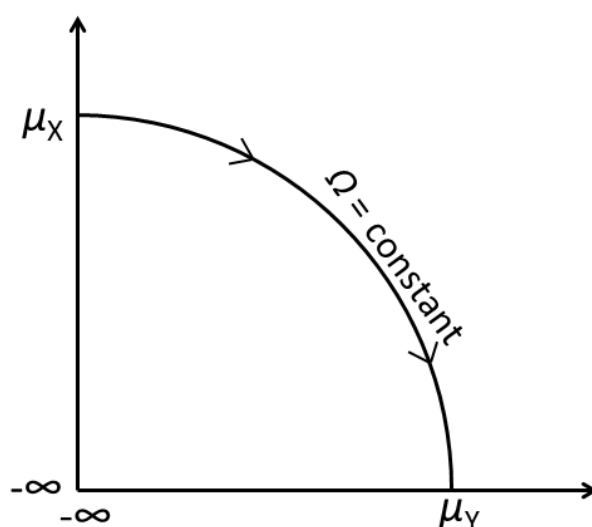


Figure 3.2. Thermodynamic integration from the chemical potential of compound X to the chemical potential of compound Y while keeping the grand potential density, Ω , constant.

The activity coefficient for the adsorbed species i can be obtained as:

$$\ln \gamma_i = \left[\frac{\partial(\psi^e/RT)}{\partial N_i} \right]_{T,P,a_1,N_j} \quad (i = 2,3, \dots n; j \neq i) \quad (3.2)$$

In Eq. 3.2, the index $i = 1$ corresponds to the adsorbent (n represents the number of compounds present in the system). The derivation of the excess free energy for adsorption is performed at constant temperature, pressure (P), sorbent activity (a_1) and keeping the number of moles of the other solutes constant (N_j).

A direct consequence of the ISAC theory is that the adsorbed phase activity coefficients at constant temperature can be written as a product of two distinct functions:

$$\gamma(\pi, x) = F_1(\pi) \cdot F_2(x) \quad (3.3)$$

In Eq. 3.3, the function F_1 is dependent only on the spreading pressure and the function F_2 is dependent only on adsorbed phase mole fractions, x . If multicomponent adsorption data at constant composition or constant spreading pressure can be generated, the two dependencies can be studied independently.

From statistical thermodynamics it follows that the grand potential density, Ω , for a fluid phase consisting of a binary mixture (X+Y), can be expressed as:

$$\Omega(\mu_X, \mu_Y, T) = -P \cdot V \quad (3.4)$$

and for an adsorbed phase:

$$\Omega(\mu_X, \mu_Y, T) = -\pi \cdot A \quad (3.5)$$

where μ_X and μ_Y are the chemical potentials of compound X and Y respectively and V is the system volume. The simulations are performed at constant adsorbent area, A . Therefore, it follows from Eq. 3.5 that a simulation performed at constant grand potential density is a simulation performed at constant spreading pressure. The total derivative of the grand potential density for the same binary mixture is:

$$d\Omega = \left(\frac{\partial \Omega}{\partial \mu_X} \right)_{\mu_Y, T} \cdot d\mu_X + \left(\frac{\partial \Omega}{\partial \mu_Y} \right)_{\mu_X, T} \cdot d\mu_Y + \left(\frac{\partial \Omega}{\partial T} \right)_{\mu_X, \mu_Y} \cdot dT \quad (3.6)$$

The differential of the Helmholtz free energy for a multicomponent system is:

$$dF = -SdT - PdV + \sum_{i=1}^n \mu_i dN_i \quad (3.7)$$

where n is the number of compounds in the system and N_i the number of moles of compound i . Using Eq. 3.4, the differential Helmholtz free energy can be written as:

$$dF = d\Omega + \sum_{i=1}^n \mu_i dN_i + \sum_{i=1}^n N_i d\mu_i \quad (3.8)$$

If the simulations are performed in the grand-canonical ensemble (μVT), from Eqs. 3.7 and 3.8 follows the variation of the grand potential density with respect to changes in chemical potential, relation valid for any system:

$$\left(\frac{\partial \Omega}{\partial \mu_i}\right)_{T,V,\mu_j,j \neq i} = -\langle N_i \rangle \quad (3.9)$$

where the differentiation must be performed at constant temperature, volume and chemical potential of the other compounds. The values between angle brackets denote ensemble averages in the grand-canonical ensemble.

Combining Eqs. 3.6 and 3.9 and considering that the simulations are done at constant temperature, an expression for the variation of μ_X with respect to μ_Y is obtained:

$$\left(\frac{\partial \mu_X}{\partial \mu_Y}\right)_{T,V,\pi} = -\frac{\langle N_Y \rangle}{\langle N_X \rangle} \quad (3.10)$$

Eq. 3.10 is valid for a binary system, at constant temperature, area and spreading pressure.

Thermodynamic integration at constant spreading pressure can be performed using Eq. 3.10 by imposing the system temperature and chemical potential of compound X (see schematic representation in Fig. 3.2). Using the 2D-lattice model described in section 3.2 of this chapter and performing a thermodynamic integration on a constant spreading pressure path, adsorption data at constant spreading pressure can be generated. Using different sets of interaction parameters, adsorption data can be generated for a behavior ranging from ideal to strongly non-ideal. All simulations were carried out at constant temperature and throughout the text reduced units were used.

Calculation of activity coefficients. For a binary (or higher) system, one can calculate the activity coefficient directly from the imposed chemical potentials and the adsorbed phase mole fractions resulting from the 2D-lattice simulations. The chemical potential of the i -th component is:

$$\mu_i(T, \pi, \vec{x}) = k_B \cdot T \cdot \ln\left(\frac{f_i}{f_0}\right) \quad (3.11)$$

or, written as a function of the standard state chemical potential of pure i -th component, μ_i^* :

$$\mu_i(T, \pi, \vec{x}) = \mu_i^*(T, \pi) + k_B \cdot T \cdot \ln(x_i \cdot \gamma_i(T, \pi, \vec{x})) \quad (3.12)$$

where k_B is the Boltzmann constant, T is the absolute temperature, x_i is the adsorbed phase mole fraction (\vec{x} is a vector containing the mole fractions of all components) and $\gamma_i(T, \pi, \vec{x})$ is the activity coefficient of the i -th component in the adsorbed phase. The standard state chemical potential of pure component i can be calculated as:

$$\mu_i^*(T, \pi) = k_B \cdot T \cdot \ln\left(\frac{f_0}{P}\right) \quad (3.13)$$

In the 2D-lattice simulations, we impose the chemical potential of the fluid phase (by imposing the fugacity, f_i) and we compute the loadings (adsorbed phase mole fractions, x_i). According to Eq. 3.12, the adsorbed phase activity coefficient can be computed as:

$$\gamma_i(T, \pi, \vec{x}) = \frac{\exp(\mu_i(T, \pi, \vec{x}) - \mu_i^*(T, \pi))}{x_i} \quad (3.14)$$

The Gibbs-Duhem thermodynamic consistency test [85, 86] was imposed on all of the activity coefficient data generated with the 2D-lattice model.

3.3.2 Segregated 2D-lattice model

The goal is to test if the simple 2D-lattice model can be used to predict multicomponent adsorption data from pure component data using the segregated sites approach, similar to the SIAST model [27] of Swisher and co-workers. We assume that competition for adsorption occurs at isolated adsorption sites and molecules from each adsorption site interact with the bulk phase independently. The pure component isotherms can be parameterized using the 2D-lattice model for any number of (isolated) adsorption sites. The parameterization procedure is explained below.

For the lattice simulations we fixed the total number of lattice sites at 1600 (square lattice of size 40 x 40); a lattice with this size assures that the finite-size effects are negligible. The interaction energy between like molecules and the interaction energy between molecules and the lattice are fitted to the pure-component isotherms.

Before fitting the interaction parameters, the loadings of the pure component isotherms need to be converted to the same units as the loadings generated by the lattice model. In the 2D-lattice model, the loadings have units of [molecules/lattice sites]. The experimental loadings of the pure component isotherms are proportional to

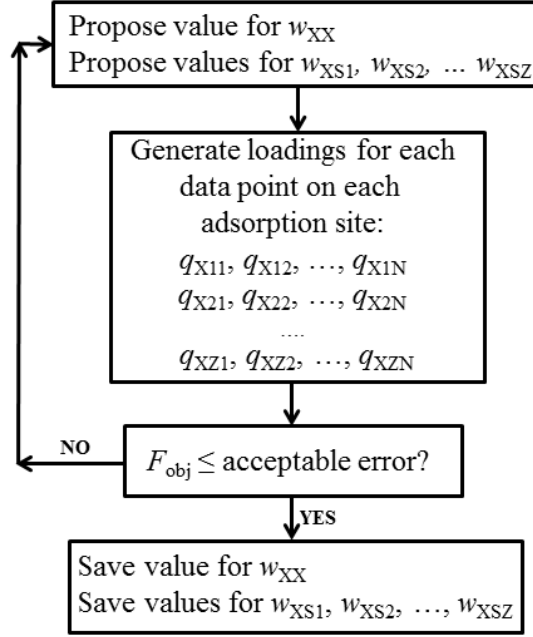


Figure 3.3. Procedure for fitting the energy interaction parameters w_{XX} , w_{XS1} , ..., w_{XSZ} for a hypothetical pure component isotherm of compound X with Z adsorption sites. The objective function is calculated as in Eq. 3.15.

the 2D-lattice loadings ([molecules/lattice sites]); the conversion factor can be obtained by examining the maximum loadings of the system.

Fig. 3.3 shows schematically the fitting procedure for a hypothetical single-component isotherm of compound X with Z adsorption sites. For a pure component isotherm with Z adsorption sites we have one energy interaction parameter between like molecules (w_{XX}) and Z energy interaction parameters between molecules and each adsorption site ($w_{XS1} \dots w_{XSZ}$).

The objective function for a least square minimization is:

$$F_{\text{obj}} = \sum_{i=1}^{n_{\text{odp}}} \left(\frac{q_{X_i}^{\text{exp}} - q_{X_i}^{\text{2D-lattice}}}{q_{X_i}^{\text{2D-lattice}}} \right)^2 \quad (3.15)$$

where n_{odp} represents the number of data points and the loadings resulting from the 2D-lattice simulations, $q_{X_i}^{\text{2D-lattice}}$, are calculated as:

$$q_{X_i}^{\text{2D-lattice}} = \sum_{j=1}^Z q_{X_{ij}} \quad (3.16)$$

$q_{X_i}^{\text{exp}}$ and $q_{X_i}^{\text{2D-lattice}}$ are experimental loadings and the 2D-lattice simulation loadings respectively.

To decrease the computational time of the proposed fitting procedure, a simpler alternative was used. The dual site Langmuir equation was fitted to the “experimental” pure component data. The 2D-lattice model was parameterized, for each adsorption site, using data generated with the fitted Langmuir model. Once all the relevant parameters were obtained from fitting the 2D-lattice model to the pure component isotherms, the mixture isotherms were generated.

3.4 Results and discussion

3.4.1 Testing of adsorbed-phase activity coefficient models using a 2D-lattice model

Using the methodology described in section 3.3.1, adsorbed phase activity coefficient data for a binary mixture (X+Y) was generated at constant spreading pressure. All simulations were carried out at constant temperature. The generated activity coefficient data obeys the Gibbs-Duhem thermodynamic consistency check [85, 86]. According to the Gibbs-Duhem equation, one activity coefficient can be expressed as a function of other activity coefficients of the mixture [85]. Therefore, it is sufficient to fit the activity coefficient models to the data of one of the components present in the binary mixture. The Wilson (see Eq. B1, Appendix B), three-parameter NRTL (NRTL3) and four-parameter NRTL (NRTL4) activity coefficient models were fitted to generated activity coefficient data using the non-linear least square minimization routine of Matlab with a relative tolerance of 10^{-8} . For a binary system, the parameters of the NRTL3 model (see Eq. B2, Appendix B) are: τ_{12} , τ_{21} and $\alpha = \alpha_{12} = \alpha_{21}$. In the NRTL4 model, α_{12} and α_{21} are not equal. The results presented below were obtained by fitting the Wilson, NRTL3 and NRTL4 models to the activity coefficient data of component X.

The deviation from non-ideal behavior of the adsorbed phase mixture, generated using the 2D-lattice model, can be influenced by changing the system fugacity and the degree of mixing in the adsorbed phase reflected by the parameter:

$$\Delta w = w_{XX} + w_{YY} - 2w_{XY} \quad (3.17)$$

Fig. 3.4 shows slightly non-ideal binary data for adsorbed phase activity coefficients and the corresponding fit with the Wilson model. The reference chemical potential was computed using Eq. 3.13. The fugacity of component X in the limit $x_X \rightarrow 1$ was 0.01 [-]. The 2D-lattice parameters used to generate the data in Fig. 3.4 are shown in Table B1 (Appendix B). As can be seen, the Wilson model overestimates the data for component Y in the low coverage regime. The NRTL3 and NRTL4 models provide a better fit (Figs. B1-B2, Appendix B). The scatter of the data for the low coverage regime is due to poor statistics obtained with the Monte Carlo simulations.

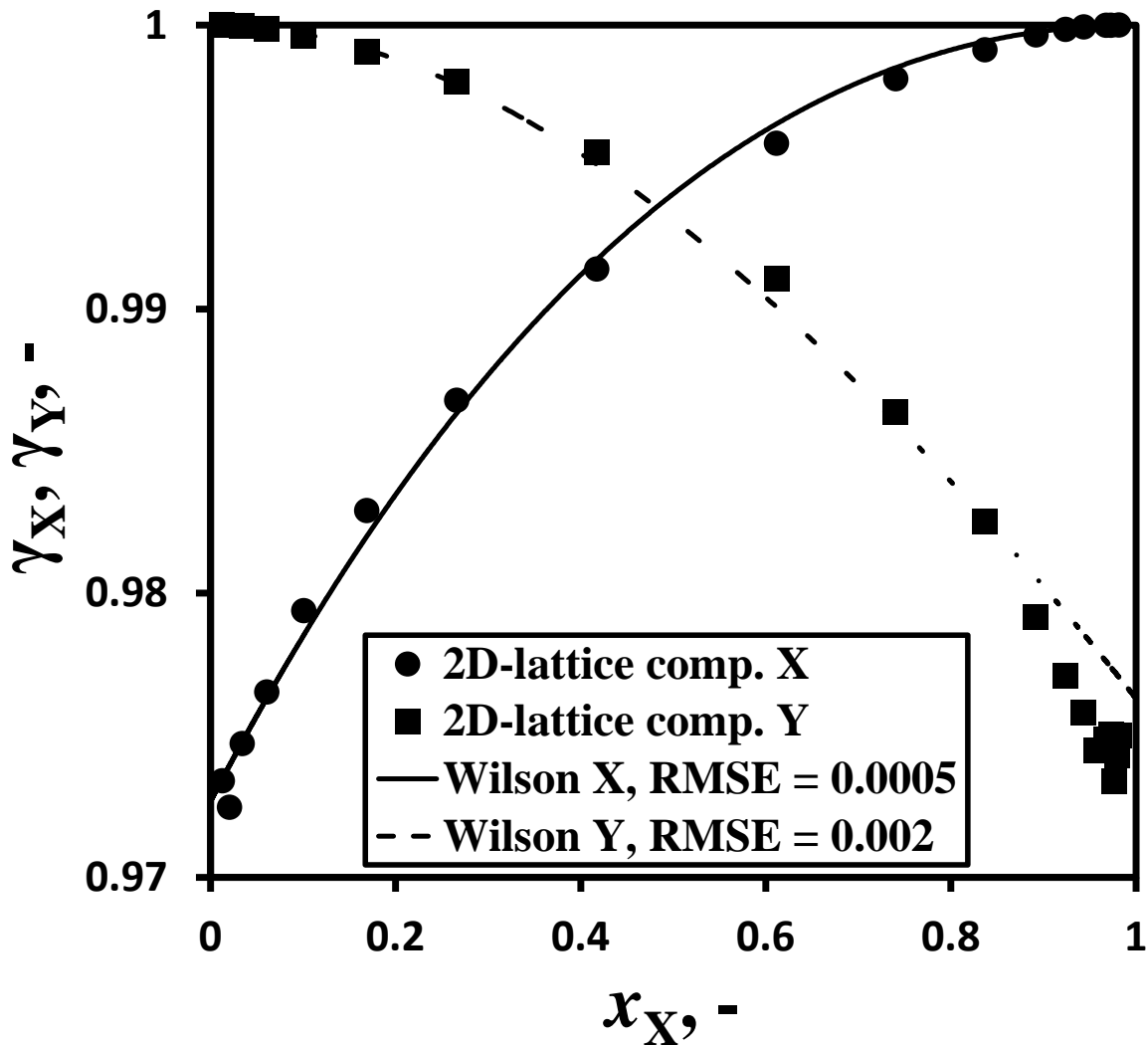


Figure 3.4. Adsorbed-phase activity coefficient data for a slightly non-ideal binary system of molecules X+Y, generated using a 2D-lattice model. Circles - 2D-lattice simulation data for compound X, squares - 2D-lattice simulation data for compound Y, lines - fit using the Wilson model. RMSE (reduced units) represents the root mean square error of the fit calculated according to Eq. B4 (Appendix B). The parameters used in the 2D-lattice simulations are listed in Table B1 (Appendix B).

To increase the non-ideal behavior of the adsorbed phase mixture, the fugacity of compound X in the limit $x_X \rightarrow 1$ was increased to 30 and the degree of mixing was increased to a Δw value of 1.6 (see Table B1, Appendix B). Using the new set of parameters, the data in Fig. 3.5 was generated. As can be observed, the activity coefficient data begins to take an S-shaped form and the Wilson model cannot accurately reproduce the shape of the data. Similar results are obtained for the NRTL model as can be observed in Figs. B3-B4 (Appendix B). The non-ideal behavior of the adsorbed phase mixture is further accentuated by increasing the degree of mixing parameter to a value of 2.6 (see Table B1, Appendix B). The strong non-ideal behavior of the data generated using the new set of parameters, for the Wilson model,

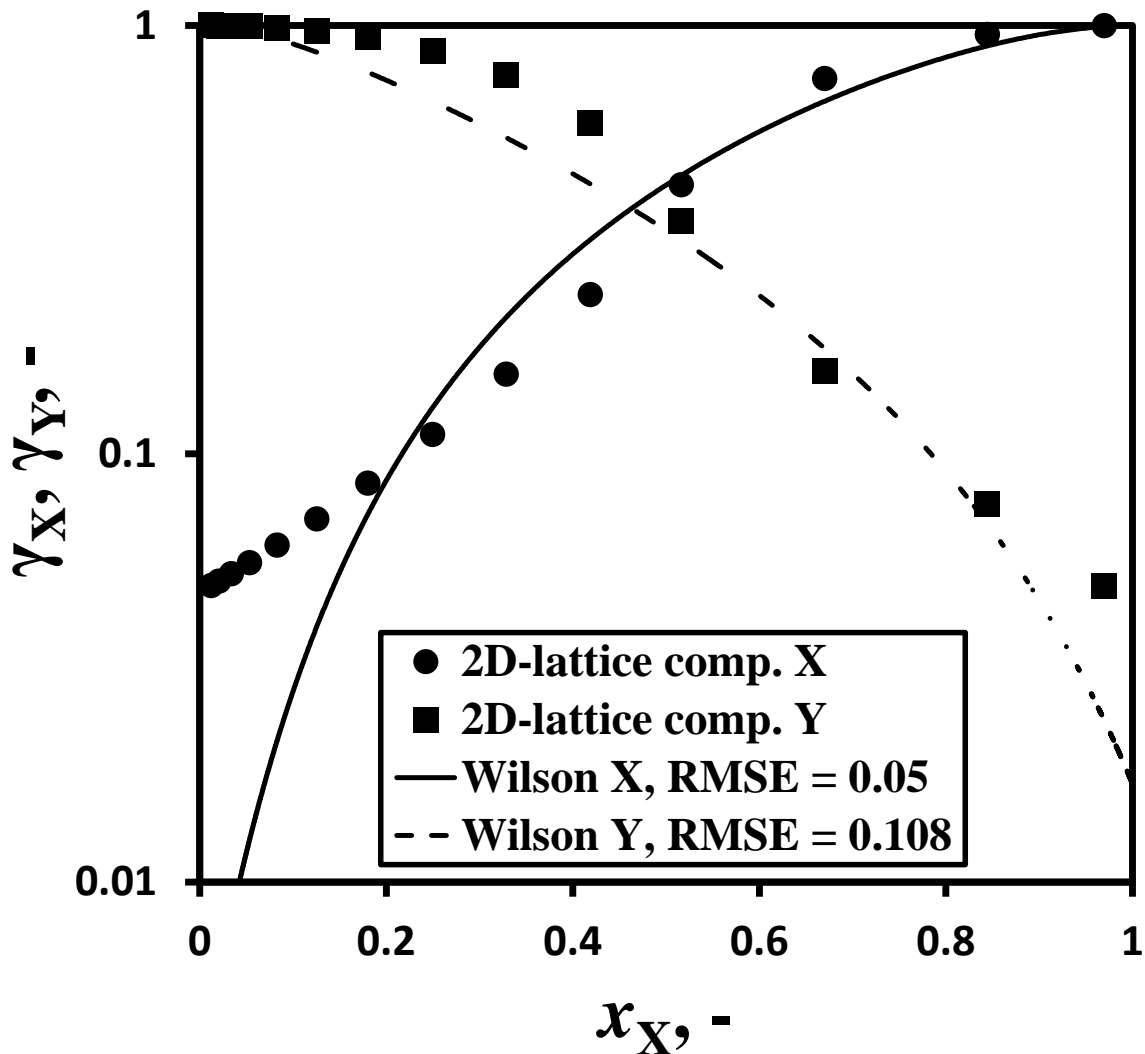


Figure 3.5. Adsorbed-phase activity coefficient data for a non-ideal binary system of molecules X+Y, generated using a 2D-lattice model. Circles - 2D-lattice simulation data for compound X, squares - 2D-lattice simulation data for compound Y, lines - fit using the Wilson model. RMSE (reduced units) represents the root mean square error of the fit calculated according to Eq. B4 (Appendix B). The parameters used in the 2D-lattice simulations are listed in Table B1 (Appendix B).

is shown in Fig. 3.6. The accentuated S-shaped form of the activity coefficient data cannot be reproduced by any of the tested models. Overall, the NRTL activity coefficient model (with three or four parameters) does not provide a significant improvement in the fitting of generated adsorption data (Figs. B1-B6, Appendix B). Neither the Wilson nor the NRTL model can provide a reasonable fit for non-ideal adsorption data generated using the simple lattice theory. The Wilson and NRTL models should be improved in order to provide an accurate description of adsorbed phase activity coefficients.

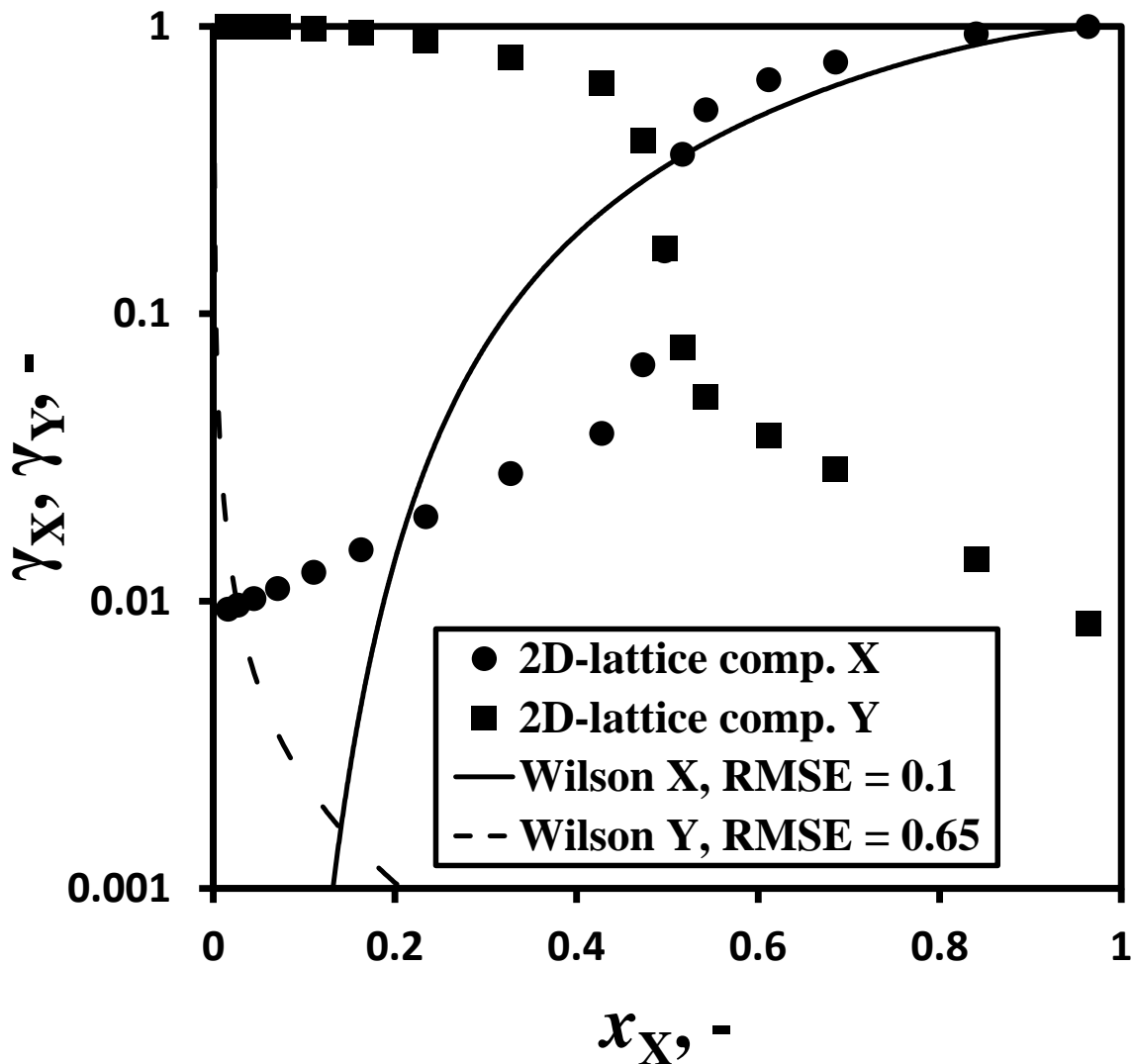


Figure 3.6. Adsorbed-phase activity coefficient data for a highly non-ideal binary system of molecules X+Y, generated using a 2D-lattice model. Circles - 2D-lattice simulation data for compound X, squares - 2D-lattice simulation data for compound Y, lines - fit using the Wilson model. RMSE (reduced units) represents the root mean square error of the fit calculated according to Eq. B4 (Appendix B). The parameters used in the 2D-lattice simulations are listed in Table B1 (Appendix B).

3.4.2 Testing the spreading pressure dependency of adsorbed-phase activity coefficients using a 2D-lattice model

As explained in section 3.3.1 of this chapter, Kopatsis and Myers [46], using the ISAC theory and based on similarities between solution thermodynamics and adsorption thermodynamics, proposed an empirical equation to describe the spreading pressure dependency of adsorbed phase activity coefficients (Eq. 3.1). According to Eqs. 3.1-3.3, the constant-composition (and constant temperature) adsorbed phase activity coefficients can be calculated using:

$$\ln \gamma_i(\pi) = 1 - e^{C \cdot (\pi \cdot A / RT)} \quad (3.18)$$

where C is a constant specific to each adsorbent. The spreading pressure can be calculated from the pure component isotherms as:

$$\pi_i = \frac{R \cdot T}{A} \cdot \int_0^{f_i^0} n_i^0(t) d \ln t, \quad i = 1, \dots, n \quad (3.19)$$

where f_i^0 is the fugacity of pure component i adsorbed at the same temperature and spreading pressure as the (adsorbed) mixture and $n_i^0(t)$ is the loading of component i .

According to Eq. 3.18, the plot of $\ln(1 - \ln \gamma_i)$ vs $\pi A / RT$ should be a straight line. However, as can be observed in Fig. 3.7, the spreading pressure dependency of $\ln(1 - \ln \gamma_X)$ at different mole fractions is not linear. For mole fractions below 0.5 the equation proposed by Kopatsis and Myers [46] cannot describe the adsorption data. Additional effort is required for developing new models to account for the spreading pressure dependency of activity coefficients.

3.4.3 Predicting adsorption of mixtures using a segregated 2D-lattice model

For testing the proposed segregated 2D-lattice model described in section 3.3.2 of this chapter, two binary adsorption data sets were used: (1) the adsorption data for the system $\text{CO}_2\text{-N}_2$ in the pure silica hypothetical zeolite PCOD8200029 and (2) the adsorption data for the system $\text{CO}_2\text{-C}_3\text{H}_8$ in pure silica MOR, both from the work of Swisher and co-workers [27]. According to the authors, both PCOD8200029 and MOR are materials with two distinct adsorption sites. Using snapshots taken during GCMC simulations, the authors concluded that the system $\text{CO}_2\text{-N}_2$ in PCOD8200029 exhibits a normal site preference, that is, both components present in the mixture will occupy the adsorption sites in the same order. The mixture $\text{CO}_2\text{-C}_3\text{H}_8$, however, exhibits a reverse site preference, that is, one component will occupy the adsorption sites in a reverse order compared to the other component.

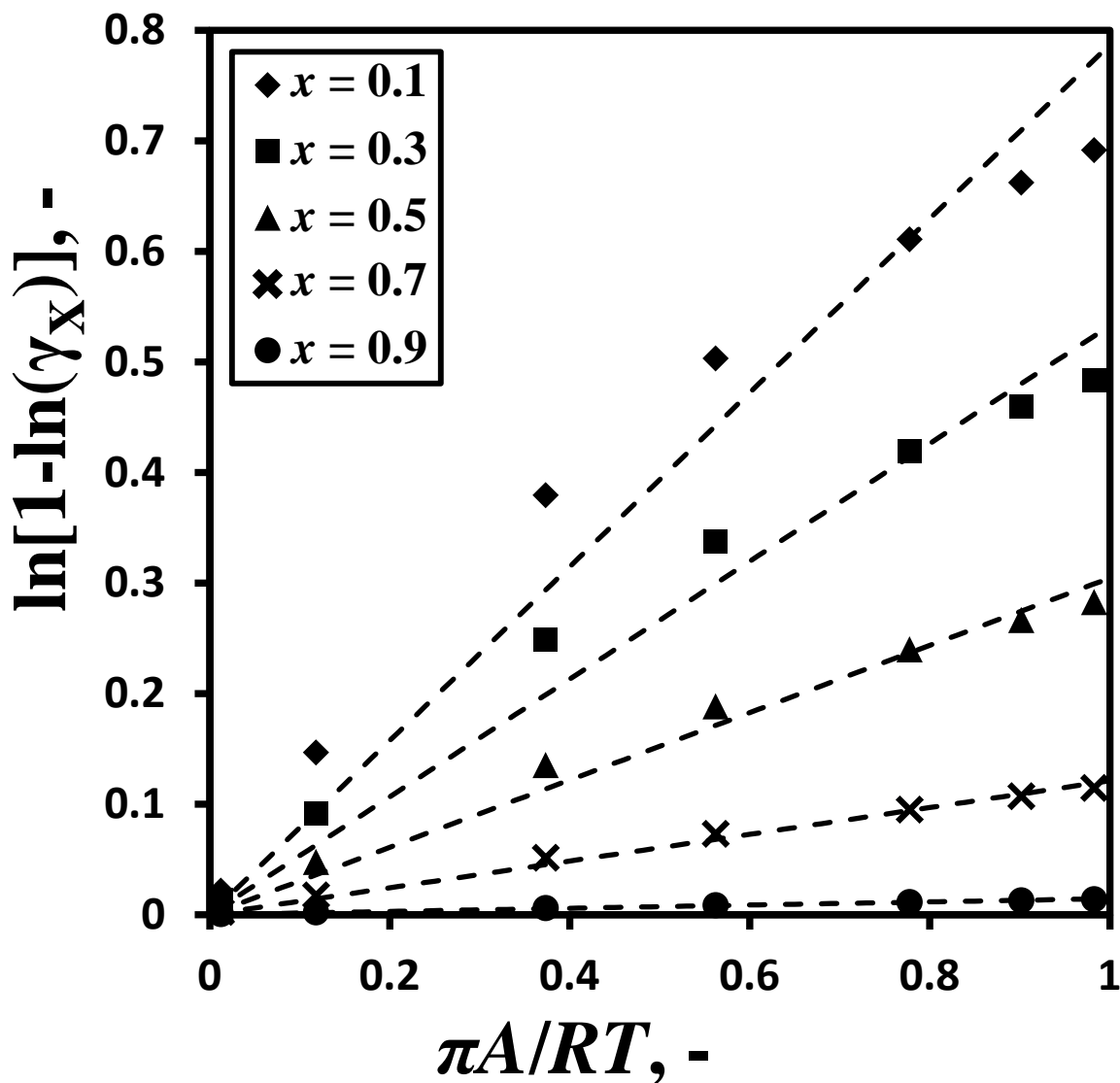


Figure 3.7. Spreading pressure dependency of adsorbed phase activity coefficient of compound X at different mole fractions (x). The error bars are smaller than the symbol size. Symbols - 2D-lattice simulations for the mole fractions given in the legend, lines - fit using Eq. 3.18. The parameters used in the 2D-lattice simulations are listed in Table B1 (Appendix B).

Materials with isolated adsorption sites and normal site preference. Swisher and co-workers [27] showed that there are two distinct adsorption sites for CO₂ and N₂ in PCOD8200029. Therefore, we parameterized the 2D-lattice model by fitting the pure component isotherms of CO₂ and N₂ from the work of Swisher and co-workers [27] on two distinct adsorption sites. To simplify the parameterization procedure described in section 3.3.2, the pure component isotherms of CO₂ and N₂ were fitted using the dual-site (DS) Langmuir equation. Using the DS Langmuir fit, adsorption data was generated for each compound on each adsorption site and the 2D-lattice model was parameterized using the generated data. For this specific case, the parameters required

to simulate the binary mixture CO₂-N₂ using the 2D-lattice model are: the interaction parameter between CO₂ molecules, $w_{\text{CO}_2-\text{CO}_2}$, the interaction parameter between N₂ molecules, $w_{\text{N}_2-\text{N}_2}$, the interaction parameter between CO₂ molecules and N₂ molecules, $w_{\text{CO}_2-\text{N}_2}$, the interaction parameter between CO₂ molecules and the lattice surface for site 1, $w_{\text{CO}_2-\text{S}_1}$, the interaction parameter between CO₂ molecules and the lattice surface for site 2, $w_{\text{CO}_2-\text{S}_2}$, the interaction parameter between N₂ molecules and the lattice surface for site 1, $w_{\text{N}_2-\text{S}_1}$ and the interaction parameter between N₂ molecules and the lattice surface for site 2, $w_{\text{N}_2-\text{S}_2}$. The cross interaction parameters between unlike molecules are approximated from the like parameters using a geometric mean:

$$w_{XY} = \sqrt{w_{XX} \cdot w_{YY}} \quad (3.20)$$

Figs. B7 and B8 (Appendix B) show the pure-component adsorption isotherms of CO₂ and N₂ respectively in PCOD8200029 for the two distinct adsorption sites, along with the fit using the parameterized 2D-lattice code. The values obtained for the 2D-lattice parameters are listed in Table B2 (Appendix B). As can be seen, the 2D-lattice model fits the pure-component data of CO₂ and N₂ in PCOD8200029 well.

The result for the binary mixture is presented and compared to SIAST predictions in Fig. 3.8. The predictions of the segregated 2D-lattice model are identical to the predictions of SIAST. It appears that for systems exhibiting normal site preference, the performance of the segregated 2D-lattice model is similar to that of the SIAST model.

Materials with isolated adsorption sites and reverse site preference. As shown by Swisher and co-workers [27], there are two distinct adsorption sites for the system CO₂-C₃H₈ in MOR. The authors concluded that the compounds have a reverse site preference in MOR, that is, at low fugacity, C₃H₈ occupies the main channels while CO₂ resides in the side pockets of MOR. At high fugacity however, CO₂ competes for the main channels with C₃H₈ [27]. In order to obtain a good prediction with SIAST, Swisher and co-workers [27] reversed the sense of the two sites in the isotherms of CO₂ and C₃H₈ such that the first site in the CO₂ isotherm competes with the second site in the C₃H₈ isotherm and vice versa.

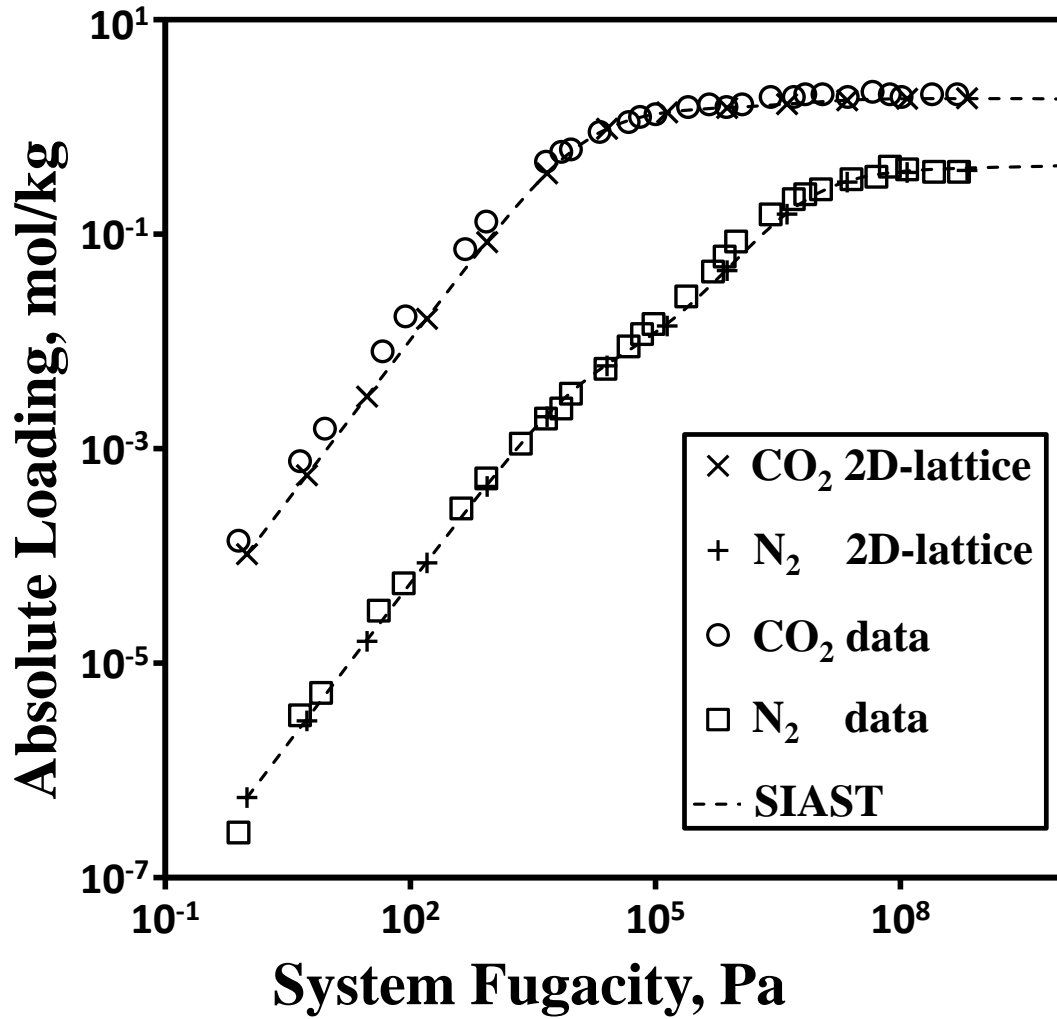


Figure 3.8. Binary adsorption isotherm for a 14% CO₂, 86% N₂ mixture in PCOD8200029. Circles and squares - GCMC simulation data of Swisher and co-workers [27], crosses - 2D-lattice simulation predictions, lines - SIAST predictions. The system fugacity is defined as the sum of partial fugacities of the two components.

In our application of the 2D-lattice model, no site reversal can be observed. The 2D-lattice model was parameterized by fitting the pure component isotherms of CO₂ and C₃H₈ on two distinct adsorption sites. For this specific case, the parameters required to simulate the binary mixture CO₂-C₃H₈ using the 2D-lattice model are: the interaction parameter between CO₂ molecules, $w_{\text{CO}_2-\text{CO}_2}$, the interaction parameter between C₃H₈ molecules, $w_{\text{C}_3\text{H}_8-\text{C}_3\text{H}_8}$, the interaction parameter between CO₂ molecules and C₃H₈ molecules, $w_{\text{CO}_2-\text{C}_3\text{H}_8}$, the interaction parameter between CO₂ molecules and the lattice surface for site 1, $w_{\text{CO}_2-\text{S1}}$, the interaction parameter between CO₂ molecules and the lattice surface for site 2, $w_{\text{CO}_2-\text{S2}}$, the interaction parameter between C₃H₈ molecules and the lattice surface for site 1, $w_{\text{C}_3\text{H}_8-\text{S1}}$ and the interaction parameter between C₃H₈ molecules and the lattice surface for site 2, $w_{\text{C}_3\text{H}_8-\text{S2}}$.

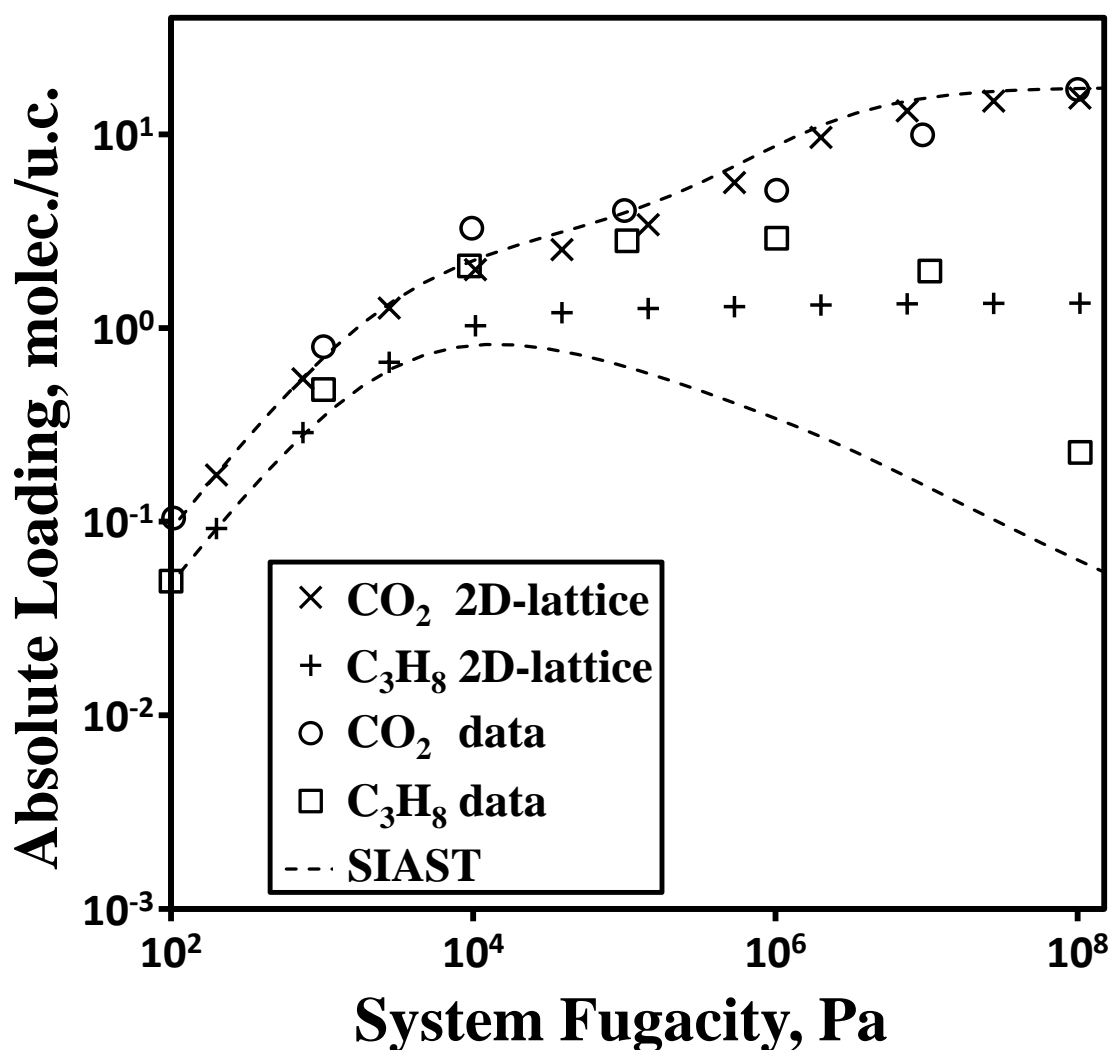


Figure 3.9. Binary adsorption isotherm for a 50% CO₂, 50% C₃H₈ mixture in MOR. Circles and squares - GCMC simulation data of Swisher and co-workers [27], crosses - 2D-lattice simulation predictions, lines - SIAST predictions. The system fugacity is defined as the sum of partial fugacities of the two components.

The cross interaction parameters between unlike molecules were approximated from the like parameters using Eq. 3.20. To simplify the parameterization procedure described in section 3.3.2, the pure component isotherms of CO₂ and C₃H₈ were fitted using the dual-site Langmuir (DSL) equation. Using the DSL fit, adsorption data was generated for each compound on each adsorption site and the 2D-lattice model was parameterized using the generated data. Figs. B9 and B10 (Appendix B) show the pure component adsorption isotherms of CO₂ and C₃H₈ respectively in MOR for the two distinct adsorption sites, along with the fit using the parameterized 2D-lattice model. The values obtained for the 2D-lattice parameters are listed in Table B3 (Appendix B). As can be seen, the 2D-lattice model fits the pure component data of CO₂ and C₃H₈ in MOR well.

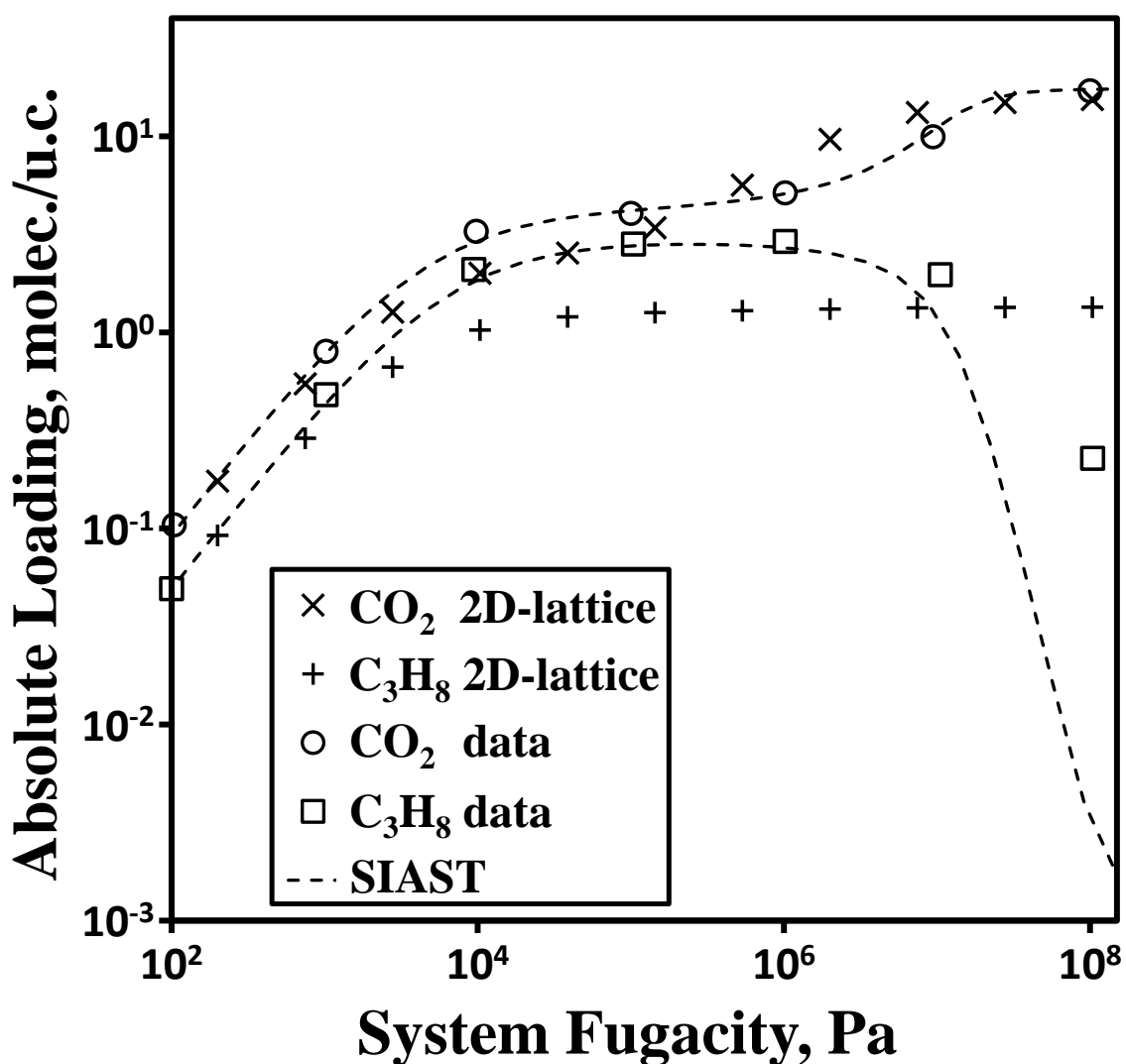


Figure 3.10. Binary adsorption isotherm for a 50% CO₂, 50% C₃H₈ mixture in MOR. Circles and squares - GCMC simulation data of Swisher and co-workers [27], crosses - 2D-lattice simulation predictions, lines - SIAST predictions with reversal of site preference (as explained in the main text). The system fugacity is defined as the sum of partial fugacities of the two components.

Using the parameterized 2D-lattice model, the 50% CO₂ – 50% C₃H₈ binary mixture was simulated. The comparison of the segregated 2D-lattice predictions and SIAST with no site inversion and the raw data of Swisher are presented in Fig. 3.9. The performance of the two models is similar. The 2D-lattice model does not predict a decrease in the C₃H₈ loading, most probably due to limitations of the 2D-lattice model. The comparison of the 2D-lattice predictions with SIAST predictions for reverse site preference is shown in Fig. 3.10. The SIAST predictions are accurate up to the high fugacity regime.

The reversal of site preference as discussed in detail by Moon and co-workers [87], Ritter and co-workers [88] and Swisher and co-workers [27] requires prior knowledge of adsorption behavior for the studied mixture. For predictive purposes, if the reverse site preference cannot be foreseen, the performance of the segregated 2D-lattice model is reasonable and comparable to SIAST.

3.5 Conclusions

The accuracy of the Wilson and NRTL models towards evaluating adsorbed phase activity coefficients was tested using a 2D-lattice model. We showed that the commonly used Wilson and NRTL models cannot describe the adsorbed phase activity coefficients for slightly non-ideal to strong non-ideal mixtures. Until new models for adsorbed phase activity coefficients are developed, one should use the models borrowed from the gas-liquid theory with care. We show that the empirical equation proposed by Kopatsis and Myers [46] for correlating the spreading pressure dependency of adsorbed phase activity coefficients does not provide accurate results. Additional effort is required for developing new models to account for the spreading pressure dependency of activity coefficients.

In the second part of this chapter, we used Monte Carlo simulations with a segregated 2D-lattice model to predict adsorption of mixtures. The segregated model assumes that the competition for adsorption occurs at isolated adsorption sites and the molecules from each adsorption site interact with the bulk phase independently. For systems with normal site preference, the precision of the segregated 2D-lattice model is comparable to the SIAST model. For systems with reverse site preference and prior knowledge of adsorption behavior, the SIAST model provides a better fit of adsorption data.

The available activity coefficient models cannot accurately describe the adsorbed phase behavior. At the same time, the spreading pressure dependency of adsorbed phase activity coefficients cannot be described using the empirical equation proposed by Kopatsis and Myers [46]. With the models that are currently available for adsorbed-phase activity coefficients, RAST cannot provide accurate predictions.

Chapter 4

Multicomponent Equilibrium and Breakthrough Adsorption of Volatile Organic Compounds

4.1 Introduction

There are several separation processes used in the industry to deal with VOCs separation. Recuperative technologies such as distillation and adsorption are preferred over destructive technologies such as incineration and biofiltration [89]. When the boiling points of the fluid components are too close, distillation becomes impractical and other alternative technologies are needed [10]. Adsorption has been widely recognized as an effective separation technology for VOCs removal [13, 15, 31, 47, 90].

The design of adsorption separation units depends mainly on the adsorbent capacity at equilibrium conditions [80]. The performance of such units is determined by the competitive adsorption of the different compounds simultaneously present in the bulk (gas or liquid) solution [19]. Therefore, the assessment of the adsorption capacity of a compound in the presence of other solutes, as well as the definition of appropriate theoretical models for predicting the adsorption behavior of multicomponent mixtures is imperative for a proper design of adsorption processes [19].

Throughout the years, various studies were published which treat the removal of VOCs using adsorption [90-94]. Studies of multicomponent systems, containing three or more components, are very important as most industrial separations involve a large number of components [10]. In addition, multicomponent adsorption data are considerably more difficult to measure than pure component data [13]. Santacesaria et al. [91] modelled the breakthrough of a five component mixture of xylenes on a Y zeolite bed using the multicomponent Langmuir equation for the calculation of adsorption equilibrium. These authors obtained good agreement between experimental and calculated breakthrough curves. Ahmad et al. [92] successfully modelled the breakthrough curves of a ternary mixture of complex organic solutes on granular activated carbon using the Freundlich isotherm together with the Ideal Adsorbed Solution Theory (IAST) for the calculation of multicomponent equilibrium. The diffusivities of each compound present in the mixture were fitted to the experimental breakthrough curves. Yun et al. [90] studied the dynamics of a ternary vapor mixture comprising toluene, benzene and p-xylene on an activated carbon bed using the multicomponent Langmuir and the Langmuir-IAST models for the calculation of adsorption equilibrium. The authors fitted a lumped mass transfer coefficient on pure and binary breakthrough curves to improve the model predictions. Sulaymon and Ahmed [93] studied the breakthrough curves of an aqueous solution containing furfural, phenol and para-chlorophenol. The authors used the multicomponent Langmuir equation to calculate the adsorption equilibrium and obtained an accurate description of the adsorption process for the furfural and phenolic compounds in a fixed adsorption bed. Silva et al. [95] studied the adsorption of a mixture containing

C₈ isomers (p-xylene, o-xylene, m-xylene and ethylbenzene) on a Ba-exchanged faujasite-type zeolite. Using the multicomponent Langmuir equation to calculate the adsorption equilibrium, the authors obtained a satisfactory agreement between simulated and experimental breakthrough curves without the need of fitting any model parameters.

In this chapter, the adsorption of traces of five volatile organic compounds comprising butanal (Bt), 2-ethyl-2-hexenal (2E2H), 2,6-dimethylcyclohexanone (dMc), 2,4,6-trimethylphenol (3Mp), and 2,4,6-trimethylanisole (3Ma) present in liquid toluene (Tol) was investigated. The first goal of this work was to find the best performing multicomponent equilibrium model for the chosen system. Therefore, binary (impurity-toluene) and multicomponent (six component mixture) equilibrium batch adsorption experiments onto an ammonium form of Y zeolite were performed to determine which equilibrium model works best for this system. Four equilibrium models were parameterized using binary equilibrium experimental data: the multicomponent Langmuir model, the multicomponent dual-site Langmuir model, the coupled IAST – dual site Langmuir model (IAST-DSL) and the coupled Segregated Ideal Adsorbed Solution Theory [27] – Langmuir model (SIASL-L). The accuracy of the parameterized equilibrium models was validated using multicomponent (six-component) equilibrium experiments. The best performing equilibrium models were used in a dynamic model for the prediction of breakthrough curves. The predicted breakthrough curves are compared to experimental breakthrough curves.

This remainder of this chapter is organized as follows. The experimental procedure followed for performing equilibrium and dynamic column experiments is explained in section 4.2. The equilibrium models, the parameterization of the equilibrium models along with the dynamic model used to obtain multicomponent breakthrough curves are explained in section 4.3. The results of the parameterization of equilibrium models, the performance of the equilibrium models towards predicting the adsorption behavior of a six-component mixture, along with the predicted and experimental breakthrough curves are presented in section 4.4. Our findings are summarized in section 4.5.

4.2 Experimental section

4.2.1 Chemicals and adsorbents.

Toluene (99.99 % anhydrous), 2,6-dimethylcyclohexanone (mixture of isomers, 98 %) and 2,4,6-trimethylphenol (99 %) were obtained from Sigma-Aldrich Chemie B.V., Netherlands; 2-ethyl-2-hexenal (+96 %) was purchased from Fluorochem Limited (UK) and 2,4,6-trimethylanisole (98 %) was purchased from Apollo Scientific (UK).

Table 4.1. Characteristics of the fixed bed column.

| Adsorbent | Ammonium form of Y zeolite |
|---|----------------------------|
| Column useful length, L (cm) | 5.4 |
| Column useful diameter, D_c (cm) | 1 |
| Bulk porosity [96], ε | 0.45 |
| Particle porosity, ε_p | 0.31 |
| Particle apparent density [97], ρ_p (g/cm ³) | 1.48 |
| Adsorbent particle radius, R_p (mm) | 0.12 |

The ammonium form of Y zeolite (CBV500) was purchased from Zeolyst International. For the sake of simplicity, throughout the chapter we will use the term zeolite Y (or Y zeolite) when referring to the ammonium form of zeolite Y.

4.2.2 Equilibrium experiments.

The zeolite Y samples were added to 20 ml vials and heated overnight in an oven at 500 °C, under nitrogen flow, in order to remove any water and impurities present in the pores. The vials were cooled to around 70 °C and, while keeping the nitrogen flow running, the stirrers were added to the bottles and the caps were placed on the bottles to avoid water adsorption on the samples. After regeneration, the vials were immediately sealed to avoid water uptake and weighted. For the binary experiments, the solution comprising traces of either butanal, 2-ethyl-2-hexenal, 2,6-dimethylcyclohexanone, 2,4,6-trimethylphenol or 2,4,6-trimethylanisole in liquid toluene, was injected through the septum into the vials and part of the solution was analyzed as a blank. In the measurement of the six-component mixture, the six-component solution was injected through the septum into the vials and part of the solution was analyzed as a blank. The test vials were stirred continuously at room temperature (25 °C) and samples were collected after 1, 2, and 3 days to ensure that the equilibrium was reached. The samples and blanks were analyzed using a Varian 430 gas chromatograph (GC). A CPSIL8 CB column was used to determine the composition of all blanks and samples. The amount adsorbed at equilibrium was calculated using the mass balance equation:

$$q_i = \frac{wt_{\text{blank},i} \cdot M_{L,0} - wt_{\text{sample},i} \cdot M_{L,A}}{m_{\text{adsorbent}}} \quad (4.1)$$

where $wt_{\text{blank},i}$ is the mass fraction of the i -th component in the blank, $wt_{\text{sample},i}$ is the mass fraction of the i -th component in the solution after adsorption, $m_{\text{adsorbent}}$ is the mass of adsorbent (grams) and $M_{L,0}$ is the mass of fresh solution (grams). The mass of solution after adsorption is calculated as:

$$M_{L,A} = M_{L,0} - 0.31 \cdot m_{\text{adsorbent}} \cdot \rho_{\text{ad.phase}} \quad (4.2)$$

Eq. 4.2 is used to correct for the change of mass in the external liquid phase due to the adsorbent uptake. There is no accurate experimental procedure for measuring the adsorbed phase mass of solution. A common practice is to assume that the density of the adsorbed phase ($\rho_{\text{ad.phase}}$) is equal to the density of the solution (which approximately equals the density of the solvent) [49]. A specific void volume of 0.31 l/g for the Y zeolite was assumed in this work [50]. The loading of the impurity compounds is not sensitive to the void fraction. By varying the void fraction of the adsorbent from 0.2 to 0.4, deviations below 1% in the impurity loadings are obtained. These assumptions allow for the calculation of the mass of liquid in the adsorbed phase.

4.2.3 Breakthrough Experiments.

The adsorption runs were performed at room temperature (25 °C) using an adsorption column (whose characteristics are summarized in Table 4.1) filled with zeolite Y powder. To obtain the zeolite Y powder with a desired particle radius of 120 μm , the supplied powder was compressed into pills, grinded and sieved to the desired particle size. The column, filled with zeolite powder, was placed in an oven where nitrogen was flushed through the column at a temperature of 250 °C for 24 hours. The column was weighted before and after this procedure to ensure a 19% weight loss of the adsorbent (corresponding to the complete elimination of water). A diaphragm dosing pump with integrated flowmeter and pulsation damper (from KNF Verder BV) was used to pump the six-component solution through the column at a constant flowrate of 10 cm^3/min . The experimental breakthrough curves were constructed by analyzing (using the same GC and chromatographic column as for the equilibrium experiments) the small samples withdrawn at different times from the column exit.

4.3 Mathematical Models

4.3.1 Equilibrium Models.

Four equilibrium models were parameterized using binary adsorption experiments obtained as explained in section 4.2: the multicomponent Langmuir and dual-site Langmuir, the coupled IAST - dual-site Langmuir and the coupled SIAST - Langmuir models.

Toluene was the solvent in all the binary experimental data. Therefore, the multicomponent model parameters were fitted to the binary experimental data simultaneously, using the non-linear least square minimization routine of Matlab with

a relative tolerance of 10^{-8} in the loadings. The objective function used for the minimization was:

$$F_{\text{obj}} = \sum_{i=1}^{n_{\text{odp}}} \left(\frac{q_i^{\text{exp}} - q_i^{\text{model}}}{q_i^{\text{model}}} \right)^2 \quad (4.3)$$

where n_{odp} represents the number of data points, q_i^{exp} the experimental loadings and q_i^{model} the loadings from the equilibrium model.

4.3.1.1 Multicomponent Langmuir model.

As shown in section 4.1 of this chapter, for simulating the dynamics of an adsorption process, the most common model used by authors to calculate multicomponent adsorption equilibrium is the multicomponent Langmuir isotherm:

$$q_{Li}^* = \frac{q_{mi} k_i C_i}{1 + \sum_{j=1}^{NC} k_j C_j} \quad (4.4)$$

where q_{mi} are the saturation capacities (mol/kg of adsorbent), k_i are the Langmuir affinity constants (m^3/mol), C_i the bulk liquid concentration of component i (mol/m^3) and NC the number of components present in the mixture. The model can be used to predict multicomponent adsorption data from pure isotherm data.

4.3.1.2 Multicomponent Dual-Site Langmuir (MDSL) model.

Mathias et al. [29] was the first to use the binary form of the MDSL model for predicting the binary adsorption equilibria of oxygen and nitrogen on 5A zeolite. The MDSL equation used to calculate the equilibrium loading for component i in a multicomponent system can be written as:

$$q_{\text{MDSL}i}^* = \frac{q_{m1i} k_{1i} C_i}{1 + \sum_{j=1}^{NC} k_{1j} C_j} + \frac{q_{m2i} k_{2i} C_i}{1 + \sum_{j=1}^{NC} k_{2j} C_j} \quad (4.5)$$

where q_{m1i} and q_{m2i} are the saturation capacities (mol/kg of adsorbent) for site 1 and 2 respectively, and k_{1i} and k_{2i} are the MDSL affinity constants for site 1 and 2 respectively (m^3/mol). The saturation capacities and the affinity constants were fitted simultaneously to the binary experimental data using the fitting procedure described in section 4.3.1.

4.3.1.3. Coupled IAST-DSL model.

The Ideal Adsorbed Solution Theory (IAST) was derived by Myers and Prausnitz [21] for a two-dimensional homogenous adsorbed phase. The adsorbed phase is considered as a temperature-invariant area equally accessible to all compounds (the so-called spreading pressure). The main assumption of IAST is that the adsorbed mixture forms an ideal solution in equilibrium with the bulk (gas or liquid) phase at a constant spreading pressure for each solute [21]. The spreading pressure of a solute is an intensive thermodynamic variable for adsorption equilibria; it is defined as the difference between the interfacial tension of the pure solvent-solid interface and that of the solution-solid interface [10]. A summary of the equations used in the IAST model can be found in Chapter 2 (section 2.3.2).

The non-ideality of the liquid phase is expressed by fugacity coefficients of the compounds in the liquid phase mixture, $\hat{\phi}_i$. The fugacity coefficients were computed using the Peng-Robinson equation of state (Appendix C, Eqs. C.1-C.12).

The saturation capacities and the affinity constants of the dual-site Langmuir equation are the fitting parameters for the coupled IAST-DSL model. The fitting procedure is explained in section 4.3.1.

4.3.1.4. Coupled SIAST-Langmuir model (SIAST-L).

As shown by Swisher and co-workers [27], by assuming that competition for adsorption occurs at isolated adsorption sites and molecules from each adsorption site interact with the bulk phase independently, one can apply IAST to each adsorption site to calculate the adsorption equilibrium. This approach is called the Segregated Ideal Adsorbed Solution Theory, SIAST. More details on the SIAST model can be found in Chapter 3 of this thesis or in the work of Swisher and co-workers [27]. The SIAST model provides a significant improvement of IAST predictions with just a few simple assumptions.

In this work, two adsorption sites are considered. Therefore, Eqs. 2.3-2.6 together with the Langmuir equation were applied to each adsorption site. The overall total loading for each compound present in the mixture is simply the sum of the loading obtained for each individual adsorption site. The Langmuir parameters for each adsorption site are the fitting parameters for the coupled SIAST-Langmuir model.

4.3.2 Breakthrough Model.

The multicomponent column breakthrough model, developed for isothermal conditions, is a constant-velocity, axially dispersed, plug-flow model, with all mass

transfer resistances lumped under the form of a linear driving force (LDF) [98-101] expressed in terms of fluid phase concentrations. The radial concentration gradients are neglected. It is assumed that there is no pressure drop along the column. A mass balance for the i -th component can be written as [10,91]:

$$\frac{\partial C_i}{\partial t} + \frac{u \partial C_i}{\partial z} + \frac{3\rho_p}{R_p} \frac{1-\varepsilon}{\varepsilon} k_{g,i} (q_i^* - \bar{q}_i) = D_{ax,i} \frac{\partial^2 C_i}{\partial z^2} \quad (4.6)$$

where z and t are the spatial and respectively time dimensions, C_i the bulk liquid concentration of component i (mol/m³), u (m/s) is the interstitial fluid velocity, ρ_p is the particle density (g/cm³), $D_{ax,i}$ (m²/s) is the axial dispersion coefficient of component i in the mobile phase, ε is the bulk porosity, q_i^* (mol component/kg adsorbent) is the adsorbed concentration of component i in equilibrium with the interparticle fluid with composition C_i , \bar{q}_i (mol component/kg adsorbent) is the average loading inside the adsorbent particle, and $k_{g,i}$ is the lumped mass transfer coefficient (m/s).

The overall mass transfer coefficient is calculated as [95]:

$$\frac{1}{k_{g,i}} = \frac{1}{k_{ext,i}} + \frac{1}{\varepsilon_p k_{int,i}} \quad (4.7)$$

where $k_{ext,i}$ (m/s) and $k_{int,i}$ (m/s) are the external and respectively internal mass transfer coefficients and ε_p is the particle porosity. The internal mass transfer coefficient is calculated as [91]:

$$k_{int,i} = \frac{5D_{mi}}{\tau R_p} \quad (4.8)$$

where D_{mi} (m²/s) is the molecular diffusivity and τ is the tortuosity factor calculated as [102]:

$$\tau = \frac{1}{\varepsilon_p} \quad (4.9)$$

The molecular diffusivities in the liquid phase were estimated using the Wilke-Chang method extended to mixtures by Perkins and Geankoplis [103, 104]:

$$D_{mi} = \frac{7.4 \cdot 10^{-8} (\bar{\theta} \bar{M}_{mi})^{1/2} T}{\eta_m V_{bi}^{0.6}} \quad (4.10)$$

$$\bar{\theta} \bar{M}_{mi} = \sum_{j=1}^{NC} y_j \theta_j M_j - y_i \theta_i M_i \quad (4.11)$$

where y_i is the mole fraction of compound i , M_i is the molar mass of compound i , η_m is the viscosity of the mixture (cP) and V_{bi} is the molar volume of compound i at the normal boiling point (cm^3/mole). The association factor (θ) is 2.6 for water, 1.9 for methanol, 1.5 for ethanol and 1 if unassociated [104].

The external mass transfer coefficient was estimated using the Wilson and Geankoplis correlation [10]:

$$Sh = 1.09\varepsilon^{-1}Re^{0.33}Sc^{0.33} \quad (4.12)$$

where $Sh = 2k_{\text{ext}}R_pD_m$ is the Sherwood number, $Re = 2\rho uR_p/\mu$ is the Reynolds number and $Sc = \mu/(\rho D_m)$ is the Schmidt number; the correlation is valid for $0.0015 < Re < 55$.

The pure component boiling points and saturated liquid densities at 298 K were taken from the literature [70]. Values and references for critical temperatures, critical pressures and acentric factors are listed in appendix A (Table A9). Except for toluene [70], the critical volumes were estimated using the method of Joback [104]. The saturated molar volumes at the boiling temperature (necessary for calculating D_m) were estimated using the method of Yamada and Gunn [104]. The liquid viscosities for Bt, 3Mp and Tol were taken from the literature [70]. For 2E2H, dMc and 3Ma, the liquid densities were estimated using the method of Orrick and Erbar [104]. The molar volume for the feed mixture was estimated using the method of Chueh and Prausnitz [105] and the mixture viscosity (necessary for calculating D_m) was estimated using the method of Grunberg and Nissan [104]. The axial dispersion coefficient, D_{axi} , was estimated using the correlation of Edwards and Richardson [10].

The boundary conditions for the adsorption breakthrough at $z = 0$ and L , and for $t > 0$ can be written as [91,95]:

$$z = 0, \quad u(C_{fi} - C_i) = -D_{\text{axi}} \frac{\partial C_i}{\partial z} \quad \text{and} \quad u = \frac{F}{A\varepsilon} \quad (4.13)$$

$$z = L, \quad \frac{\partial C_i}{\partial z} = 0 \quad (4.14)$$

where F (m^3/s) is the feed flowrate, A (m^2) is the cross-sectional area of the column and C_{fi} is the feed concentration of component i .

The initial conditions are:

$$C_i(0, z) = 0 \quad \text{and} \quad q(0, z) = 0 \quad (4.15)$$

To describe the adsorption equilibrium (calculation of q_i^*) we used the models described in section 4.3.1 of this chapter. The system of partial differential equations was reduced to a system of ordinary differential equations in time by discretization of the axial domain using finite difference approximations. The resulting system of implicit ordinary differential and algebraic equations that define the fixed-bed breakthrough model were solved using the *ode15i* solver of Matlab with an absolute error tolerance of 10^{-6} . This tolerance applies to time-derivatives of concentrations (in units of mol/m^3) and loadings (in units of mol/kg).

4.4 Results and discussion

4.4.1 Performance of equilibrium models.

The first goal of this study was to determine which equilibrium model can best predict multicomponent adsorption data for the chosen system. Therefore, four equilibrium models were fitted to binary experimental data toluene-impurity as explained in section 4.3.1. As mentioned earlier, the Langmuir parameters for toluene resulting from fitting the multicomponent Langmuir model to the binary data toluene-impurity have to be the same for all the binary systems. Therefore, the equilibrium models were fitted to all the binary data simultaneously as explained before. Fig. 4.1 shows the binary experimental data for the mixture toluene-butanal, together with the multicomponent Langmuir fit. It is clear that the multicomponent Langmuir model cannot describe the binary experimental data properly. Similar fitting results for the other binary systems for the multicomponent Langmuir model are obtained (Appendix C, Figs. C1-C4). On the other hand, the multicomponent dual-site Langmuir model provides good overall fits of the binary experimental data. Fig. 4.2 shows the results for the system toluene-2,4,6-trimethylphenol. The quality of the fits obtained for the other binary mixtures is similar (Appendix C, Figs. C5-C8).

The more complex coupled IAST – dual-site Langmuir (IAST-DSL) equilibrium model could not provide an accurate fit of the binary experimental data. As can be seen in Fig. 4.3, the fit for the binary system toluene – 2-ethyl-2-hexenal is far off. The results for the other binary systems are given in Appendix C (Figs. C9-C12) and show comparable results. The coupled SIAST-Langmuir equilibrium model provides a better fit. Fig. 4.4 shows the binary experimental data for the system toluene-2,4,6-trimethylanisole and the corresponding fit with the coupled SIAST-Langmuir equilibrium model. The quality of the fits of the coupled SIAST-Langmuir model for the other binary mixtures is comparable (Appendix C, Figs. C13-C16).

To test the accuracy of the equilibrium models to predict multicomponent adsorption equilibria, four experimental data sets representing the adsorption equilibrium of the

Table 4.2. Relevant parameters used for the simulation of the multicomponent breakthrough curves; global mass transfer coefficients (k_{gi}) and molecular diffusivities (D_{mi}) obtained using Eq. 4.7 and Eq. 4.10 respectively.

| Compound | k_{gi} , m/s | D_{mi} , m ² /s |
|----------|----------------------|------------------------------|
| Bt | $9.12 \cdot 10^{-6}$ | $2.4 \cdot 10^{-9}$ |
| 2E2H | $6.36 \cdot 10^{-6}$ | $1.66 \cdot 10^{-9}$ |
| dMc | $6.67 \cdot 10^{-6}$ | $1.74 \cdot 10^{-9}$ |
| 3Mp | $6.45 \cdot 10^{-6}$ | $1.68 \cdot 10^{-9}$ |
| 3Ma | $5.81 \cdot 10^{-6}$ | $1.51 \cdot 10^{-9}$ |
| Tol | $6.15 \cdot 10^{-7}$ | $1.57 \cdot 10^{-10}$ |

six-component mixture were compared to predicted data from the models. Fig. 4.5 shows the experimental loadings of the six-component mixture vs predicted loadings obtained using the multicomponent Langmuir model. Especially, but not only for the low concentration regime, the multicomponent Langmuir model strongly underestimates the loadings for the impurities, outside the +/- 95% boundary.

The predicted loadings obtained using the multicomponent dual-site Langmuir model are closer to experimental values. As can be seen in Fig. 4.6, the majority of the data lies within the +/- 95% boundary. The coupled IAST - dual-site Langmuir model underestimates most of the multicomponent adsorption data (Appendix C, Fig. C17).

The coupled SIAST - Langmuir model fitted the binary experimental data reasonably well. However, the predicted multicomponent adsorption data is less accurate than the data obtained using the multicomponent dual-site Langmuir model. As can be seen in Fig. 4.7, the model overestimates the loadings for butanal and underestimates the loadings for 2-ethyl-2-hexenal and 2,6-dimethylcyclohexanone at high concentrations.

4.4.2 Multicomponent breakthrough curves.

The multicomponent breakthrough curves were obtained using a feed solution containing traces of butanal, 2-ethyl-2-hexenal, 2,6-dimethylcyclohexanone, 2,4,6-trimethylphenol and 2,4,6-trimethylanisole in toluene (Appendix C, Table C5). Some parameters relevant for the simulation of the multicomponent breakthrough curves are listed in Table 4.2.

The predictions of multicomponent adsorption data obtained with the multicomponent dual-site Langmuir model and the coupled SIAST - Langmuir model are superior to those of the other two models. Therefore, these two models were used in the simulation of the breakthrough curves. Fig. 4.8 shows the experimental multicomponent breakthrough curves and the predicted multicomponent breakthrough

curves obtained using the multicomponent dual-site Langmuir model for calculating the equilibrium isotherms. The elution order predicted by the breakthrough model is in agreement with experimental observations. However, the elution times for 2,4,6-trimethylanisole, 2,6-dimethylcyclohexanone and specially butanal are off.

The experimental multicomponent breakthrough curves and the predicted multicomponent breakthrough curves obtained using the coupled SIAST-Langmuir model are shown in Fig. 4.9. As can be seen, the elution order is not correctly predicted; 2,4,6-trimethylphenol elutes before 2,4,6-trimethylanisole. Moreover, the elution time for butanal is delayed by approximately 1 hour. Overall, the proposed breakthrough model together with the multicomponent dual-site Langmuir model can predict the correct elution order for the components and provide a qualitative description of the multicomponent breakthrough curves.

4.5 Conclusions

Experimental adsorption data for the binary mixtures toluene - butanal, toluene - 2-ethyl-2-hexenal, toluene - 2,6-dimethylcyclohexanone, toluene - 2,4,6-trimethylphenol and toluene - 2,4,6-trimethylanisole on an ammonium form of Y zeolite are presented. These binary experimental data were used for the parameterization of four multicomponent equilibrium models: the multicomponent Langmuir model, the multicomponent dual-site Langmuir model, the coupled IAST - dual-site Langmuir model and the coupled SIAST - Langmuir model. The prediction accuracy of the four equilibrium models was compared to experimental multicomponent equilibrium adsorption data. We show that the multicomponent dual-site Langmuir and the coupled SIAST-Langmuir equilibrium models outperformed the other equilibrium models. For the studied system, the prediction accuracy of the multicomponent dual-site Langmuir model proves to be superior to that of the coupled SIAST-Langmuir model.

A multicomponent breakthrough model was introduced and compared to experimentally obtained multicomponent breakthrough curves. It is shown that, the breakthrough model, together with the multicomponent dual-site Langmuir model (used to calculate the equilibrium isotherms), can provide a very rough qualitative estimation of the breakthrough behavior for the chosen system. The breakthrough model was not fitted to any experimental breakthrough data. As explained in section 4.4.1, most of the pure component and mixture data required to calculate the molecular diffusivities were estimated. The large discrepancy between experimental and simulated data is most likely caused by errors introduced in estimating the molecular diffusivities.

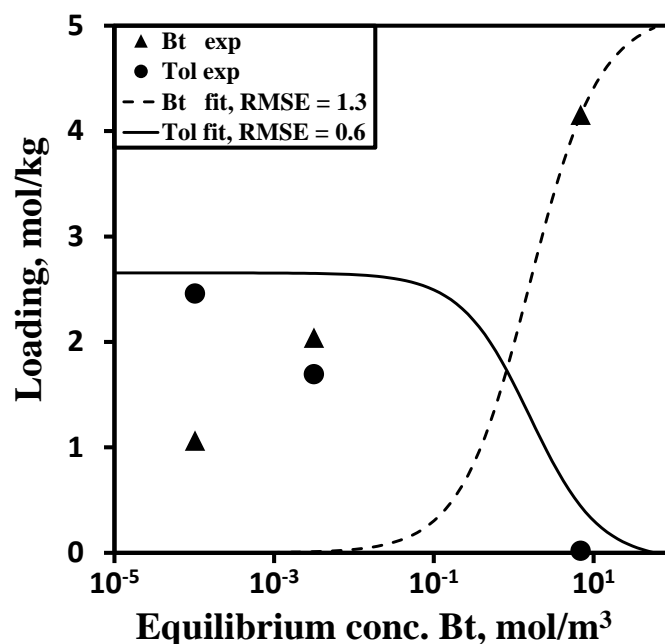


Figure 4.1. Binary adsorption data for the system toluene-butanal. Symbols - experimental data, lines - fit using the multicomponent Langmuir model. RMSE (mol/kg) represents the root mean square error of the fit calculated according to Eq. B4 (Appendix B). The fitted parameters are listed in Table C1 (Appendix C).

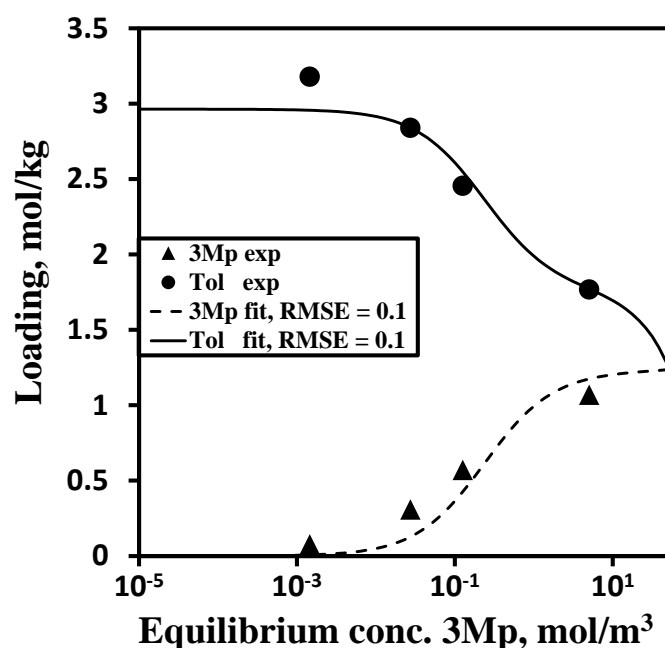


Figure 4.2. Binary adsorption data for the system toluene-2,4,6-trimethylphenol. Symbols - experimental data, lines - fit using the multicomponent dual-site Langmuir model. RMSE (mol/kg) represents the root mean square error of the fit calculated according to Eq. B4 (Appendix B). The fitted parameters are listed in Table C2 (Appendix C).

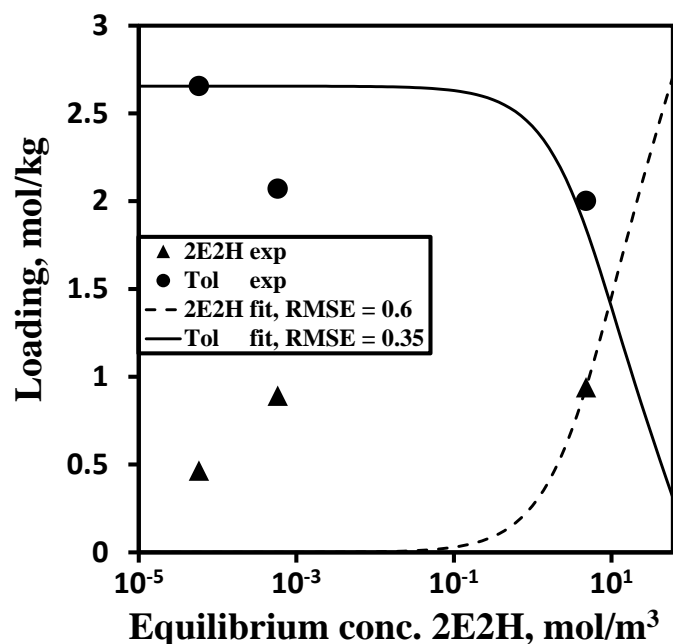


Figure 4.3. Binary adsorption data for the system toluene - 2-ethyl-2-hexenal. Symbols - experimental data, lines - fit using the coupled IAST - dual-site Langmuir model. RMSE (mol/kg) represents the root mean square error of the fit calculated according to Eq. B4 (Appendix B). The fitted parameters are listed in Table C3 (Appendix C).

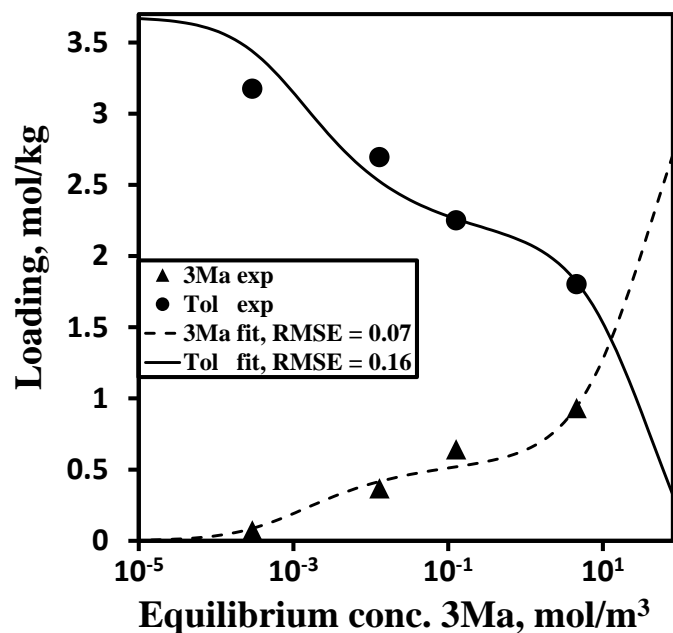


Figure 4.4. Binary adsorption data for the system toluene - 2,4,6-trimethylanisole. Symbols - experimental data, lines - fit using the coupled SIAST - Langmuir model. RMSE (mol/kg) represents the root mean square error of the fit calculated according to Eq. B4 (Appendix B). The fitted parameters are listed in Table C4 (Appendix C).

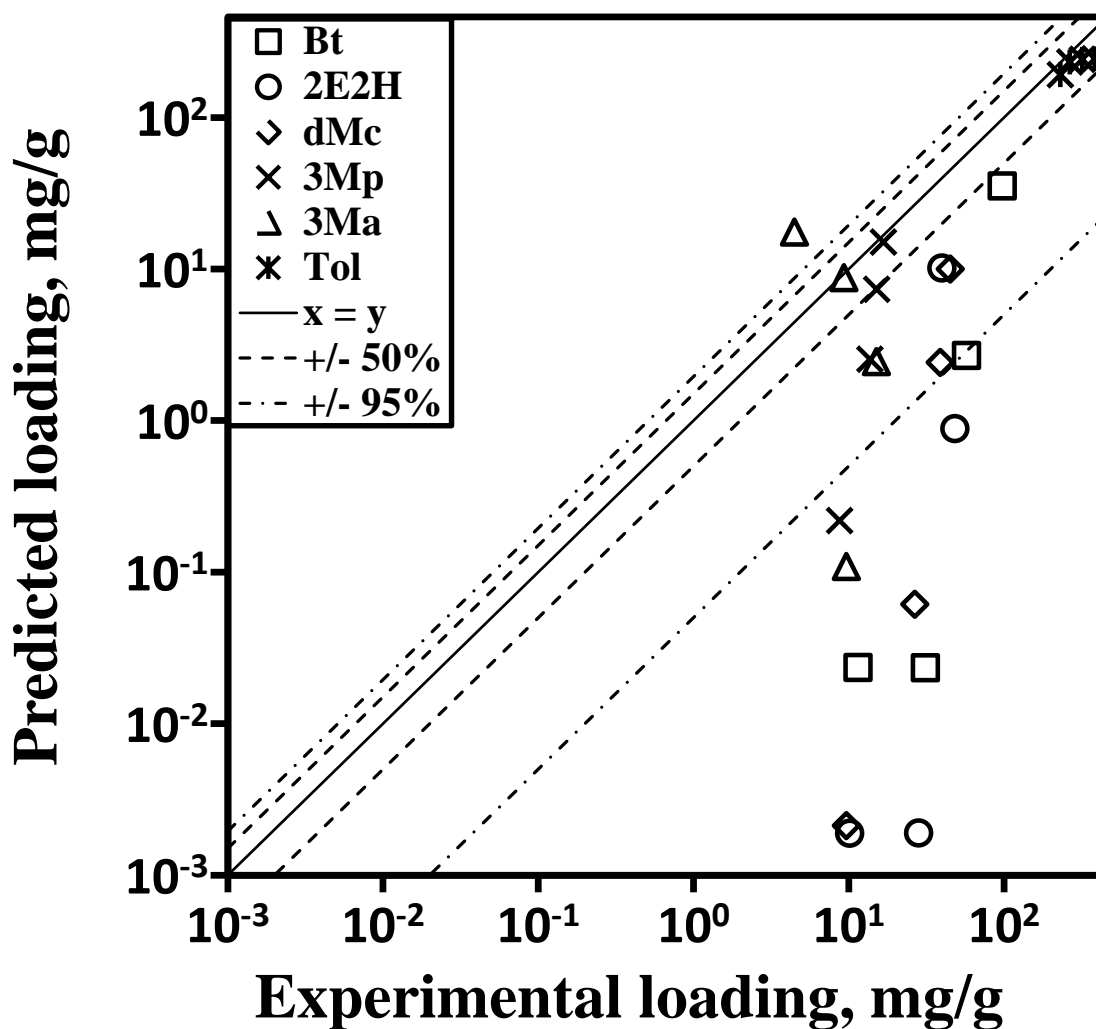


Figure 4.5. Experimental vs predicted multicomponent adsorption isotherms in zeolite Y for impurities in liquid toluene. The predicted data were obtained using the multicomponent Langmuir model. Squares - butanal, circles - 2-ethyl-2-hexenal, diamonds - 2,6-dimethylcyclohexanone, crosses - 2,4,6-trimethylphenol, triangles - 2,4,6-trimethylanisole, stars - toluene. The dashed and dotted lines represent the plus/minus 50% and respectively 90% deviation lines.

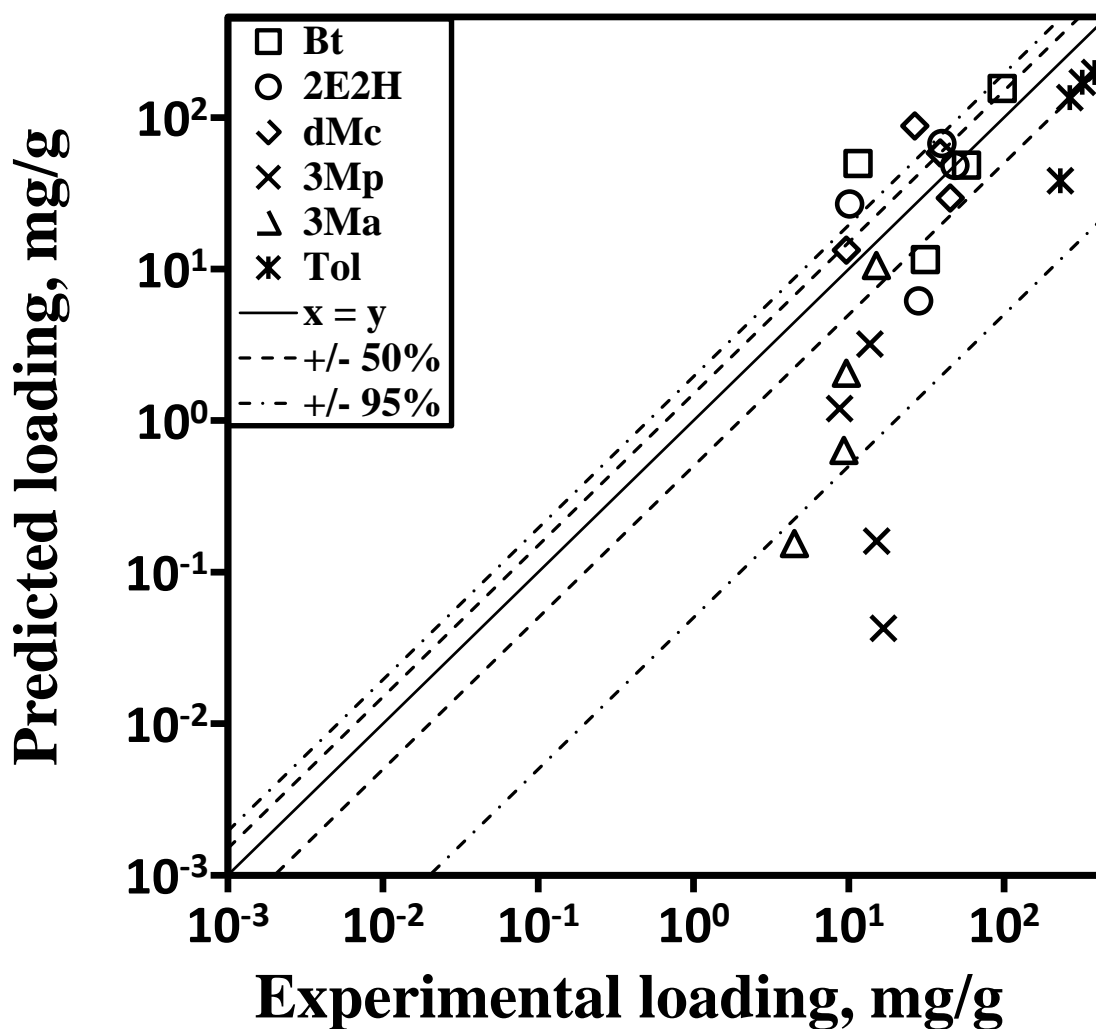


Figure 4.6. Experimental vs predicted multicomponent adsorption isotherms in zeolite Y for impurities in liquid toluene. The predicted data were obtained using the multicomponent dual-site Langmuir model. Squares - butanal, circles - 2-ethyl-2-hexenal, diamonds - 2,6-dimethylcyclohexanone, crosses - 2,4,6-trimethylphenol, triangles - 2,4,6-trimethylanisole, stars - toluene. The dashed and dotted lines represent the plus/minus 50% and respectively 90% deviation lines.

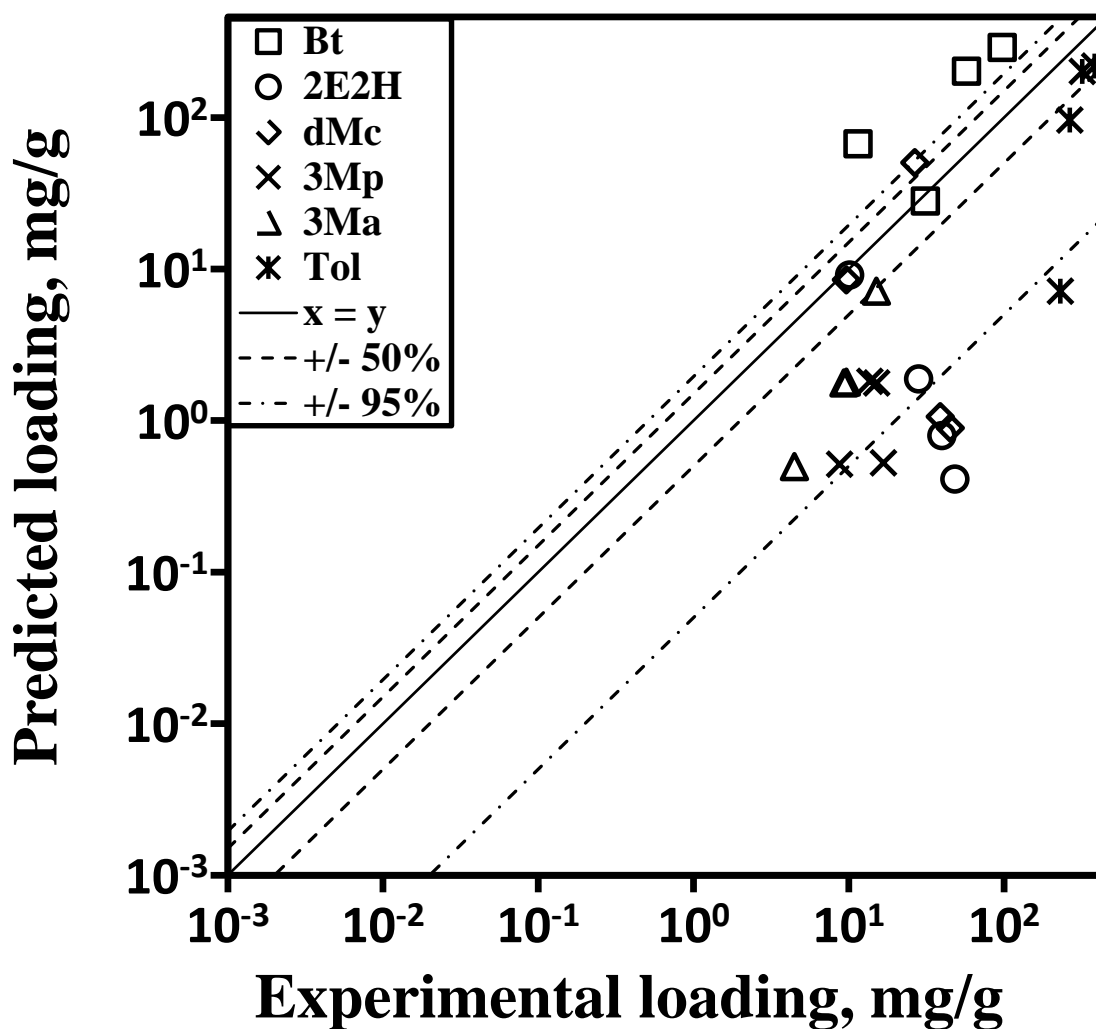


Figure 4.7. Experimental vs predicted multicomponent adsorption isotherms in zeolite Y for impurities in liquid toluene. The predicted data were obtained using the coupled SIAST - Langmuir model. Squares - butanal, circles - 2-ethyl-2-hexenal, diamonds - 2,6-dimethylcyclohexanone, crosses - 2,4,6-trimethylphenol, triangles - 2,4,6-trimethylanisole, stars - toluene. The dashed and dotted lines represent the plus/minus 50% and respectively 90% deviation lines.

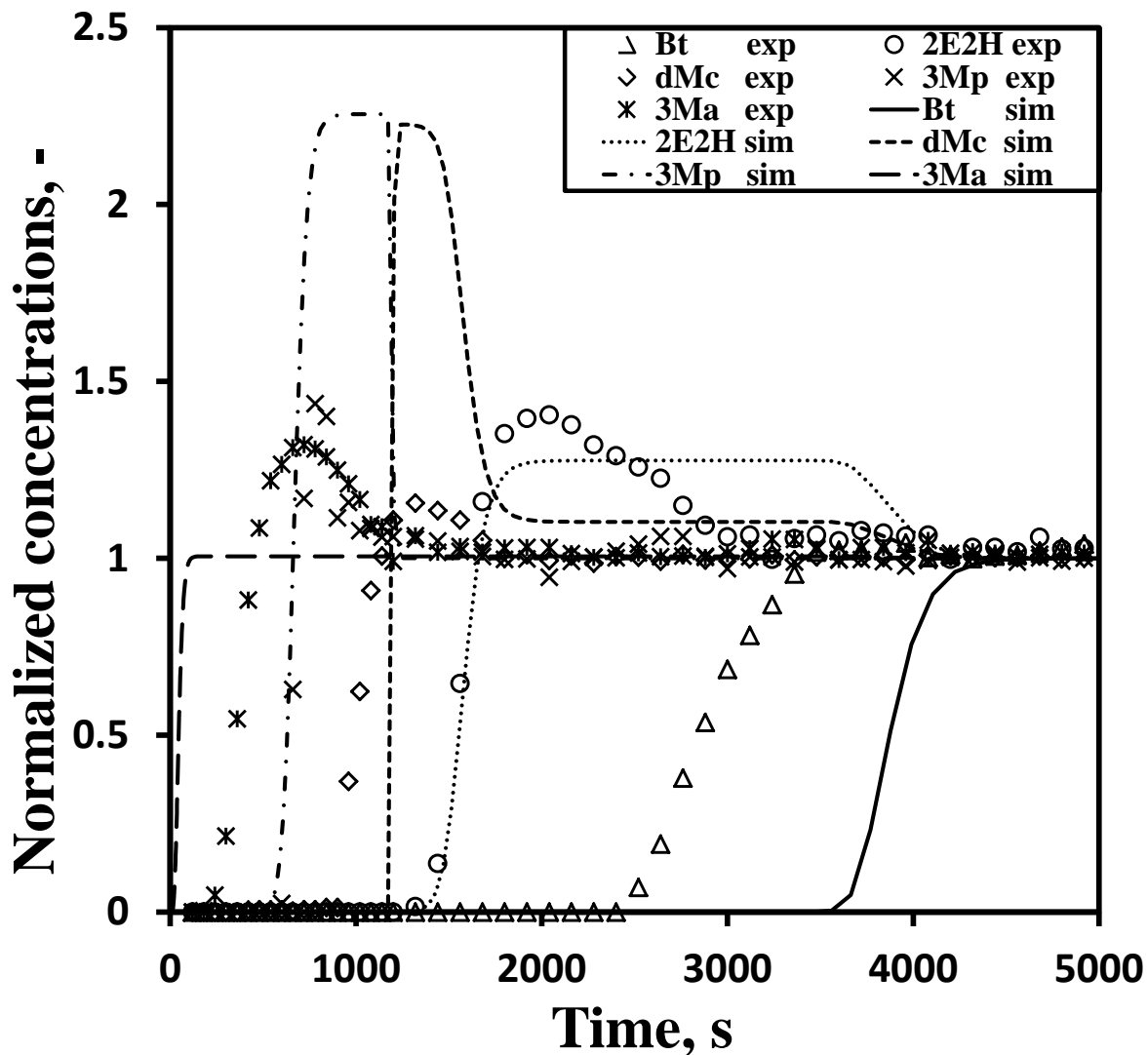


Figure 4.8. Experimental and predicted multicomponent breakthrough curves in zeolite Y for impurities in liquid toluene. The predicted data was obtained using the multicomponent dual-site Langmuir model for calculating the equilibrium isotherms. Triangles - butanal, circles - 2-ethyl-2-hexenal, diamonds - 2,6-dimethylcyclohexanone, crosses - 2,4,6-trimethylphenol, stars - 2,4,6-trimethylanisole, lines - model predictions.

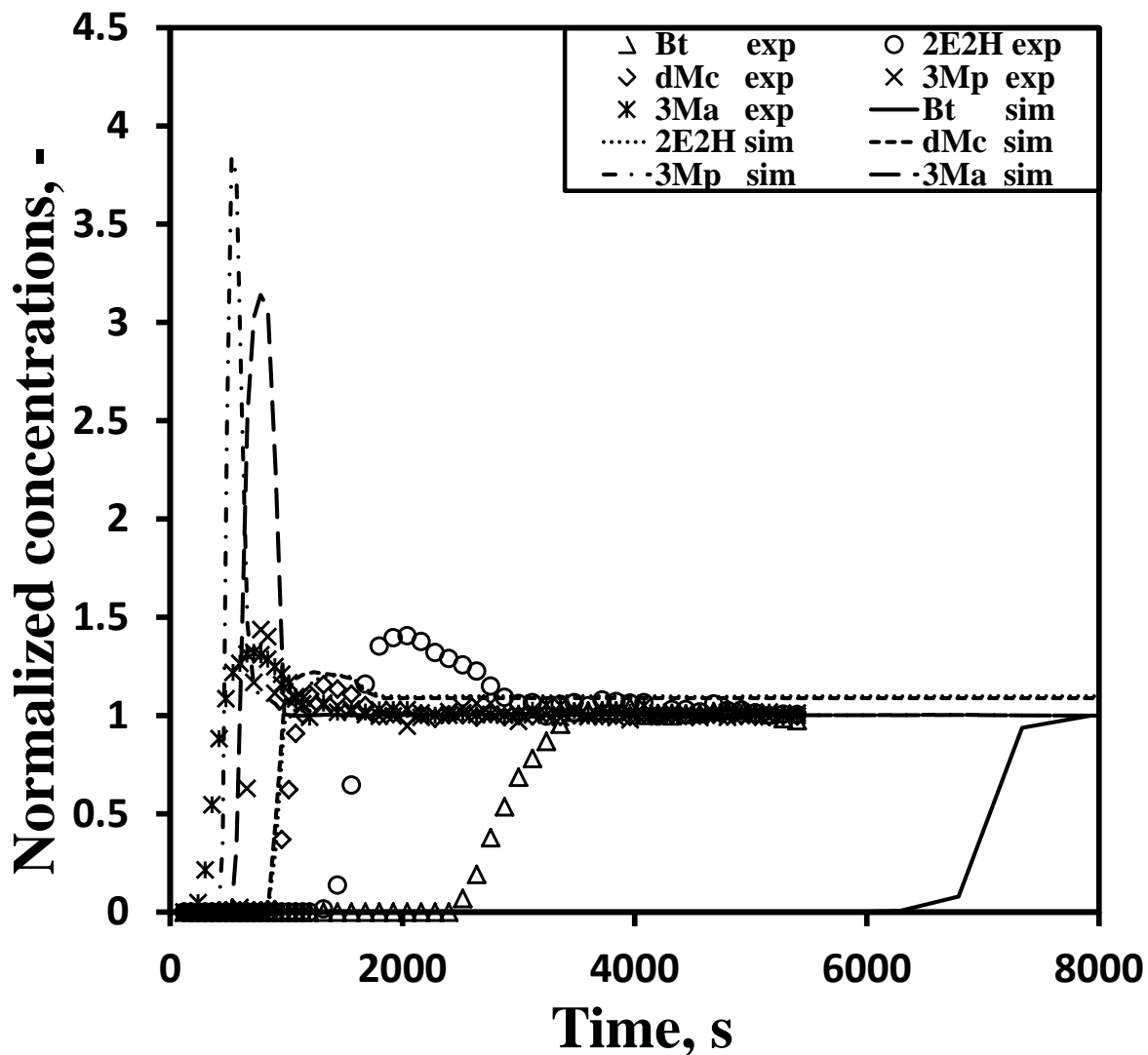


Figure 4.9. Experimental and predicted multicomponent breakthrough curves in zeolite Y for impurities in liquid toluene. The predicted data was obtained using the coupled SIAST-Langmuir model for calculating the equilibrium isotherms. Triangles - butanal, circles - 2-ethyl-2-hexenal, diamonds - 2,6-dimethylcyclohexanone, crosses - 2,4,6-trimethylphenol, stars - 2,4,6-trimethylanisole, lines - model predictions.

Appendix A

Additional Data for Chapter 2

Molecule models. The studied system was a mixture of toluene (Tol), butanal (Bt), 2-ethyl-2-hexenal (2E2H), 2,6-dimethylcyclohexanone (dMc), 2,4,6-trimethylphenol (3Mp) and 2,4,6-trimethylanisole (3Ma). The molecules were modeled as rigid and/or flexible structures using the united atom approach as described by Ryckaert and Bellemans [51]. For the flexible molecular structures, the pseudoatoms are connected through harmonic bonding potentials, harmonic bending potentials and the cosine series torsion potential described by Siepmann and co-workers [52].

The parameters for bond lengths, bond bending and torsion potentials are listed in Tables A1, A2 and A3 respectively. References for the parameters are indicated in the last column of the tables.

Pseudoatoms are connected through harmonic bonding potentials given by:

$$u_{\text{bond}} = k \cdot (r - r_0)^2 \quad (\text{A1})$$

where k is a constant in $\text{K}/\text{\AA}^2$ and r_0 is the equilibrium bond distance found in Table A1. The constant k/k_B had a value of $96500 \text{ K}/\text{\AA}^2$ in all cases.

Pseudoatoms separated by two bonds interact via a harmonic bending potential:

$$u_{\text{bend}} = \frac{k_0}{2} \cdot (\theta - \theta_0)^2 \quad (\text{A2})$$

For the torsional interactions of beads separated by three bonds, a cosine series is employed:

$$u_{\text{tors}} = c_0 + c_1[1 + \cos(\Phi)] + c_2[1 - \cos(2\Phi)] + c_3[1 + \cos(3\Phi)] \quad (\text{A3})$$

In this study we only consider the cis-form of 2-ethyl-2-hexenal. The difference between the cis- and trans – isomer of the molecule can be described by a harmonic torsional potential as described by Siepmann and co-workers [53]:

$$u_{\text{tors-cis}} = \frac{d_0}{2} (\varphi - \varphi_0)^2 \quad (\text{A4})$$

The parameters for the harmonic torsional potential needed to describe the cis-form of 2E2H can be found in Table A3.

Guest – guest interactions

The non-bonded interactions are described by a pairwise additive Lennard-Jones (LJ) and Coulombic potentials:

$$u(r_{ij}) = 4\varepsilon_{ij} \left[\left(\frac{\sigma_{ij}}{r_{ij}} \right)^{12} - \left(\frac{\sigma_{ij}}{r_{ij}} \right)^6 \right] + \frac{q_i q_j}{4\pi\varepsilon_0 r_{ij}} \quad (\text{A5})$$

where r_{ij} , ε_{ij} , σ_{ij} , q_i and q_j are bead-bead separation distance, the LJ well depth, the LJ size parameter and the partial charges on beads i and j respectively. Their values can be found in Table A4. The electrostatic interactions calculated using the Ewald summation with a relative precision of 10^{-6} [106]. The unlike interactions are computed with the Lorentz-Berthelot combining rules [65, 66]:

$$\sigma_{ij} = \frac{1}{2}(\sigma_{ii} + \sigma_{jj}) \quad (\text{A6a})$$

$$\varepsilon_{ij} = \sqrt{\varepsilon_{ii}\varepsilon_{jj}} \quad (\text{A6b})$$

The LJ size parameters for the guest-guest interactions, σ_i , and the charges of the pseudo-atoms were taken from the corresponding TraPPE force fields of Siepmann and co-workers [52-56, 61] and used without further modifications. The references for the values of the LJ parameters are listed in Table A4.

The LJ well depth parameters for guest-guest interactions, ε_i , for Bt, Tol and 3Mp were fitted to the vapor-liquid coexistence curve of the phase diagram using simulations in the μVT and NPT -ensemble. The LJ well depth parameters for guest-guest interactions, ε_i , for 2E2H, dMc and 3Ma were fitted to the experimental density at 363 K. The absolute relative difference between the predicted liquid density and the experimental one was calculated as:

$$\Delta_{\text{rel}} = \frac{|\rho_{\text{simulation}} - \rho_{\text{experimental}}|}{\rho_{\text{simulation}}} \cdot 100 \% \quad (\text{A7})$$

As can be seen in Table A5, the absolute relative difference between the predicted liquid density and the experimental one had a maximum of 4.9 % in the case of dMc.

Guest – host interactions

All the guest-host LJ interaction parameters used in this work, along with the corresponding references are listed in Table A6.

Pure component adsorption isotherms.

The pure component adsorption isotherms, obtained using molecular simulations and their fit using the dual – site Langmuir equation are shown in Figs. A1-A6.

Table A1. Adsorbents used in the experiments and their suppliers.

| Adsorbent name | Adsorbent type | Supplier |
|--|------------------------------------|-----------------|
| Al ₂ O ₃ acidic | activated alumina | 1 |
| Al ₂ PO ₃ basic | activated alumina | 1 |
| Al ₂ O ₃ neutral | activated alumina | 1 |
| Florisil | activated magnesium silicate | 1 |
| Lewatit AF5 | carbon-based microporous adsorbent | 1 |
| Dowex L-493 | polymeric resin | 1 |
| Carboxen 1000 | carbon molecular sieve | 1 |
| Carbosieve G | carbon molecular sieve | 1 |
| Carboxen 1003 | carbon molecular sieve | 1 |
| Carboxen 1021 | carbon molecular sieve | 1 |
| Carboxen 1018 | carbon molecular sieve | 1 |
| Carbosieve SIII | carbon molecular sieve | 1 |
| Carboxen 1012 | carbon molecular sieve | 1 |
| Carboxen 1016 | carbon molecular sieve | 1 |
| Carboxen 569 | carbon molecular sieve | 1 |
| Carbotrap X | graphitized carbon black | 1 |
| Carbotrap F | graphitized carbon black | 1 |
| Carbotrap Y | graphitized carbon black | 1 |
| Carbotrap C | graphitized carbon black | 1 |
| XAD2 | polymeric resin | 1 |
| Na-FAU zeolite | zeolite Y | 2 |

1, Sigma Aldrich Chemie B.V. (Netherlands)

2, Zeolyst (USA)

A total of 21 commercial adsorbents were tested in batch adsorption experiments using a solution comprising traces of butanal, 2-ethyl-2-hexenal, 2,6-dimethylcyclohexanone, 2,4,6-trimethylphenol and 2,4,6-trimethylanisole in liquid toluene. The initial concentrations of the impurity compounds in this solution is listed in Table A2.

In Tables A3-A8, the following notations are used to denote atoms in various chemical groups: *a* - atom adjacent to the aldehyde carbon, *ald* - atom in aldehyde group, *ar* - atom in aromatic group, *phen* - atom in phenol group, *anis* - atom in anisole group.

Table A2. Concentrations of the compounds in the initial solution used for the testing of 21 adsorbents (Figs. 2.1-2.5).

| Compound | Initial conc., ppmw |
|---------------------------|---------------------|
| Butanal | 1663 |
| 2-ethyl-2-hexenal | 1826 |
| 2,6-dimethylcyclohexanone | 1817 |
| 2,4,6-trimethylphenol | 1807 |
| 2,4,6-trimethylanisole | 1013 |

Table A3. Equilibrium bond lengths for the studied molecules. The following notations are used to denote atoms in various chemical groups: *a* - atom adjacent to the aldehyde carbon, *ald* - atom in aldehyde group, *ar* - atom in aromatic group, *phen* - atom in phenol group, *anis* - atom in anisol group.

| Bond Length | Molecule | r_0 (Å) | Ref. |
|---|------------------------|-----------|------|
| $\text{CH}_x - \text{CH}_y$ | all | 1.54 | [54] |
| $\text{CH}_{\text{ald}} = \text{O}_{\text{ald}}$ | aldehyde | 1.217 | [52] |
| $\text{CH}_{x\ a} - \text{CH}_{\text{ald}}$ | aldehyde/ketone | 1.52 | [52] |
| $\text{CH} = \text{C}_a$ | 2-ethyl-2-hexenal | 1.33 | [53] |
| $\text{CH}_3 - \text{C}_{\text{ar}}$ | aromatic | 1.54 | [54] |
| $\text{C}_{\text{ar}} - \text{H}_{\text{ar}}$ | aromatic | 1.08 | [55] |
| $\text{C}_{\text{ar}} - \text{C}_{\text{ar}}$ | aromatic | 1.392 | [55] |
| $\text{C}_{\text{phen}} - \text{O}_{\text{phen}}$ | 2,4,6-trymethylphenol | 1.43 | [56] |
| $\text{O}_{\text{phen}} - \text{H}_{\text{phen}}$ | 2,4,6-trymethylphenol | 0.945 | [56] |
| $\text{C}_{\text{anis}} - \text{O}_{\text{anis}}$ | 2,4,6-trymethylanisole | 1.41 | [52] |
| $\text{O}_{\text{anis}} - \text{CH}_{3\text{anis}}$ | 2,4,6-trymethylanisole | 1.41 | [52] |

Table A4. Parameters for bond-bending interactions. The following notations are used to denote atoms in various chemical groups: *a* - atom adjacent to the aldehyde carbon, *ald* - atom in aldehyde group, *ar* - atom in aromatic group, *phen* - atom in phenol group, *anis* - atom in anisol group.

| Bend | Molecule | θ_0 (deg) | k_0/k_B (K) | Ref. |
|--|------------------------|------------------|---------------|------|
| $\text{CH}_x - \text{CH}_2 - \text{CH}_y$ | all | 114 | 62500 | [54] |
| $\text{CH}_{x\ a} - \text{CH}_{\text{ald}} = \text{O}_{\text{ald}}$ | aldehyde | 121.4 | 62500 | [52] |
| $\text{CH}_2 - \text{CH} = \text{C}_a$ | 2-ethyl-2-hexenal | 119.7 | 70420 | [53] |
| $\text{C}_{\text{ar}} - \text{C}_{\text{ar}} - \text{C}_{\text{ar}}$ | aromatic | 120 | rigid | [55] |
| $\text{C}_{\text{ar}} - \text{C}_{\text{ar}} - \text{H}_{\text{ar}}$ | aromatic | 120 | rigid | [55] |
| $\text{CH}_{3\text{ar}} - \text{C}_{\text{ar}} - \text{C}_{\text{ar}}$ | aromatic | 120 | rigid | [55] |
| $\text{C}_{\text{ar}} - \text{C}_{\text{phen}} - \text{O}_{\text{phen}}$ | 2,4,6-trymethylphenol | 120 | rigid | [55] |
| $\text{C}_{\text{phen}} - \text{O}_{\text{phen}} - \text{H}_{\text{phen}}$ | 2,4,6-trymethylphenol | 108.5 | rigid | [56] |
| $\text{C}_{\text{ar}} - \text{C}_{\text{anis}} - \text{O}_{\text{anis}}$ | 2,4,6-trymethylanisole | 120 | rigid | [55] |
| $\text{C}_{\text{anis}} - \text{O}_{\text{anis}} - \text{CH}_{3\text{anis}}$ | 2,4,6-trymethylanisole | 112 | rigid | [52] |

Table A5. Parameters for the torsion potentials of the studied molecules. The following notations are used to denote atoms in various chemical groups: *a* - atom adjacent to the aldehyde carbon, *ald* - atom in aldehyde group, *ar* - atom in aromatic group, *phen* - atom in phenol group, *anis* - atom in anisol group.

| Torsion | Molecule | c_0/k_B (K) | c_1/k_B (K) | c_2/k_B (K) | c_3/k_B (K) | Ref. |
|---|-------------------|---------------------------------|-------------------------------------|---------------|---------------|------|
| $\text{CH}_x - \text{CH}_2 - \text{CH}_2 - \text{CH}_y$ | all | 0 | 355.03 | -68.19 | 791.32 | [54] |
| $\text{CH}_2 - \text{CH}_{2a} - \text{CH}_{\text{ald}} = \text{O}_{\text{ald}}$ | butanal | 2035 | -736.90 | 57.84 | -293.23 | [52] |
| $\text{CH}_2 - \text{CH}_2 - \text{CH} = \text{C}_a$ | 2-ethyl-2-hexenal | 688 | 86.36 | -109.77 | -282.24 | [53] |
| $\text{CH} = \text{C}_a - \text{CH}_2 - \text{CH}_3$ | 2-ethyl-2-hexenal | 688 | 86.36 | -109.77 | -282.24 | [53] |
| $\text{CH} = \text{C}_a - \text{CH}_{\text{ald}} = \text{O}_{\text{ald}}$ | 2-ethyl-2-hexenal | 2035 | -736.90 | 57.84 | -293.23 | * |
| $\text{CH}_3 - \text{CH}_2 - \text{C}_a - \text{CH}_{\text{ald}}$ | 2-ethyl-2-hexenal | 0 | 355.03 | -68.19 | 791.32 | ** |
| $\text{CH}_2 - \text{C}_a - \text{CH}_{\text{ald}} = \text{O}_{\text{ald}}$ | 2-ethyl-2-hexenal | 2035 | -736.90 | 57.84 | -293.23 | * |
| Torsion (eq. A4) | Molecule | d_0/k_B (K) | φ_0 (rad) | | | |
| $\text{CH}_2 - \text{CH} = \text{C}_a - \text{CH}_2$ (cis) | 2-ethyl-2-hexenal | 24800 | π | | | [53] |
| $\text{CH}_2 - \text{CH} = \text{C}_a - \text{CH}_{\text{ald}}$ (trans) | 2-ethyl-2-hexenal | 26800 | 0 | | | [53] |

* value not available in the literature, the torsion for aldehydes was used

** value not available in the literature, the torsion for alkanes was used

Table A6. Lennard-Jones guest – guest interaction parameters and partial charges. The following notations are used to denote atoms in various chemical groups: *a* - atom adjacent to the aldehyde carbon, *ald* - atom in aldehyde group, *ar* - atom in aromatic group, *phen* - atom in phenol group, *anis* - atom in anisol group.

| Site | Molecule | σ (Å) | Ref. | ϵ/k_B (K) | Ref. | q [e] | Ref. |
|--|---------------------------|--------------|------|-----------------------|------|---------|------|
| CH₃ (sp₃) | all | 3.75 | [54] | 106.8 | * | 0 | [54] |
| CH₂ (sp₃) | all | 3.95 | [54] | 56.2 | * | 0 | [54] |
| CH_{2a} | butanal | 3.95 | [52] | 56.2 | * | -0.043 | [52] |
| O_{ald} | butanal | 3.05 | [52] | 49.56 | * | -0.482 | [52] |
| CH_{ald} | aldehyde | 3.52 | [52] | 50.64 | * | 0.525 | [52] |
| CH (sp₂) | 2-ethyl-2-hexenal | 3.73 | [53] | 50.6 | * | 0 | [53] |
| C_a | 2-ethyl-2-hexenal | 3.85 | [53] | 23.12 | * | -0.043 | [53] |
| C_{ar} | aromatic | 3.6 | [55] | 34.3 | * | -0.095 | [55] |
| CH_{3ar} | aromatic | 3.75 | [54] | 98 | [54] | 0.095 | [55] |
| H_{ar} | aromatic | 2.36 | [55] | 25.45 | [55] | 0.095 | [55] |
| C_{phen} | 2,4,6-trymethylphenol | 3.6 | [55] | 34.3 | * | 0.265 | [56] |
| O_{phen} | 2,4,6-trymethylphenol | 3.02 | [56] | 93 | [56] | -0.7 | [56] |
| H_{phen} | 2,4,6-trymethylphenol | 0 | [56] | 0 | [56] | 0.435 | [56] |
| C_{anis} | 2,4,6-trymethylanisole | 3.6 | [55] | 34.3 | * | 0.25 | [52] |
| O_{anis} | 2,4,6-trymethylanisole | 2.8 | [52] | 55 | [52] | -0.5 | [52] |
| CH_{3anis} | 2,4,6-trymethylanisole | 3.75 | [54] | 98 | [54] | 0.25 | [52] |
| CH (sp₃) | 2,6-dimethylcyclohexanone | 4.68 | [61] | 17.04 | * | 0 | [61] |
| C_{ket} | 2,6-dimethylcyclohexanone | 3.82 | [52] | 45.44 | * | 0.424 | [52] |
| O_{ket} | 2,6-dimethylcyclohexanone | 3.05 | [52] | 49.56 | * | -0.424 | [52] |

* values fitted to liquid densities (at 25°C and 1 bar) using simulations in the *NPT* ensemble.

Table A7. Relative difference between the computed liquid density and the experimental liquid density.

| Compound | Temp., K | Liquid density, kg/m ³ | | | Δ_{rel} , % |
|---------------------------|----------|-----------------------------------|--------------|------|--------------------|
| | | Computed | Experimental | Ref. | |
| Toluene | 250 | 907.5 | 906.7 | [70] | 0.079 |
| | 400 | 761.4 | 761.9 | [70] | 0.060 |
| | 500 | 629.4 | 638.1 | [70] | 1.368 |
| Butanal | 300 | 819.8 | 794.9 | [70] | 3.133 |
| | 400 | 678.1 | 671.2 | [70] | 1.029 |
| 2-ethyl-2-hexenal | 363 | 785.1 | 793.5 | * | 1.061 |
| 2,6-dimethylcyclohexanone | 290 | 871.5 | 915 | * | 4.754 |
| | 363 | 810.4 | 852 | * | 4.882 |
| 2,4,6-trimethylphenol | 450 | 871.9 | 881 | [70] | 1.034 |
| | 550 | 762.2 | 790.7 | [70] | 3.593 |
| 2,4,6-trimethylanisole | 363 | 886.1 | 885.2 | * | 0.098 |

* value measured experimentally at 25 °C

Table A8. Lennard-Jones guest – host interaction parameters and partial charges. The following notations are used to denote atoms in various chemical groups: *a* - atom adjacent to the aldehyde carbon, *ald* - atom in aldehyde group, *ar* - atom in aromatic group, *phen* - atom in phenol group, *anis* - atom in anisole group.

| Site | Molecule | σ (Å) | Ref. | ϵ/k_B (K) | Ref. | q (e) | Ref. |
|------------------------------------|---------------------------|--------------|-------|--------------------|-------|---------|------|
| CH ₃ (sp ₃) | all | 3.48 | [62] | 93 | [62] | 0 | [54] |
| CH ₂ (sp ₃) | all | 3.58 | [62] | 60.5 | [62] | 0 | [54] |
| CH _{2a} | butanal | 3.38 | * | 70.96 | * | -0.043 | [52] |
| O _{ald} | butanal | 2.93 | * | 66.64 | * | -0.482 | [52] |
| CH _{ald} | aldehyde | 3.16 | * | 67.36 | * | 0.525 | [52] |
| CH (sp ₂) | 2-ethyl-2-hexenal | 3.502 | [107] | 55.215 | [107] | 0 | [53] |
| C _a | 2-ethyl-2-hexenal | 3.33 | * | 45.51 | * | -0.043 | [53] |
| C _{ar} | aromatic | 3.01 | [40] | 73.6 | [40] | -0.095 | [55] |
| CH _{3ar} | aromatic | 3.365 | [40] | 80.32 | [40] | 0.095 | [55] |
| H _{ar} | aromatic | 2.61 | [40] | 49.1 | [40] | 0.095 | [55] |
| C _{phen} | 2,4,6-trimethylphenol | 3.01 | [40] | 73.6 | [40] | 0.265 | [56] |
| O _{phen} | 2,4,6-trimethylphenol | 2.91 | * | 91.3 | * | -0.7 | [56] |
| H _{phen} | 2,4,6-trimethylphenol | 0 | * | 0 | * | 0.435 | [56] |
| C _{anis} | 2,4,6-trimethylanisole | 3.01 | [40] | 73.6 | [40] | 0.25 | [52] |
| O _{anis} | 2,4,6-trimethylanisole | 4.56 | [67] | 10 | [67] | -0.5 | [52] |
| CH _{3anis} | 2,4,6-trimethylanisole | 3.365 | [40] | 80.32 | [40] | 0.25 | [52] |
| CH (sp ₃) | 2,6-dimethylcyclohexanone | 3.92 | [62] | 40 | [62] | 0 | [61] |
| C _{ket} | 2,6-dimethylcyclohexanone | 3.31 | * | 63.81 | * | 0.424 | [52] |
| O _{ket} | 2,6-dimethylcyclohexanone | 2.93 | * | 66.64 | * | -0.424 | [52] |

Numbers in brackets are corresponding references.

* obtained using geometric and arithmetic mean combining rules as explained in section 2.3.1 (Chapter 2)

Table A9. Critical temperatures, pressures and acentric factors used in this thesis.

| Comp. | T_c, K | Ref. T_c | P_c, Pa | Ref. P_c | ω | Ref ω |
|--------------|----------------------------|---|-----------------------------|--|----------------------------|---|
| Tol | 591.79 | [70] | 4109000 | [70] | 0.264 | [70] |
| Bt | 537 | [108] | 4890214 | Est. Met. Marrero &Pardillo [104] | 0.3319 | [109], P_{vap} from [70] |
| 2E2H | 615.9 | Est. Met. Const- Gani [104] | 2301790 | Est. Met. Const-Gani [104] | 0.406 | [110] |
| dMc | 637.693 | Est. Met. Marrero &Pardillo [104] | 2811361 | Est. Met. Marrero &Pardillo [104] | 0.388 | [111] |
| 3Mp | 708.23 | Est. Met. Marrero &Pardillo [104] | 3637734 | Est. Met. Marrero &Pardillo [104] | 0.535 | [109], P_{vap} from [70] |
| 3Ma | 674.262 | Est. Met. Marrero &Pardillo [104] | 2665267 | Est. Met. Marrero &Pardillo [104] | 0.352 | [109] |

Est. Met. = estimation method;

P_{vap} = vapor pressure.

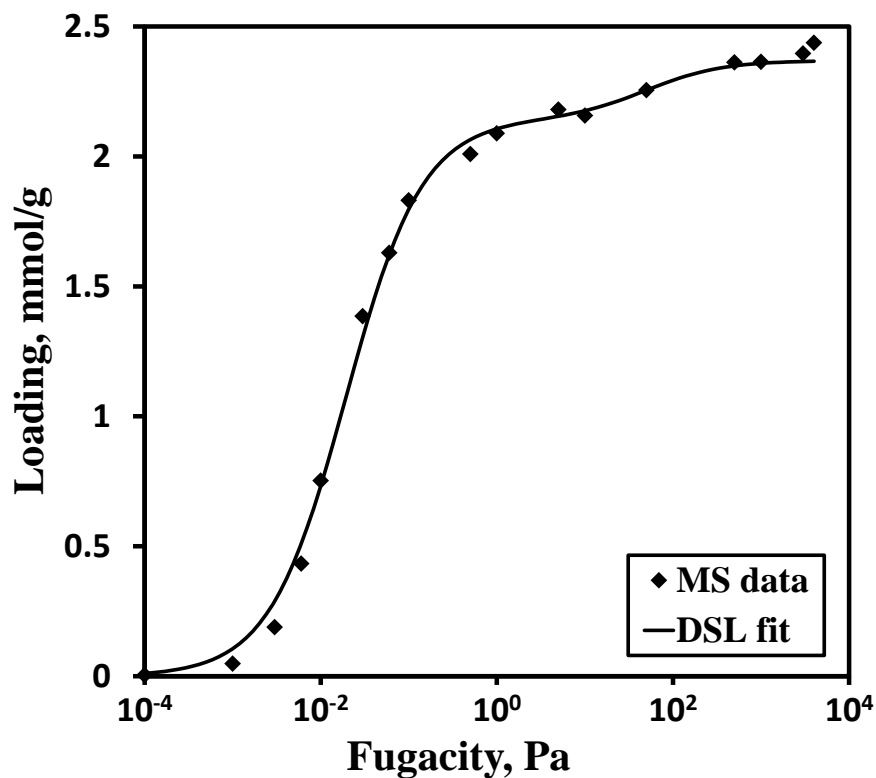


Figure A1. Adsorption isotherm of pure toluene in NaY zeolite; symbols - molecular simulation (MS) results; line - dual-site Langmuir (DSL) fit.

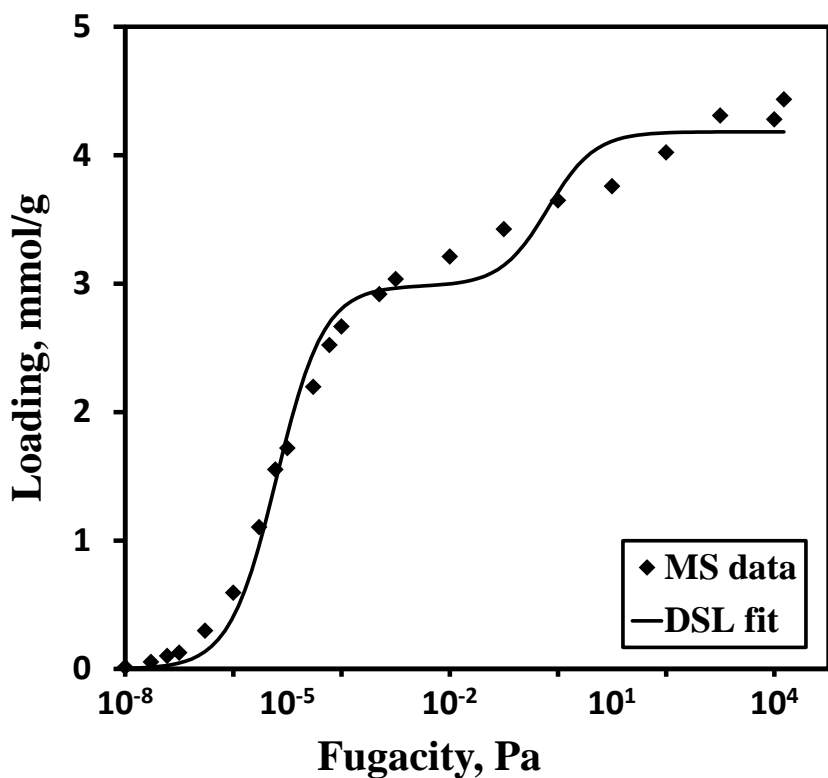


Figure A2. Adsorption isotherm of pure butanal in NaY zeolite; symbols - molecular simulation (MS) results; line - dual-site Langmuir (DSL) fit.

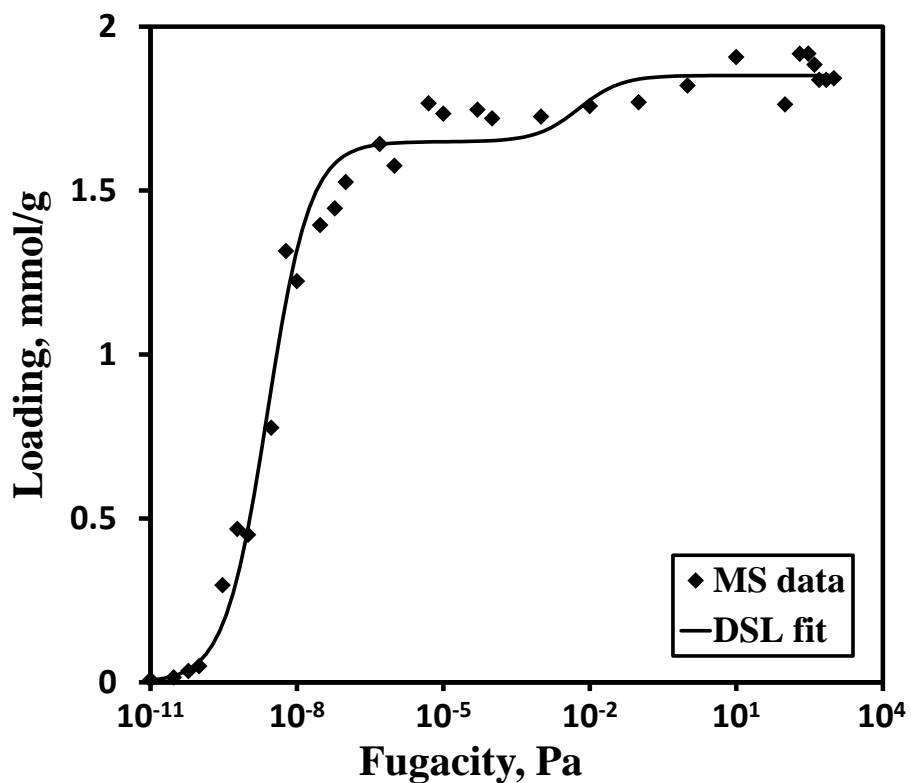


Figure A3. Adsorption isotherm of pure 2-ethyl-2-hexenal in NaY zeolite; symbols - molecular simulation (MS) results; line - dual-site Langmuir (DSL) fit.

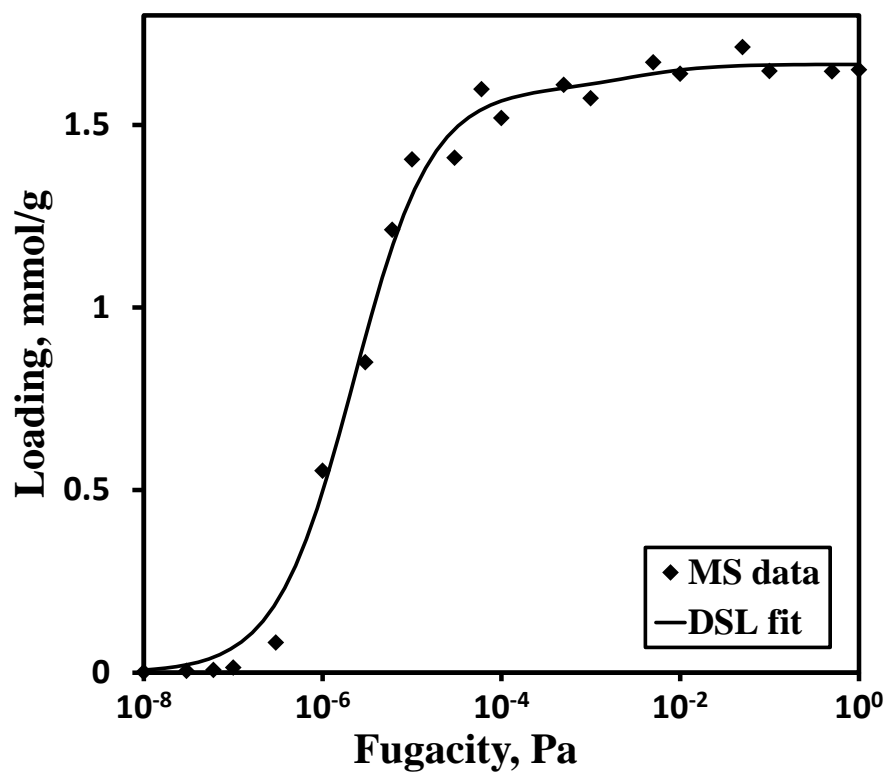


Figure A4. Adsorption isotherm of pure 2,6-dimethylcyclohexanone in NaY zeolite; symbols - molecular simulation (MS) results; line - dual-site Langmuir (DSL) fit.

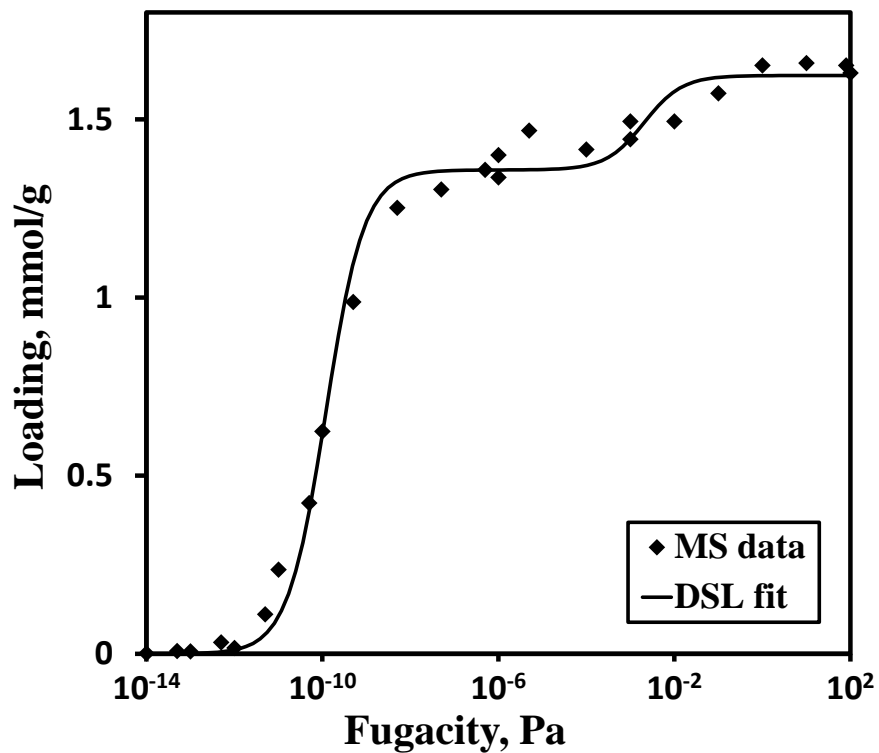


Figure A5. Adsorption isotherm of pure 2,4,6-trimethylphenol in NaY zeolite; symbols - molecular simulation (MS) results; line - dual-site Langmuir (DSL) fit.

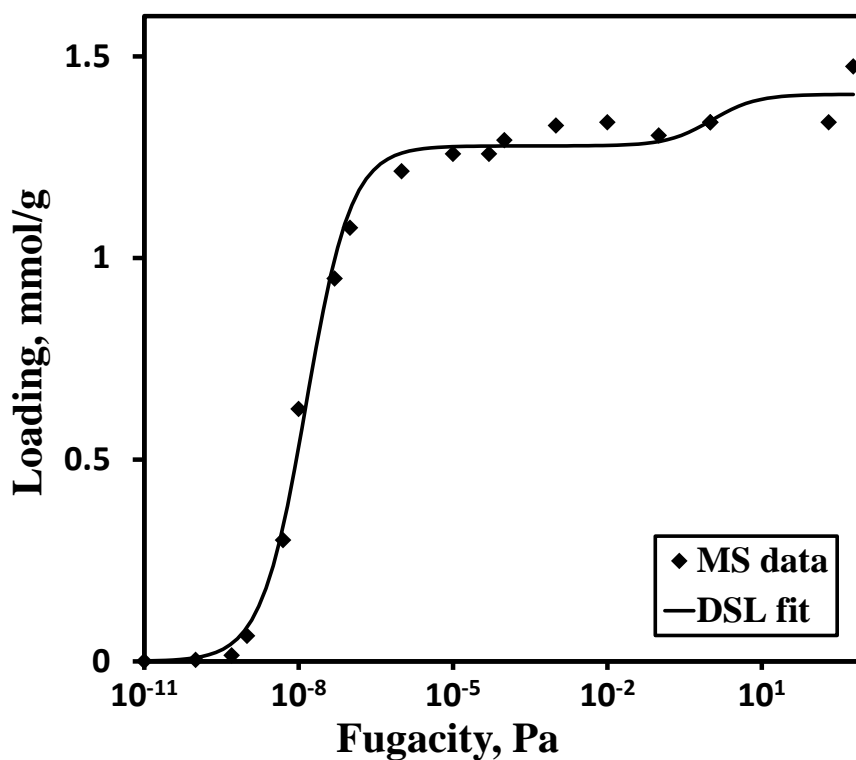


Figure A6. Adsorption isotherm of pure 2,4,6-trimethylanisole in NaY zeolite; symbols - molecular simulation (MS) results; line - dual-site Langmuir (DSL) fit.

Appendix B

Additional Data for Chapter 3

The Wilson activity coefficient model [45]:

$$\ln \gamma_i = 1 - \ln \sum_{j=1}^n (x_j s_{ij}) - \sum_{k=1}^n \frac{x_k s_{ki}}{\sum_{j=1}^n x_j s_{kj}} \quad s_{ii} = s_{jj} = 1 \quad (\text{B1})$$

where n represents the number of species in the system, x_j is the adsorbed phase mole fraction of species j , and s_{ij} are fitting parameters of the Wilson model.

The NRTL activity coefficient model [43]:

$$\ln \gamma_i = \frac{\sum_{j=1}^n x_j \tau_{ji} g_{ji}}{\sum_{k=1}^n x_k g_{ki}} + \sum_{j=1}^n \left[\frac{x_j g_{ij}}{\sum_{k=1}^n x_k g_{kj}} \cdot \left(\tau_{ij} - \frac{\sum_{k=1}^n x_k \tau_{kj} g_{kj}}{\sum_{k=1}^n x_k g_{kj}} \right) \right] \quad (\text{B2})$$

$$g_{ij} = \exp[-\alpha_{ij} \cdot \tau_{ij}], \quad \tau_{ii} = \tau_{jj} = 0, \quad g_{ii} = g_{jj} = 1 \quad (\text{B3})$$

where τ_{ij} and α_{ij} are fitting parameters of the NRTL model.

The 2D-lattice parameters used to generate the adsorption data of Figs. 3.4-3.7 and B1-B6 are shown in Table B1. The 2D-lattice parameters obtained from fitting the binary adsorption data for the systems $\text{CO}_2\text{-N}_2$ in PCOD8200029 and $\text{CO}_2\text{-C}_3\text{H}_8$ in MOR are listed in Tables B2 and B3. The NRTL model predictions of data generated with the 2D-lattice model are shown in Figs. B1-B6. The fit of the pure component adsorption isotherms for the systems $\text{CO}_2\text{-N}_2$ in the hypothetical zeolite PCOD8200029 [27] and $\text{CO}_2\text{-C}_3\text{H}_8$ in MOR are shown in Figs. B7-B10.

In Figs. B1-B6, the root mean square error of the fit, RMSE, was calculated using the formula:

$$RMSE = \sqrt{\frac{1}{n_{\text{odp}}} \sum_{i=1}^{n_{\text{odp}}} (\text{fit.result}_i - \text{exp.result}_i)^2} \quad (\text{B4})$$

where n_{odp} is the number of data points.

Table B1. 2D-lattice parameter values used to generate adsorption data presented in Figs. 3.4-3.7, B1-B6. f_X -imposed fugacity for pure component X in the thermodynamic integration. x_X -mole fraction of component X. The fugacity and interaction parameters are expressed in reduced units.

| Fig. nr. | w_{XX} | w_{YY} | w_{XY} | Δw (Eq. 17) | $f_X (x_X \rightarrow 1)$ |
|-------------|----------|----------|----------|---------------------|-------------------------------|
| 3.4, B1, B2 | -0.1 | -0.3 | -0.5 | 0.6 | 0.01 |
| 3.5, B3, B4 | -0.1 | 0.7 | -0.5 | 1.6 | 30 |
| 3.6, B5, B6 | 0.1 | 1.1 | -0.7 | 2.6 | 30 |
| 3.7 | -0.1 | -0.3 | -0.5 | 0.6 | 0.01, 0.1, 0.4, 0.8, 2, 5, 30 |

Table B2. 2D-lattice interaction parameters ($w_{CO_2-CO_2}$, $w_{CO_2-N_2}$, $w_{CO_2-S_1}$, $w_{CO_2-S_2}$, $w_{N_2-N_2}$, $w_{N_2-S_1}$, $w_{N_2-S_2}$) for the system CO_2-N_2 in the pure silica hypothetical zeolite PCOD8200029. The hypothetical zeolite PCOD8200029 has two distinct adsorption sites. The interaction parameters are expressed in reduced units.

| Interaction parameter, w | CO_2 | N_2 | Adsorption site 1 | Adsorption site 2 |
|----------------------------|---------|---------|-------------------|-------------------|
| CO_2 | -0.0005 | 0.0448 | 2627.5 | 573.2 |
| N_2 | 0.0448 | -4.0107 | 3160.4 | 2728.9 |

Table B3. 2D-lattice interaction parameters ($w_{CO_2-CO_2}$, $w_{CO_2-C_3H_8}$, $w_{CO_2-S_1}$, $w_{CO_2-S_2}$, $w_{C_3H_8-C_3H_8}$, $w_{C_3H_8-S_1}$, $w_{C_3H_8-S_2}$) for the system $CO_2-C_3H_8$ in MOR. MOR-type zeolite has two distinct adsorption sites. The interaction parameters are expressed in reduced units.

| Interaction parameter, w | CO_2 | C_3H_8 | Adsorption site 1 | Adsorption site 2 |
|----------------------------|--------|----------|-------------------|-------------------|
| CO_2 | 0.0028 | 0.0021 | 600.9 | 2377.4 |
| C_3H_8 | 0.0021 | 0.0013 | 691.3 | 3667.7 |

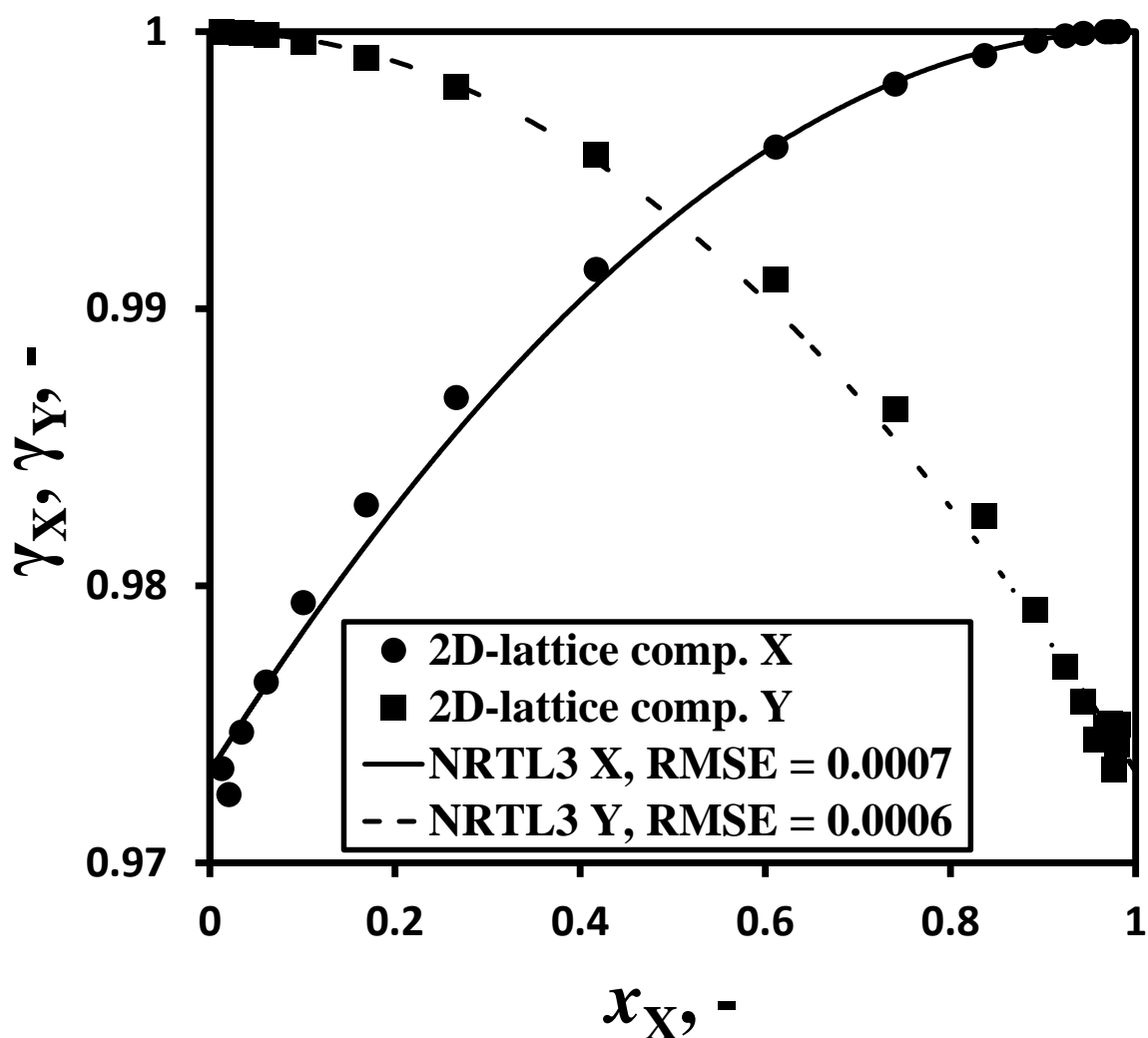


Figure B1. Adsorbed-phase activity coefficient data for a slightly non-ideal binary system of molecules X+Y, generated using a 2D-lattice model. Circles - 2D-lattice simulation data for compound X, squares - 2D-lattice simulation data for compound Y, lines - fit using the three-parameter NRTL model (NRTL3). RMSE (reduced units) represents the root mean square error of the fit calculated according to Eq. B4. The parameters used in the 2D-lattice simulations are listed in Table B1.

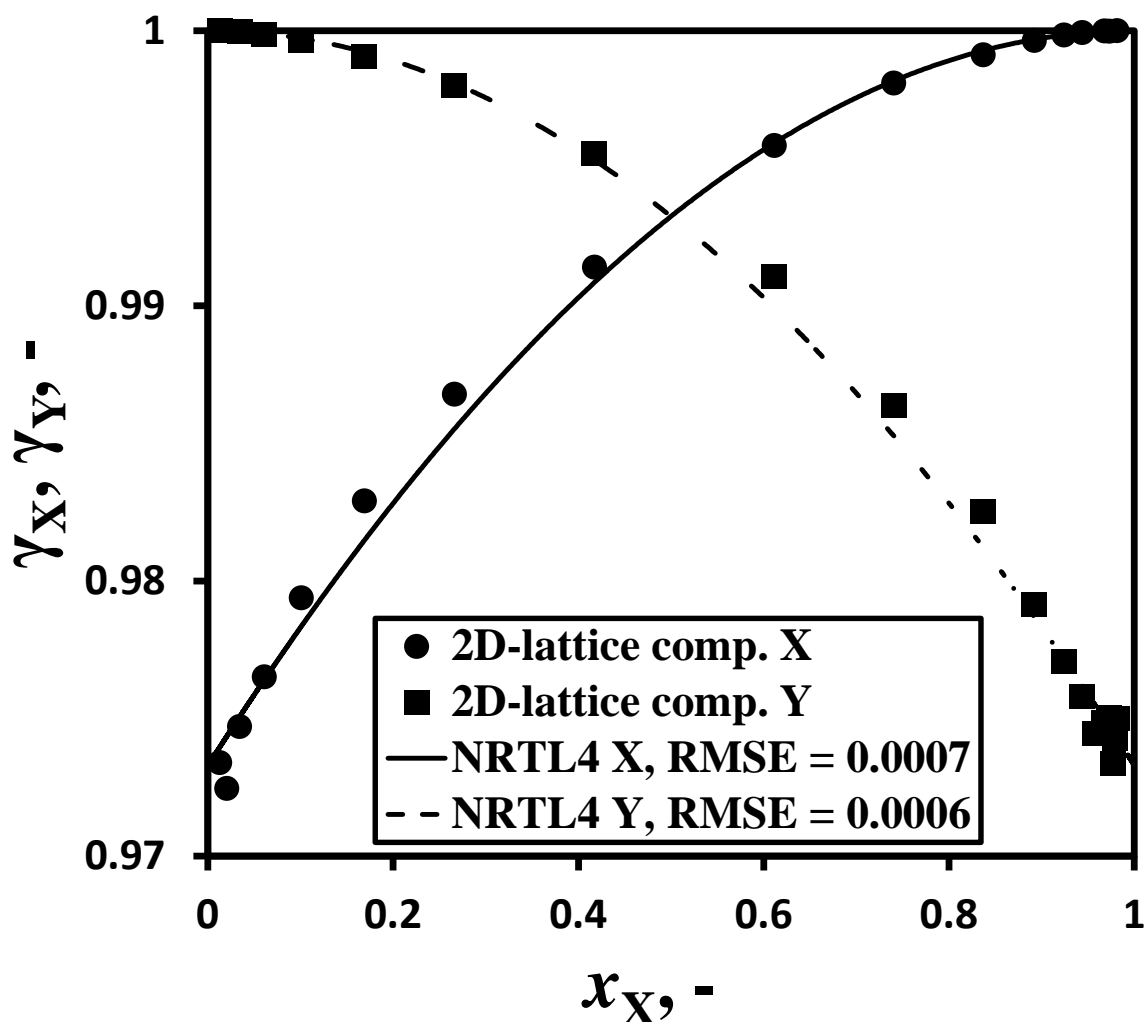


Figure B2. Adsorbed-phase activity coefficient data for a slightly non-ideal binary system of molecules X+Y, generated using a 2D-lattice model. Circles - 2D-lattice simulation data for compound X, squares - 2D-lattice simulation data for compound Y, lines - fit using the four-parameter NRTL model (NRTL4). RMSE (reduced units) represents the root mean square error of the fit calculated according to Eq. B4. The parameters used in the 2D-lattice simulations are listed in Table B1.

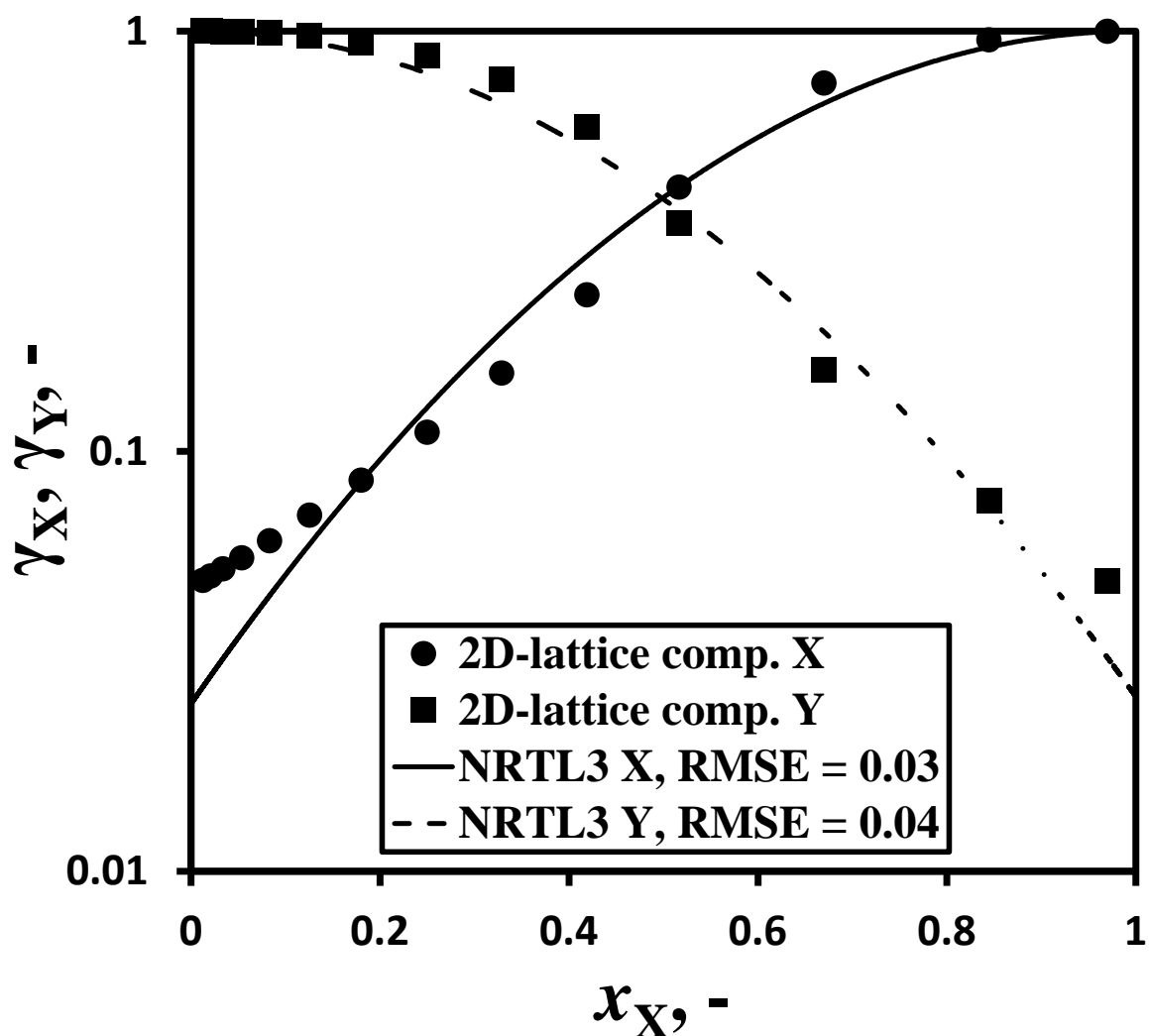


Figure B3. Adsorbed-phase activity coefficient data for a non-ideal binary system of molecules X+Y, generated using a 2D-lattice model. Circles - 2D-lattice simulation data for compound X, squares - 2D-lattice simulation data for compound Y, lines - fit using the three-parameter NRTL model (NRTL3). RMSE (reduced units) represents the root mean square error of the fit calculated according to Eq. B4. The parameters used in the 2D-lattice simulations are listed in Table B1.

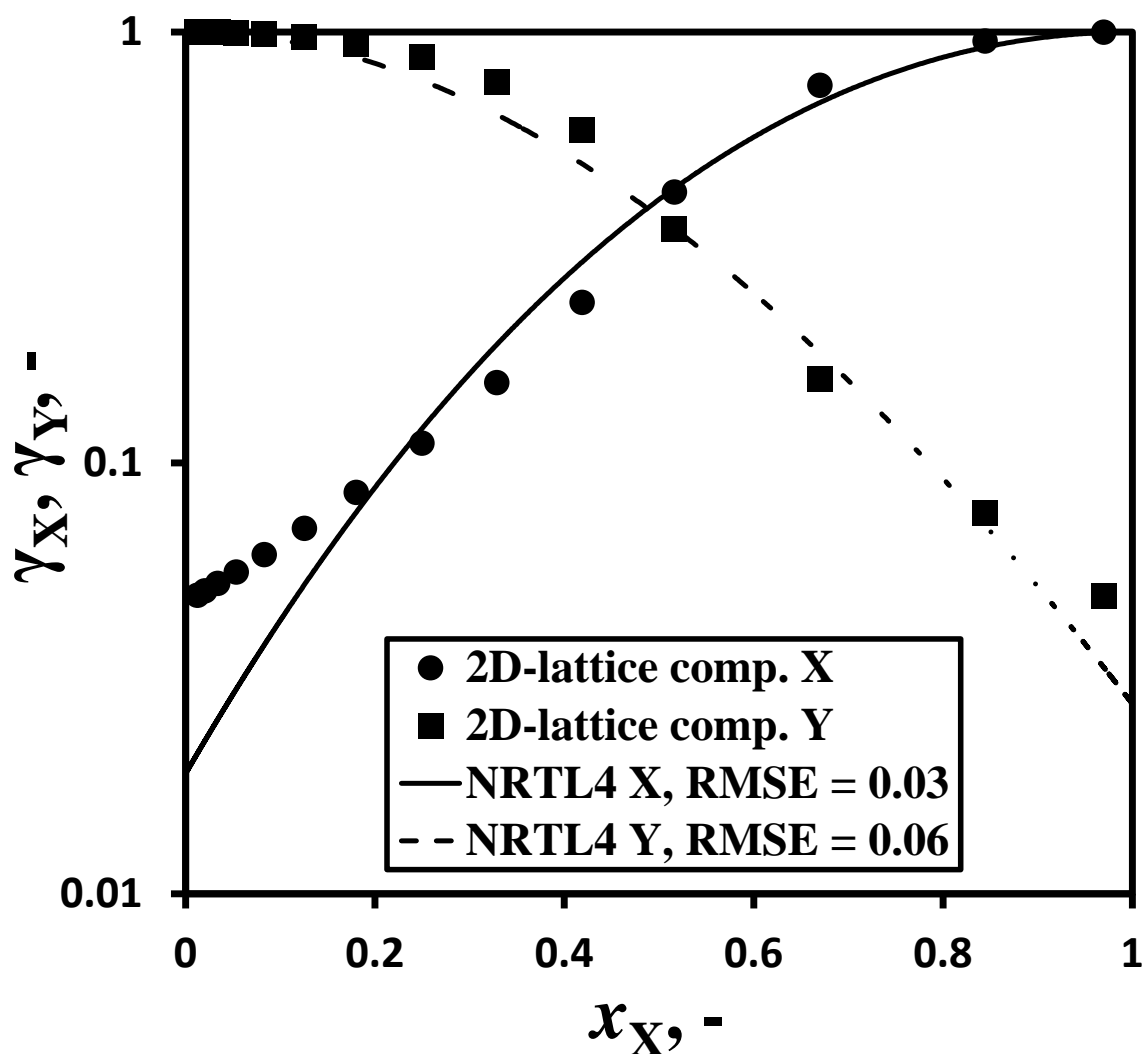


Figure B4. Adsorbed-phase activity coefficient data for a non-ideal binary system of molecules X+Y, generated using a 2D-lattice model. Circles - 2D-lattice simulation data for compound X, squares - 2D-lattice simulation data for compound Y, lines - fit using the four-parameter NRTL model (NRTL4). RMSE (reduced units) represents the root mean square error of the fit calculated according to Eq. B4. The parameters used in the 2D-lattice simulations are listed in Table B1.

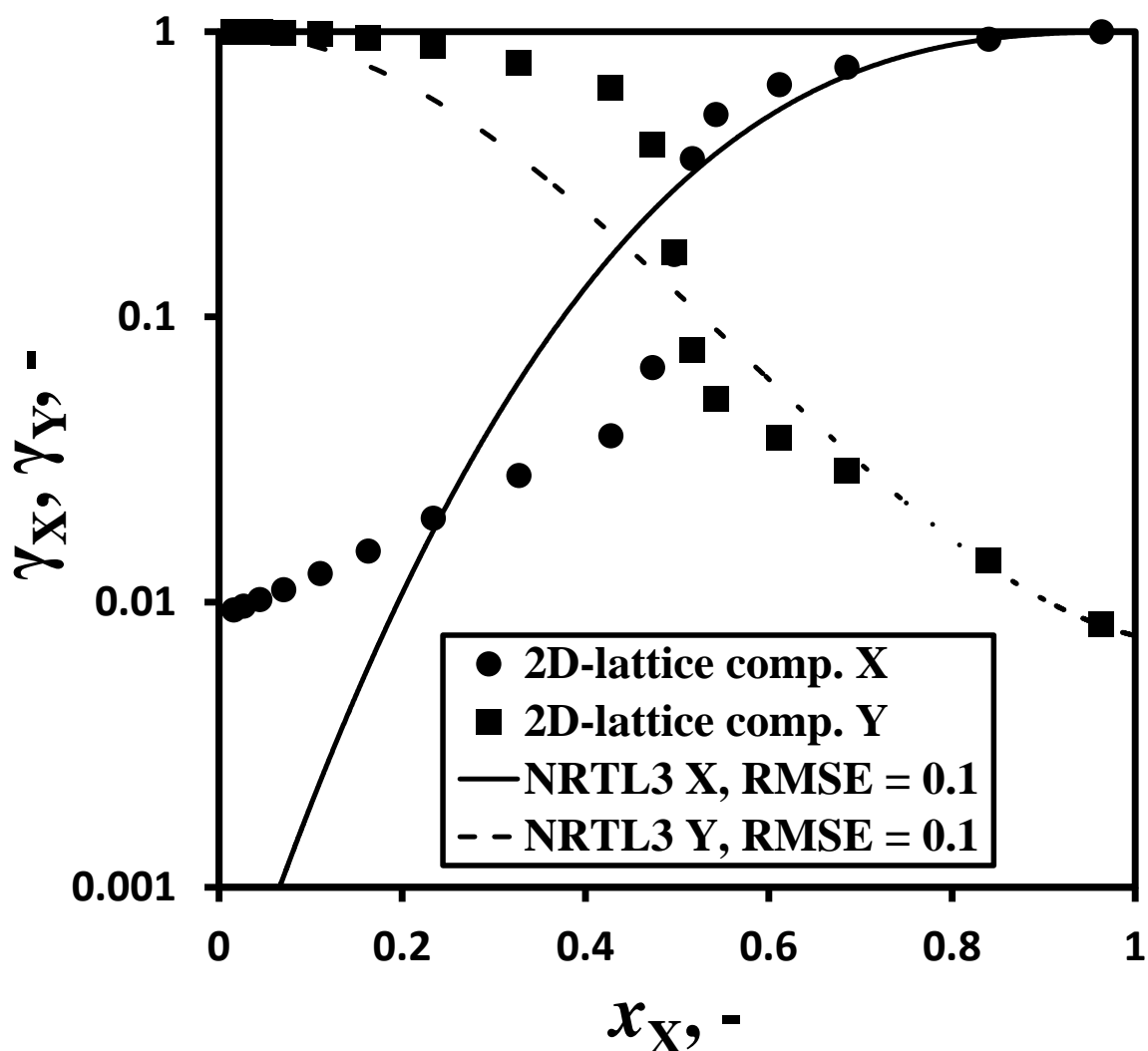


Figure B5. Adsorbed-phase activity coefficient data for a highly non-ideal binary system of molecules X+Y, generated using a 2D-lattice model. Circles - 2D-lattice simulation data for compound X, squares - 2D-lattice simulation data for compound Y, lines - fit using the three-parameter NRTL model (NRTL3). RMSE (reduced units) represents the root mean square error of the fit calculated according to Eq. B4. The parameters used in the 2D-lattice simulations are listed in Table B1.

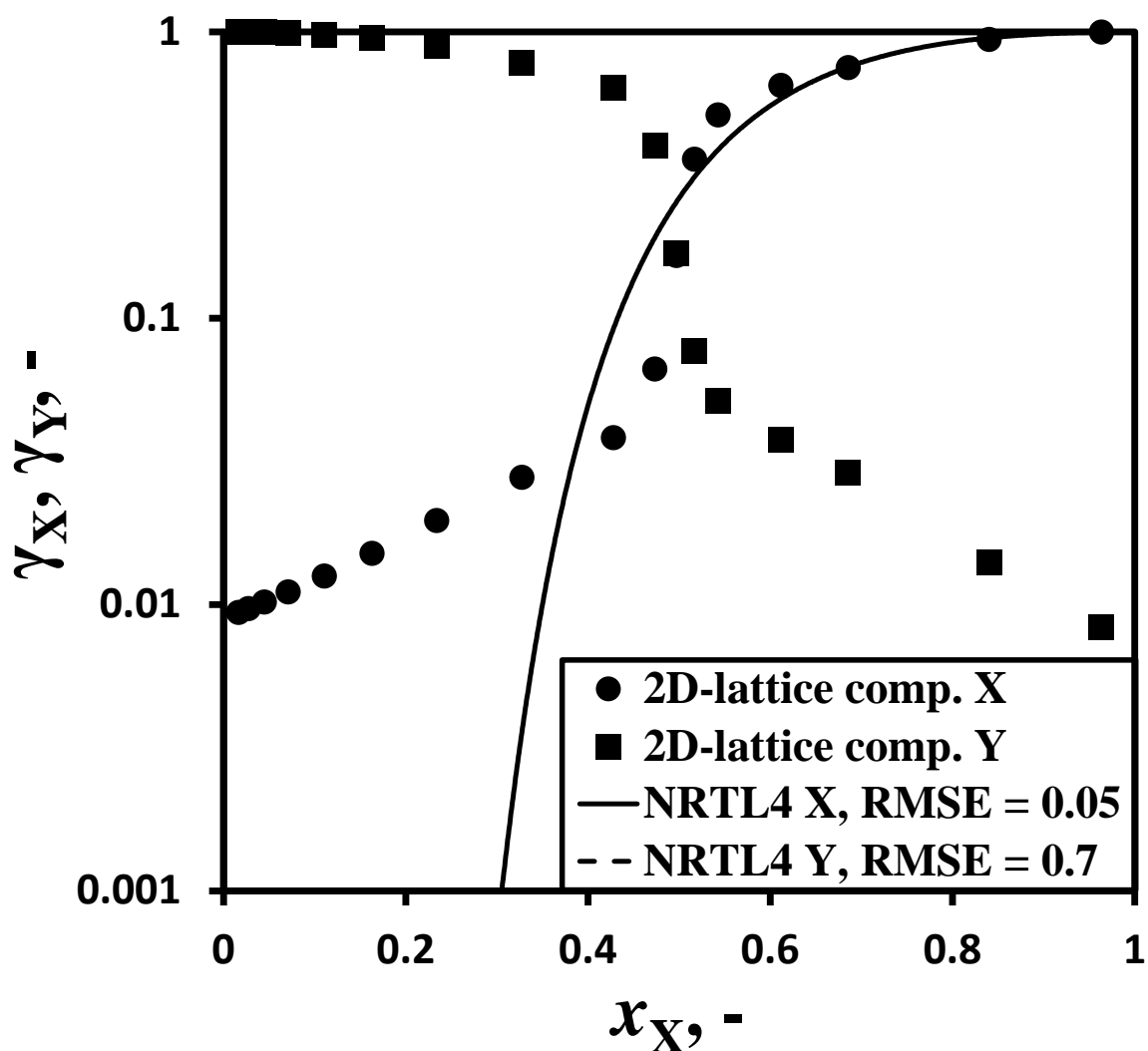


Figure B6. Adsorbed-phase activity coefficient data for a highly non-ideal binary system of molecules X+Y, generated using a 2D-lattice model. Circles - 2D-lattice simulation data for compound X, squares - 2D-lattice simulation data for compound Y, lines - fit using the four-parameter NRTL model (NRTL4); the fit for compound Y does not fit the scale. RMSE (reduced units) represents the root mean square error of the fit calculated according to Eq. B4. The parameters used in the 2D-lattice simulations are listed in Table B1.

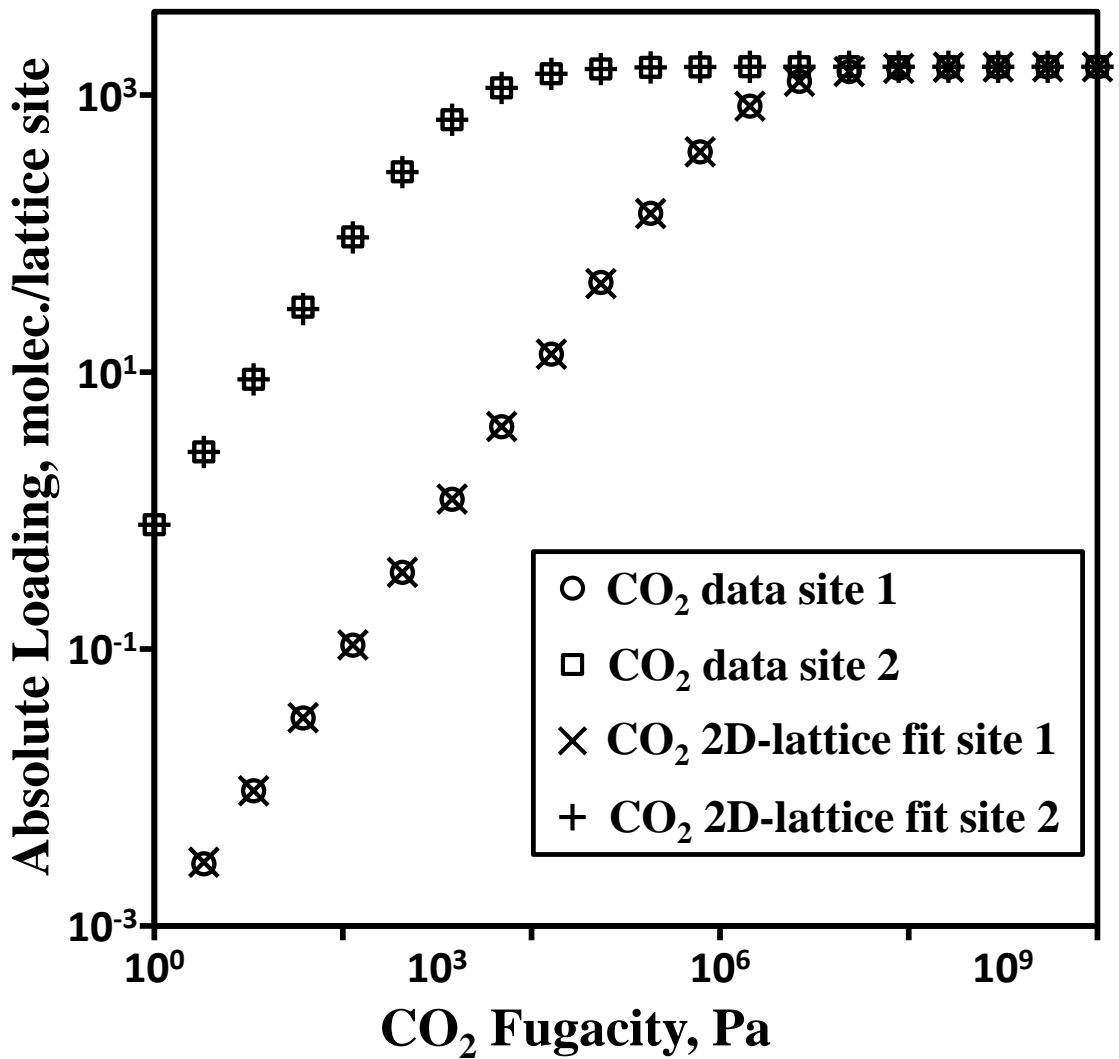


Figure B7. Pure component adsorption isotherm of CO₂ in pure silica hypothetical zeolite PCOD8200029 for two distinct adsorption sites. Circles and squares - data of Swisher and co-workers [27], crosses - fit using the parameterized 2D-lattice model. The values for the 2D-lattice parameters obtained from fitting this dataset are listed in Table B2.

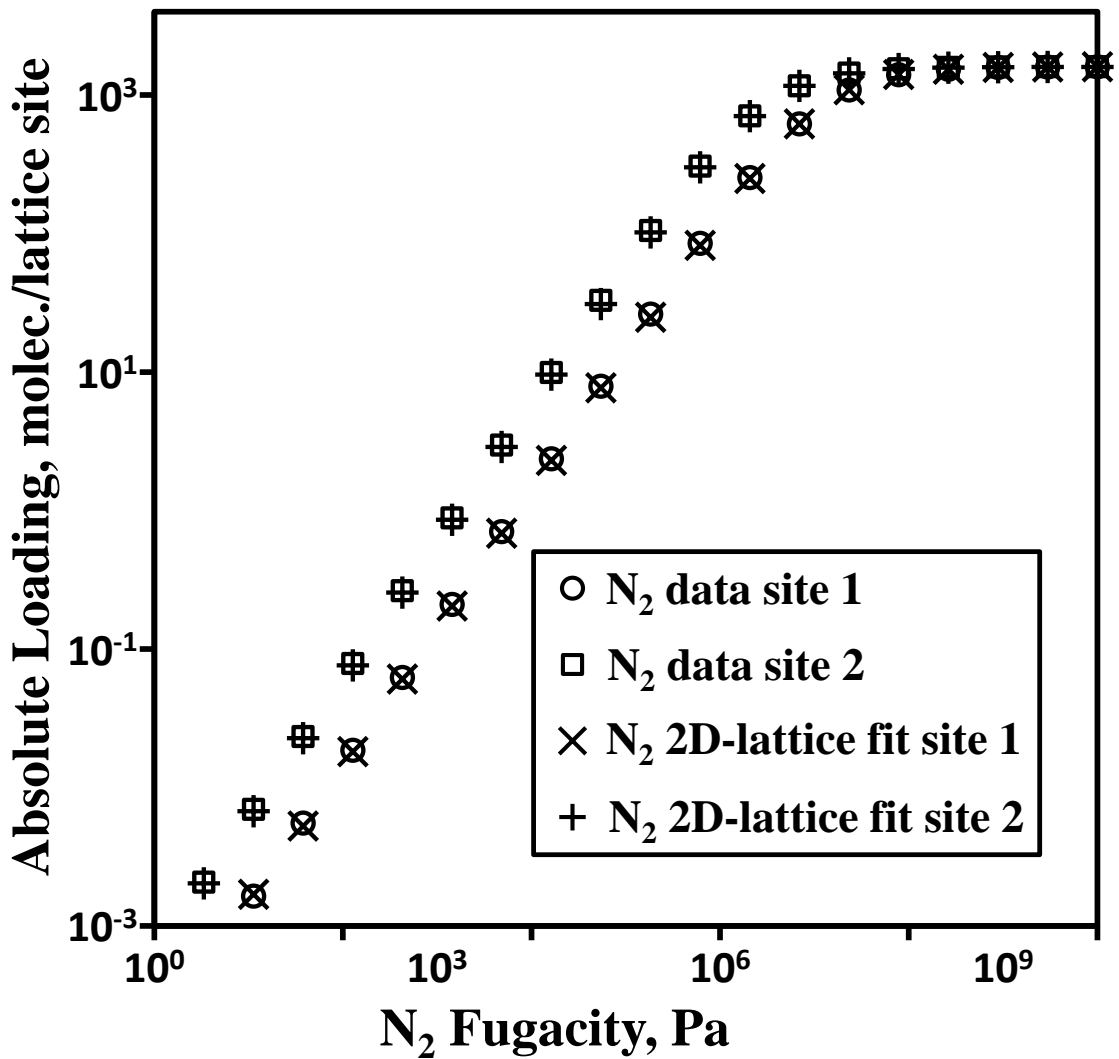


Figure B8. Pure component adsorption isotherm of N₂ in pure silica hypothetical zeolite PCOD8200029 for two distinct adsorption sites. Circles and squares - data of Swisher and co-workers [27], crosses - fit using the parameterized 2D-lattice model. The values for the 2D-lattice parameters obtained from fitting this dataset are listed in Table B2.

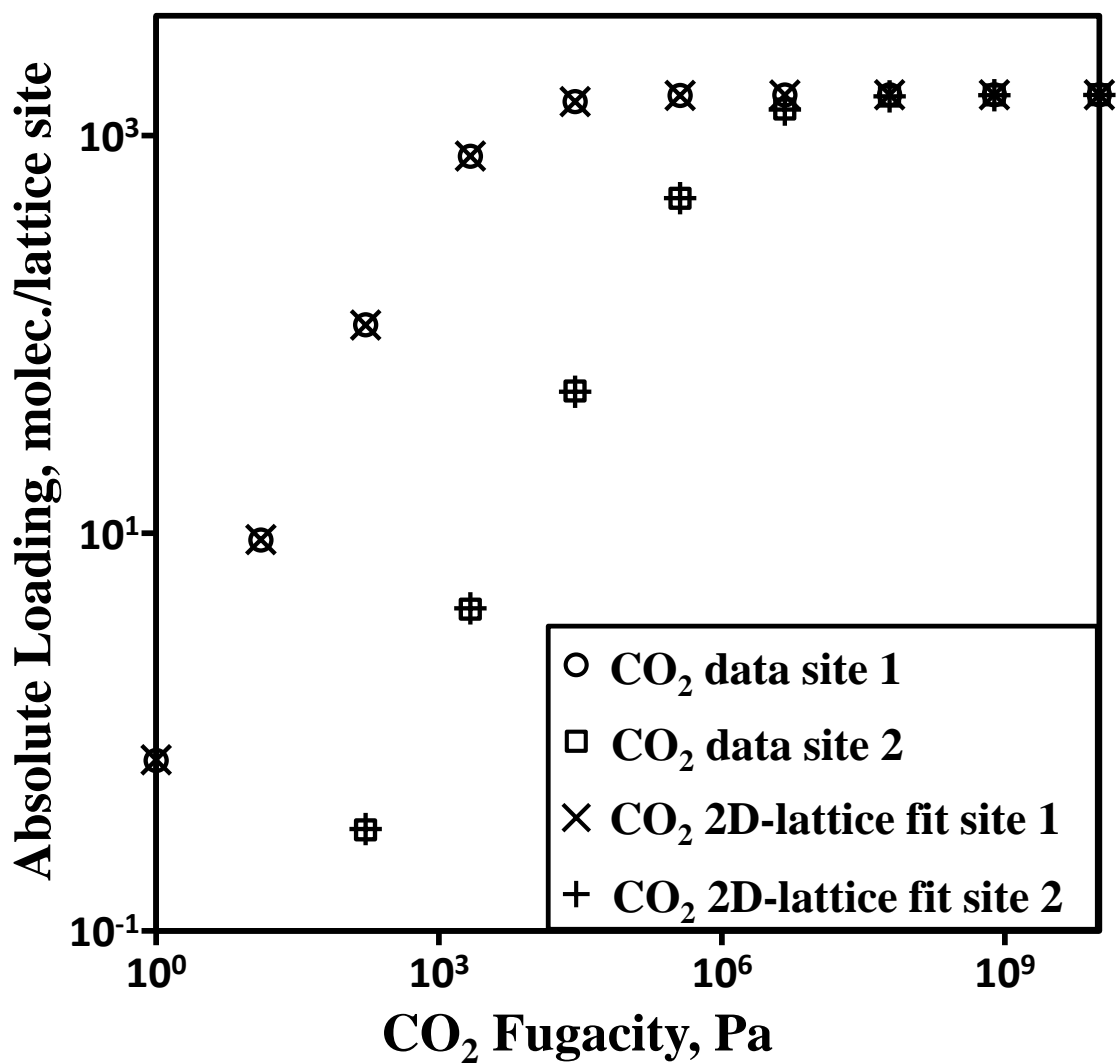


Figure B9. Pure component adsorption isotherm of CO₂ in MOR for two distinct adsorption sites. Circles and squares - data of Swisher and co-workers [27], crosses - fit using the parameterized 2D-lattice model. The values for the 2D-lattice parameters obtained from fitting this dataset are listed in Table B3.

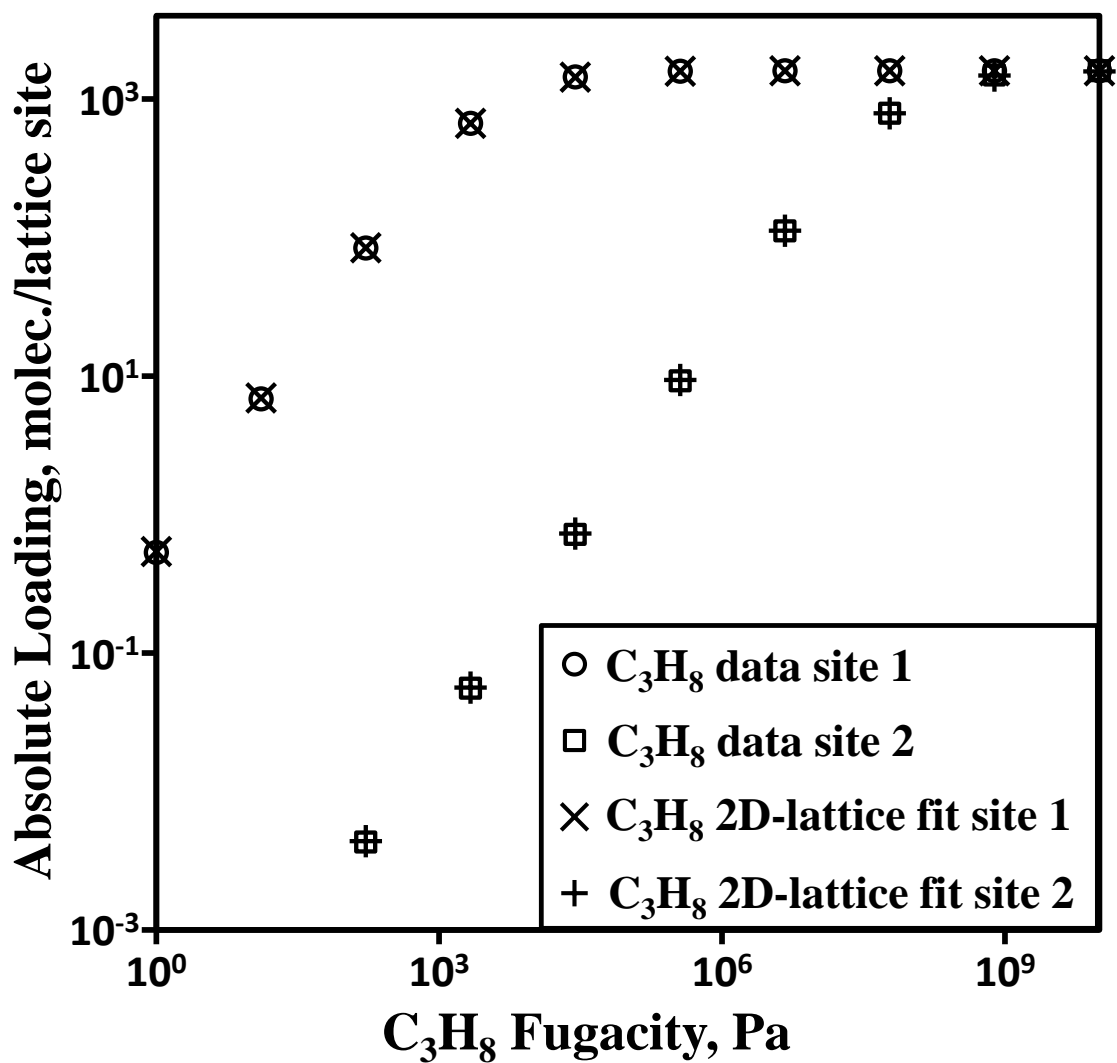


Figure B10. Pure component adsorption isotherm of C_3H_8 in MOR for two distinct adsorption sites. Circles and squares - data of Swisher and co-workers [27], crosses - fit using the parameterized 2D-lattice model. The values for the 2D-lattice parameters obtained from fitting this dataset are listed in Table B3.

Appendix C

Additional Data for Chapter 4

Table C1. Multicomponent Langmuir (ML) parameter values obtained by simultaneously fitting the multicomponent Langmuir model (Eq. 4.3) to experimental binary adsorption data toluene-impurity. q_{mML} - maximum loading parameter, k_{ML} - affinity parameter.

| Compound | q_{mML} , mol/kg | k_{ML} , m ³ /mol |
|----------|--------------------|--------------------------------|
| Bt | 4.98 | $9.51 \cdot 10^{13}$ |
| 2E2H | 3.34 | $1.16 \cdot 10^{13}$ |
| dMc | 3.49 | $1.25 \cdot 10^{13}$ |
| 3Mp | 3.51 | $1.27 \cdot 10^{13}$ |
| 3Ma | 2.97 | $1.47 \cdot 10^{13}$ |
| Tol | 2.65 | $1.85 \cdot 10^{12}$ |

Table C2. Multicomponent dual-site Langmuir (MDSL) parameter values obtained by simultaneously fitting the multicomponent dual-site Langmuir model (Eq. 4.5) to experimental binary adsorption data toluene-impurity. $q_{mMDSL1,2}$ - maximum loading parameter for site 1 and 2; $k_{MDSL1,2}$ - affinity parameter for site 1 and 2.

| Compound | q_{mMDSL1} , mol/kg | q_{mMDSL2} , mol/kg | k_{MDSL1} , m ³ /mol | k_{MDSL2} , m ³ /mol |
|----------|-----------------------|-----------------------|-----------------------------------|-----------------------------------|
| Bt | 1.99 | 2.19 | $1.23 \cdot 10^{14}$ | $1.92 \cdot 10^{14}$ |
| 2E2H | 1.03 | 0.0029 | $1.31 \cdot 10^{14}$ | $1 \cdot 10^5$ |
| dMc | 0.98 | 3.99 | $6.83 \cdot 10^{13}$ | $4.73 \cdot 10^{10}$ |
| 3Mp | 1.23 | 0.043 | $4.87 \cdot 10^{10}$ | $6.82 \cdot 10^{10}$ |
| 3Ma | 0.96 | 0.048 | $2.11 \cdot 10^{11}$ | $1 \cdot 10^{-8}$ |
| Tol | 1.19 | 1.77 | $1.45 \cdot 10^8$ | $1.43 \cdot 10^{11}$ |

Table C3. Dual-site Langmuir (DSL) parameter values obtained by simultaneously fitting the coupled IAST-DSL model (Eqs. 2.3-2.6) to experimental binary adsorption data toluene-impurity. $q_{mDSL1,2}$ - maximum loading parameter for site 1 and 2; $k_{DSL1,2}$ - affinity parameter for site 1 and 2.

| Compound | q_{mDSL1} , mol/kg | q_{mDSL2} , mol/kg | k_{DSL1} , 1/Pa | k_{DSL2} , 1/Pa |
|----------|----------------------|----------------------|-------------------|-------------------|
| Bt | 1 | 3.14 | $9.8 \cdot 10^6$ | $3.47 \cdot 10^6$ |
| 2E2H | 1.87 | 1.19 | $2.82 \cdot 10^6$ | $7.22 \cdot 10^6$ |
| dMc | 1.59 | 1.74 | $2.17 \cdot 10^6$ | $1.44 \cdot 10^6$ |
| 3Mp | 1.2 | 2.47 | $7.26 \cdot 10^6$ | $9.17 \cdot 10^6$ |
| 3Ma | 1.82 | 1.5 | $4.42 \cdot 10^6$ | $3.37 \cdot 10^6$ |
| Tol | 1.98 | 0.68 | $6.65 \cdot 10^6$ | $4.94 \cdot 10^4$ |

Table C4. Langmuir parameter values obtained by simultaneously fitting the coupled SIAST-Langmuir model to experimental binary adsorption data toluene-impurity. $q_{mL1,2}$ - maximum loading parameter for site 1 and 2; $k_{L1,2}$ - affinity parameter for site 1 and 2.

| Compound | q_{mL1} , mol/kg | q_{mL2} , mol/kg | k_{L1} , 1/Pa | k_{L2} , 1/Pa |
|----------|--------------------|--------------------|----------------------|----------------------|
| Bt | 2.57 | 1.56 | $6.4 \cdot 10^{11}$ | $4.74 \cdot 10^5$ |
| 2E2H | 4.99 | 0.69 | $4.83 \cdot 10^3$ | $1.73 \cdot 10^{11}$ |
| dMc | 5 | 0.68 | $1.29 \cdot 10^4$ | $3.49 \cdot 10^{11}$ |
| 3Mp | 2.53 | 0.57 | $6.48 \cdot 10^{11}$ | $3.67 \cdot 10^{11}$ |
| 3Ma | 2.52 | 0.57 | $4.74 \cdot 10^{10}$ | $2.35 \cdot 10^{11}$ |
| Tol | 2.09 | 1.59 | $1.84 \cdot 10^{11}$ | 0.57 |

Table C5. Feed mixture used for obtaining the multicomponent breakthrough curves in Figs. 4.8 and 4.9.

| Compound | Concentration, ppmw |
|----------|---------------------|
| Bt | 1089 |
| 2E2H | 1097 |
| dMc | 1193 |
| 3Mp | 910.5 |
| 3Ma | 1122 |
| Tol | 994588.5 |

Calculation of mixture fugacity coefficients from the generic cubic EOS. The fugacity coefficients can be calculated from the generic cubic equation of state [112]:

$$\ln \hat{\phi}_i = \frac{b_i}{b} (Z - 1) - \ln(Z - \beta) - \bar{q}_i I \quad (C.1)$$

where Z is the compressibility factor and b_i , b , β , \bar{q}_i , and I are parameters specific to each particular EOS [112]. In Eqs. C.1-C.12, the subscript i denotes that the property is for compound i . The parameters without a subscript denote mixture properties. The vapour root of the cubic EOS is [112]:

$$Z = 1 + \beta - q\beta \frac{Z - \beta}{(Z + \beta\varepsilon)(Z + \beta\sigma)} \quad (C.2)$$

and the liquid root of the cubic EOS is [112]:

$$Z = \beta + (Z + \beta\varepsilon)(Z + \beta\sigma) \left(\frac{1 + \beta - Z}{q\beta} \right) \quad (C.3)$$

where q is a parameter specific to each particular EOS; ε and σ are calculated as:

$$\sigma = 1 + \sqrt{2} \quad (C.4)$$

$$\varepsilon = 1 - \sqrt{2} \quad (\text{C.5})$$

In the case of Peng-Robinson EOS, the rest of the parameters can be calculated using the following equations [112]:

$$I = \frac{1}{\sigma - \varepsilon} \ln \left(\frac{Z + \sigma\beta}{Z + \varepsilon\beta} \right) \quad (\text{C.6})$$

$$\bar{q}_i = q \left(1 + \frac{\bar{a}_i}{a} - \frac{b_i}{b} \right), \quad q = \frac{a}{bRT}, \quad \beta = \frac{bP}{RT} \quad (\text{C.7})$$

The mixture parameters a and b are calculated as [112]:

$$a = \sum_i \sum_j x_i x_j a_{ij}, \quad b = \sum_i x_i b_i \quad (\text{C.8})$$

$$a_{ij} = (a_i a_j)^{\frac{1}{2}}, \quad b_i = 0.0778 \frac{RT_c}{P_c} \quad (\text{C.9})$$

The parameter \bar{a}_i is calculated using the following mixing rule [112]:

$$\bar{a}_i = 2 \sum_j x_j \sqrt{a_j a_i} - a \quad (\text{C.10})$$

where x_j is the mole fraction of compound j .

The component specific parameter a_i is calculated as:

$$a_i(T) = 0.45724 \frac{R^2 T_c^2}{P_c} \alpha(T_r, \omega), \quad T_r = \frac{T}{T_c} \quad (\text{C.11})$$

where T is the absolute temperature, R is the gas constant ($\text{m}^3\text{Pa}/\text{mol}/\text{K}$), T_c is the critical temperature (K), P_c is the critical pressure (Pa) and ω is the acentric factor. The parameter $\alpha(T_r, \omega)$ is calculated as [112]:

$$\alpha(T_r, \omega) = \left(1 + (0.37464 + 1.54226\omega - 0.26992\omega^2) \left(1 - T_r^{\frac{1}{2}} \right) \right)^2 \quad (\text{C.12})$$

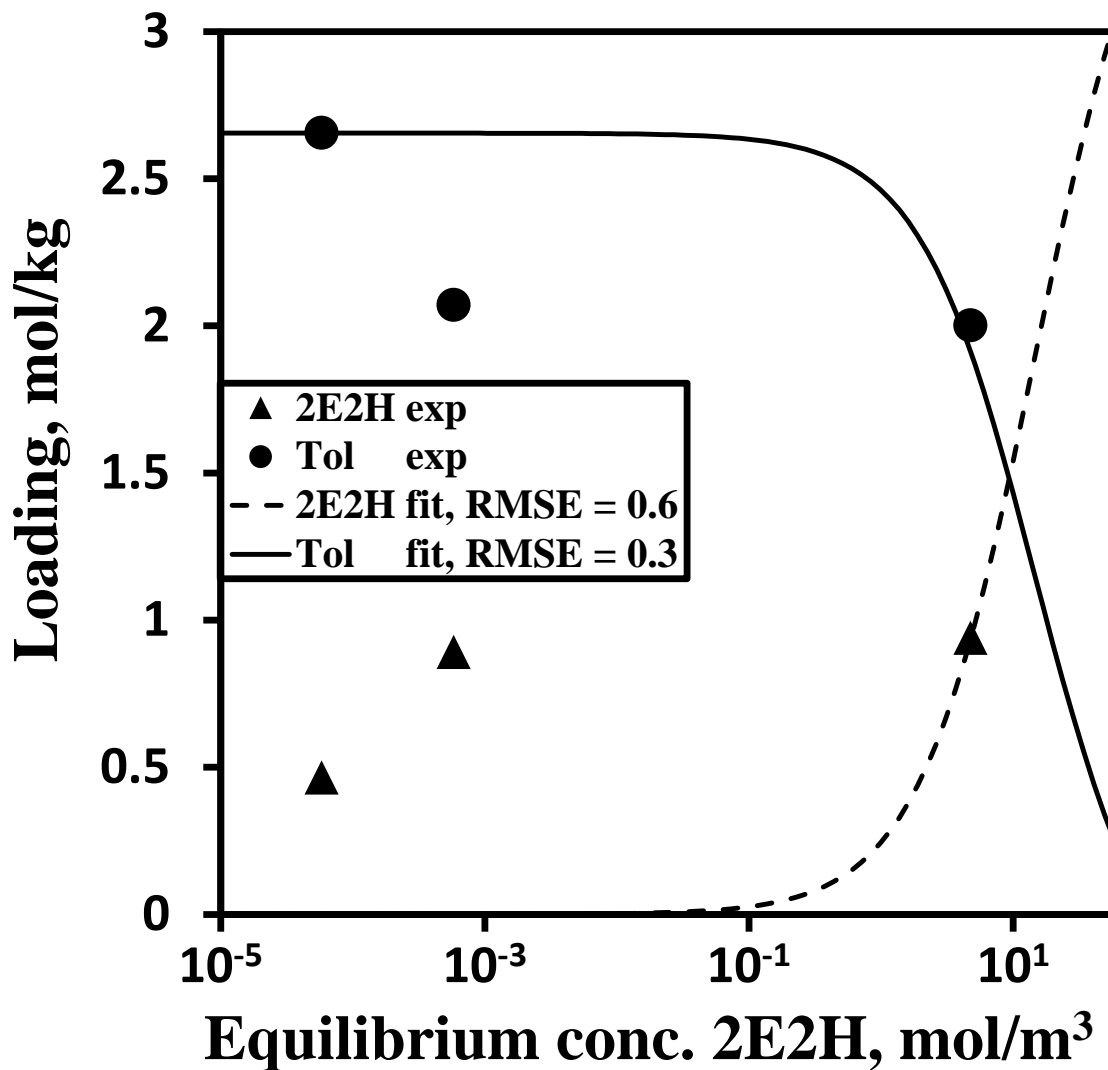


Figure C1. Binary adsorption data for the system toluene - 2-ethyl-2-hexenal (2E2H). Circles - toluene experimental data, triangles - 2-ethyl-2-hexenal experimental data, lines - fit using the multicomponent Langmuir model. RMSE (mol/kg) represents the root mean square error of the fit calculated according to Eq. B4 (Appendix B). The parameters resulting from the fit are listed in Table C1.

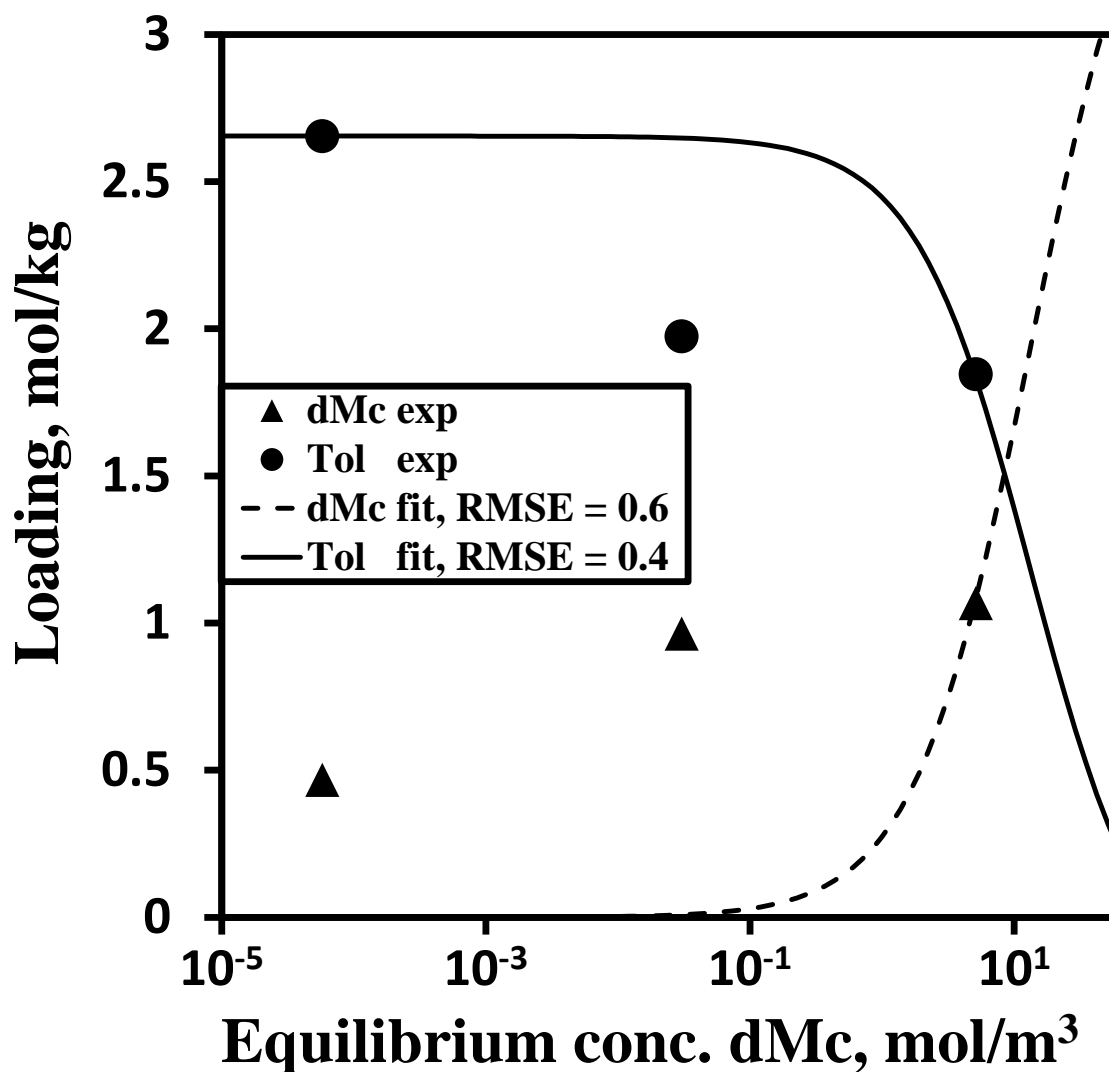


Figure C2. Binary adsorption data for the system toluene-2,6-dimethylcyclohexanone (dMc). Circles - toluene experimental data, triangles - 2,6-dimethylcyclohexanone experimental data, lines - fit using the multicomponent Langmuir model. RMSE (mol/kg) represents the root mean square error of the fit calculated according to Eq. B4 (Appendix B). The parameters resulting from the fit are listed in Table C1.

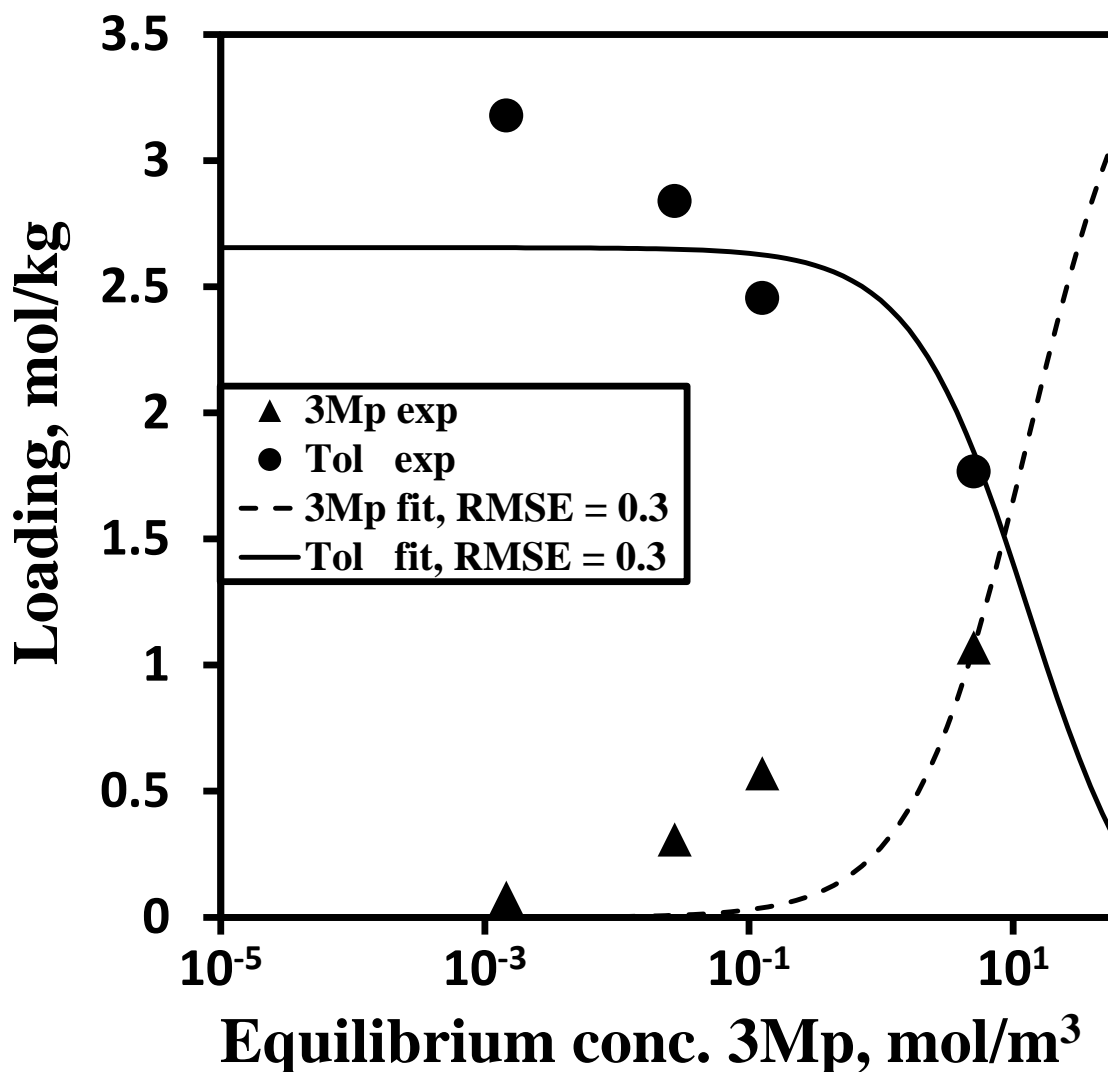


Figure C3. Binary adsorption data for the system toluene - 2,4,6-trimethylphenol (3Mp). Circles - toluene experimental data, triangles - 2,4,6-trimethylphenol experimental data, lines - fit using the multicomponent Langmuir model. RMSE (mol/kg) represents the root mean square error of the fit calculated according to Eq. B4 (Appendix B). The parameters resulting from the fit are listed in Table C1.

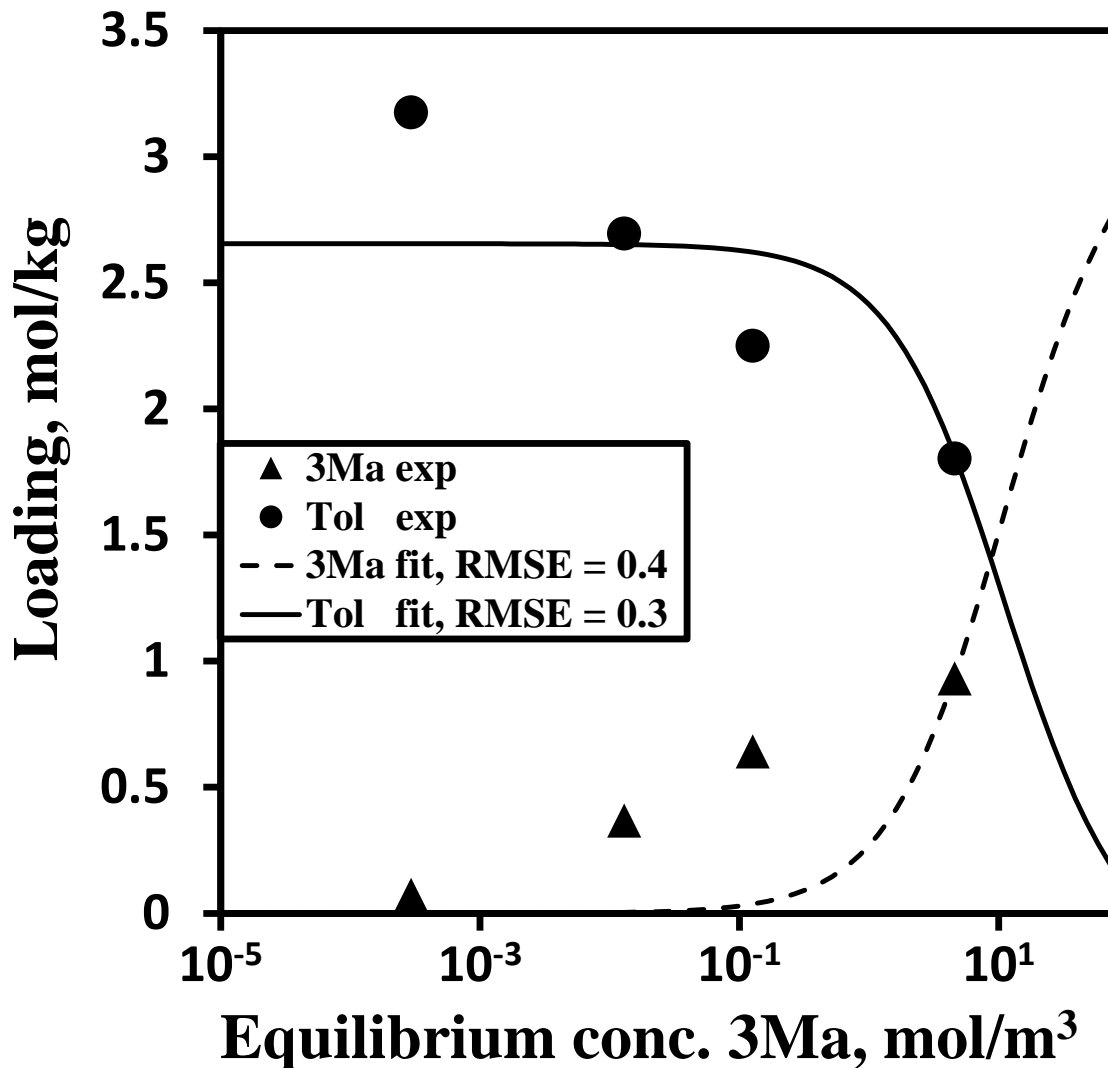


Figure C4. Binary adsorption data for the system toluene - 2,4,6-trimethylanisole (3Ma). Circles - toluene experimental data, triangles - 2,4,6-trimethylanisole experimental data, lines - fit using the multicomponent Langmuir model. RMSE (mol/kg) represents the root mean square error of the fit calculated according to Eq. B4 (Appendix B). The parameters resulting from the fit are listed in Table C1.

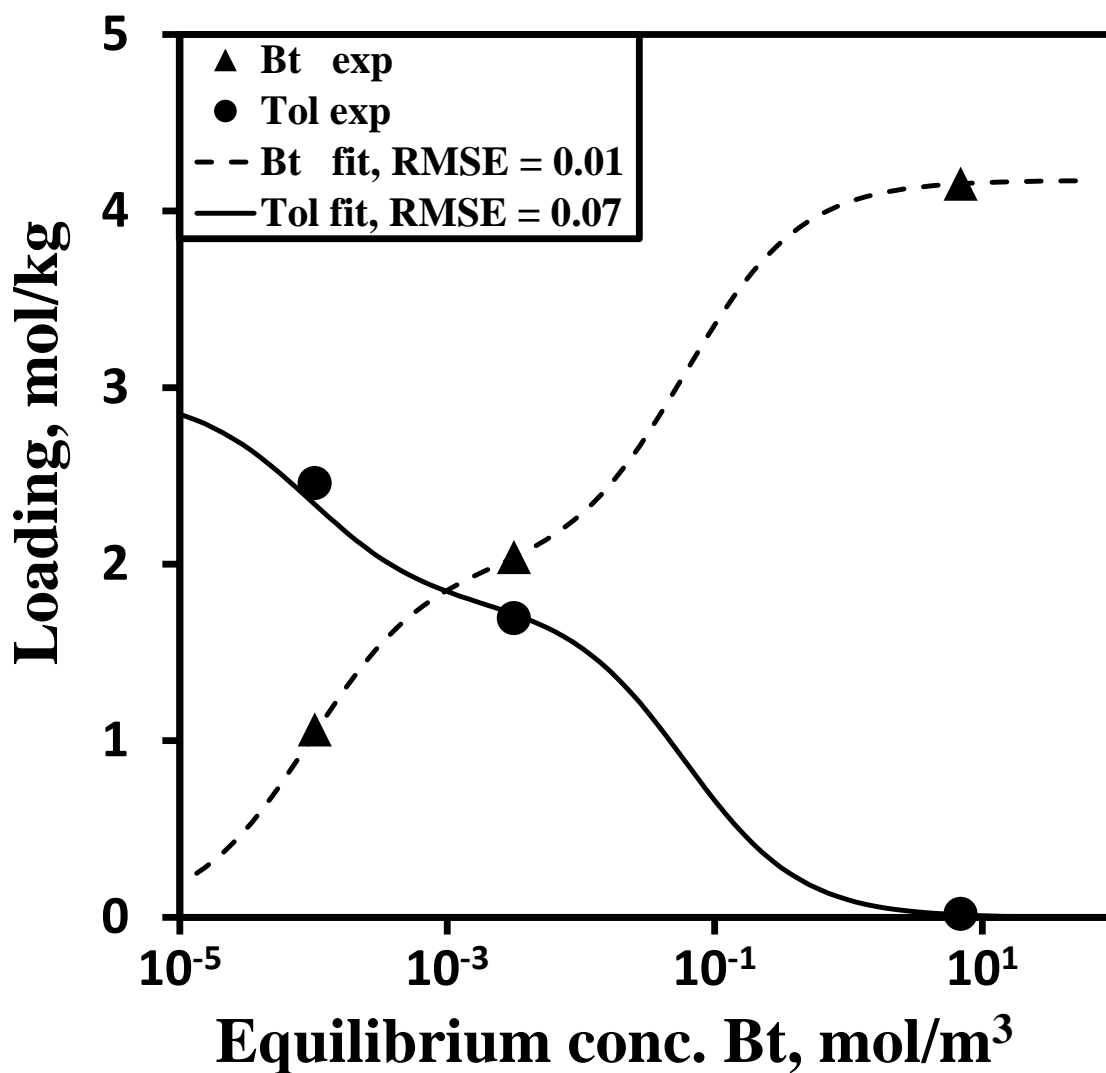


Figure C5. Binary adsorption data for the system toluene-butanal. Circles - toluene (Tol) experimental data, triangles - butanal (Bt) experimental data, lines - fit using the multicomponent dual-site Langmuir model. RMSE (mol/kg) represents the root mean square error of the fit calculated according to Eq. B4 (Appendix B). The parameters resulting from the fit are listed in Table C2.

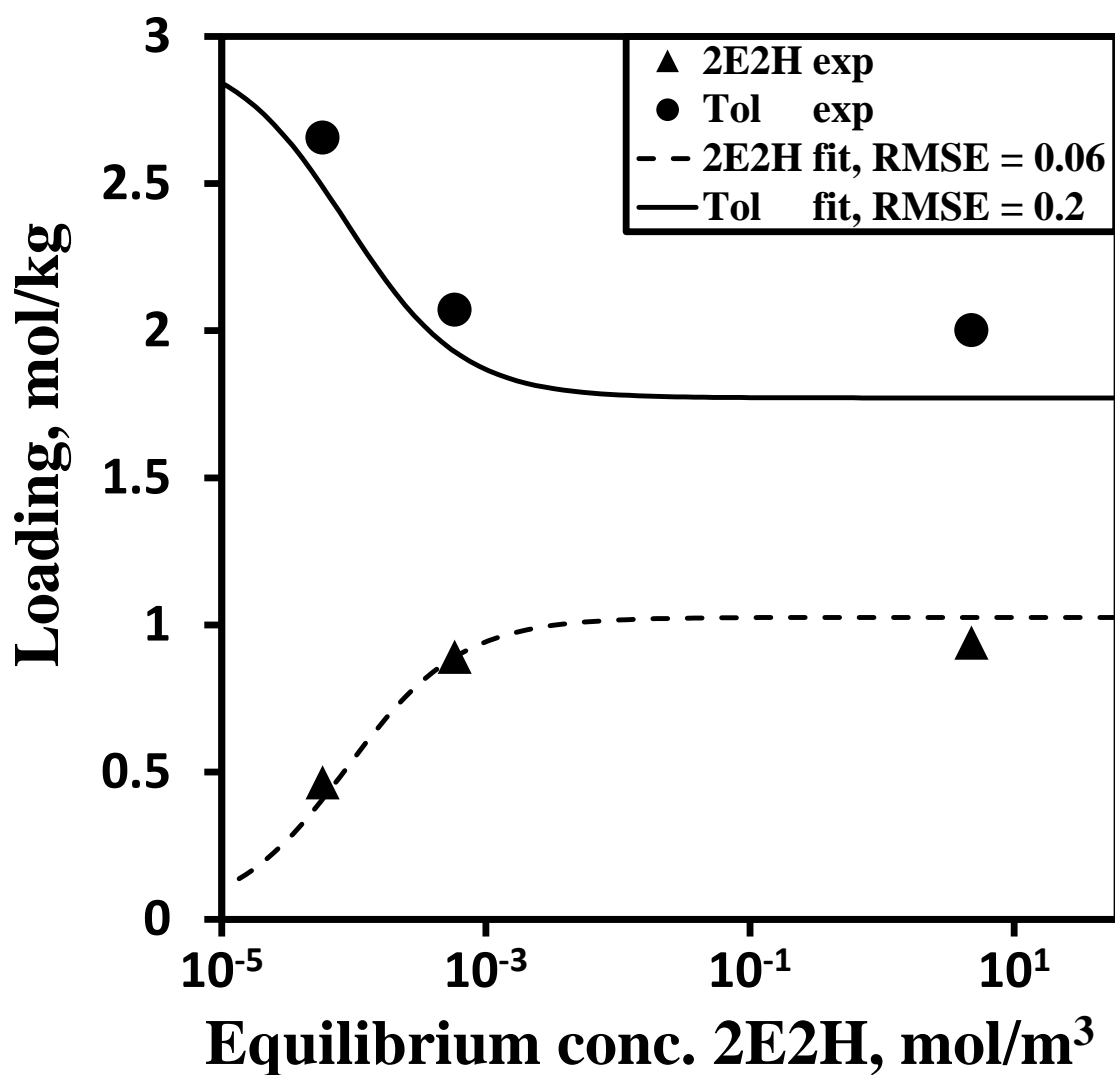


Figure C6. Binary adsorption data for the system toluene - 2-ethyl-2-hexenal. Circles - toluene (Tol) experimental data, triangles - 2-ethyl-2-hexenal (2E2H) experimental data, lines - fit using the multicomponent dual-site Langmuir model. RMSE (mol/kg) represents the root mean square error of the fit calculated according to Eq. B4 (Appendix B). The parameters resulting from the fit are listed in Table C2.

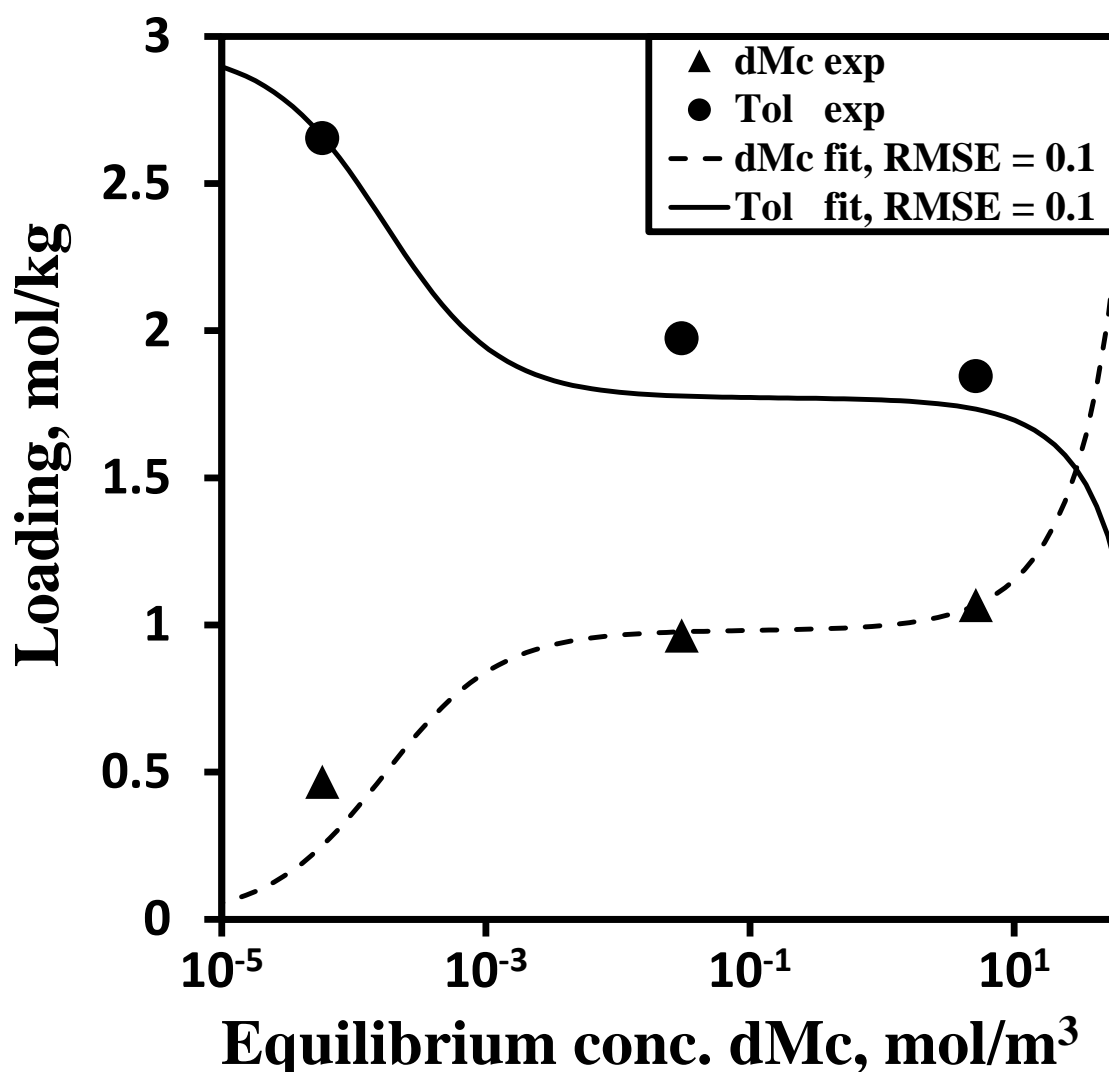


Figure C7. Binary adsorption data for the system toluene - 2,6-dimethylcyclohexanone. Circles - toluene (Tol) experimental data, triangles - 2,6-dimethylcyclohexanone (dMc) experimental data, lines - fit using the multicomponent dual-site Langmuir model. RMSE (mol/kg) represents the root mean square error of the fit calculated according to Eq. B4 (Appendix B). The parameters resulting from the fit are listed in Table C2.

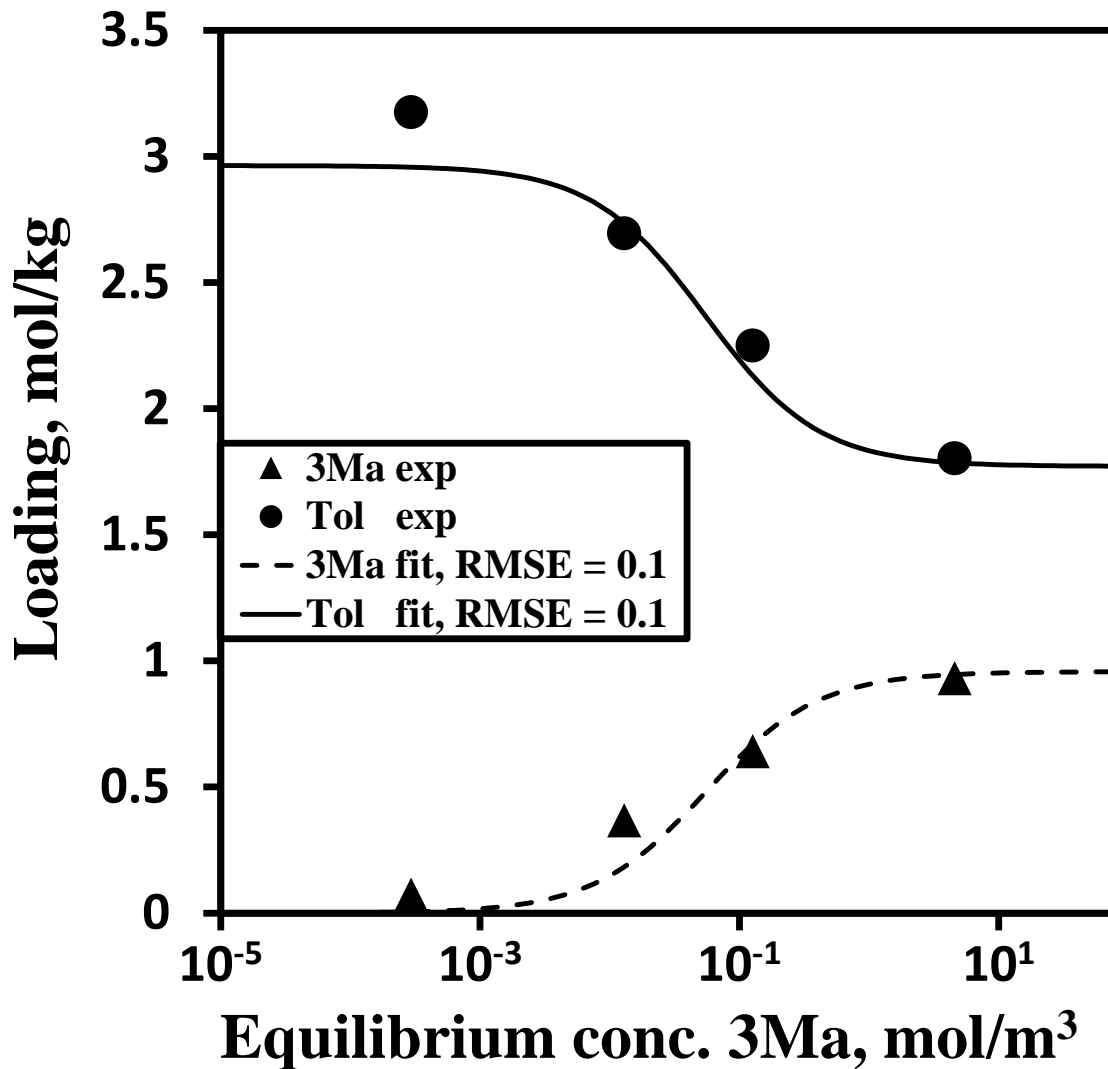


Figure C8. Binary adsorption data for the system toluene - 2,4,6-trimethylanisole. Circles - toluene (Tol) experimental data, triangles - 2,4,6-trimethylanisole (3Ma) experimental data, lines - fit using the multicomponent dual-site Langmuir model. RMSE (mol/kg) represents the root mean square error of the fit calculated according to Eq. B4 (Appendix B). The parameters resulting from the fit are listed in Table C2.

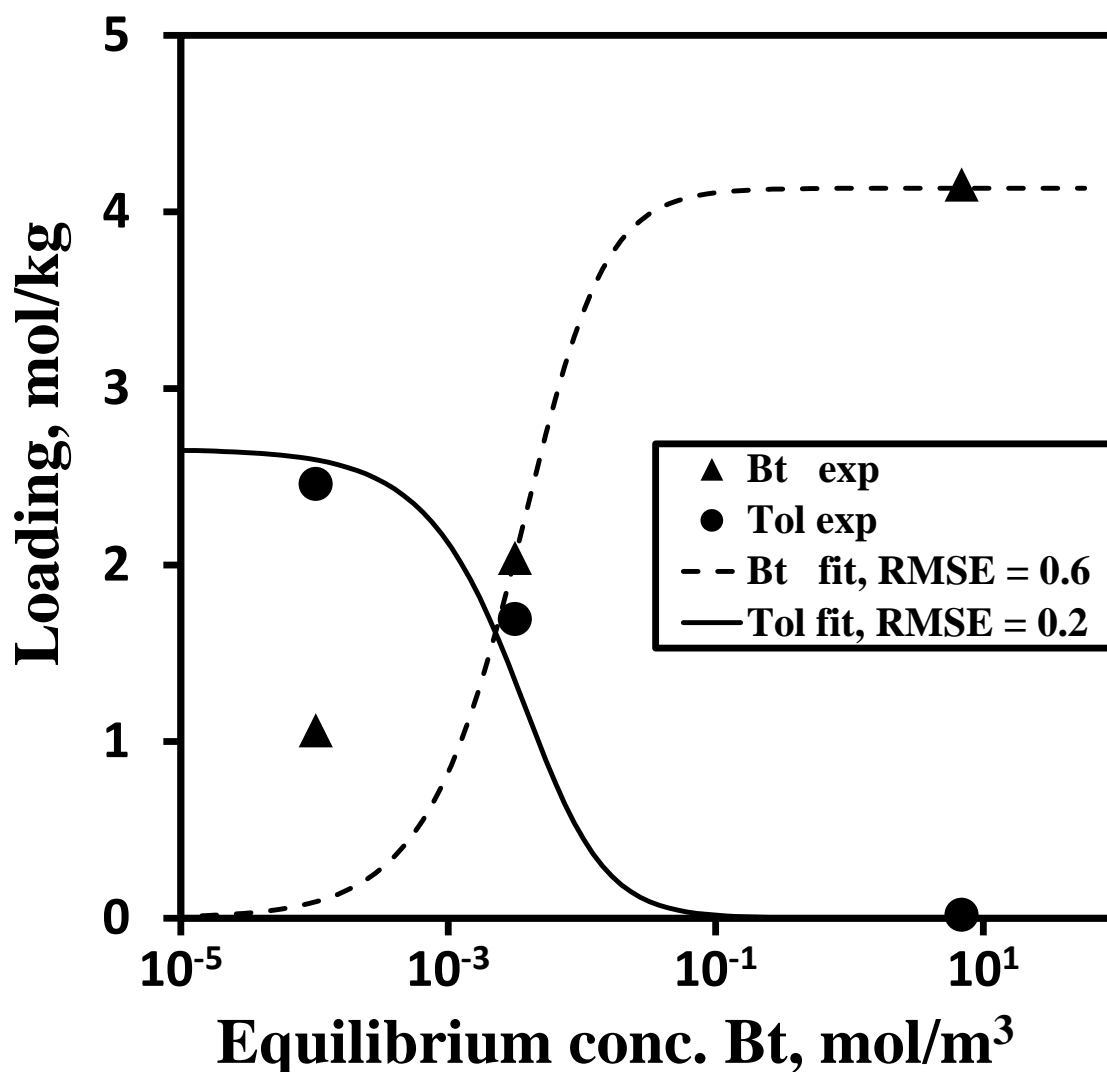


Figure C9. Binary adsorption data for the system toluene - butanal. Circles - toluene (Tol) experimental data, triangles - butanal (Bt) experimental data, lines - fit using the coupled IAST - dual-site Langmuir model. RMSE (mol/kg) represents the root mean square error of the fit calculated according to Eq. B4 (Appendix B). The parameters resulting from the fit are listed in Table C3.

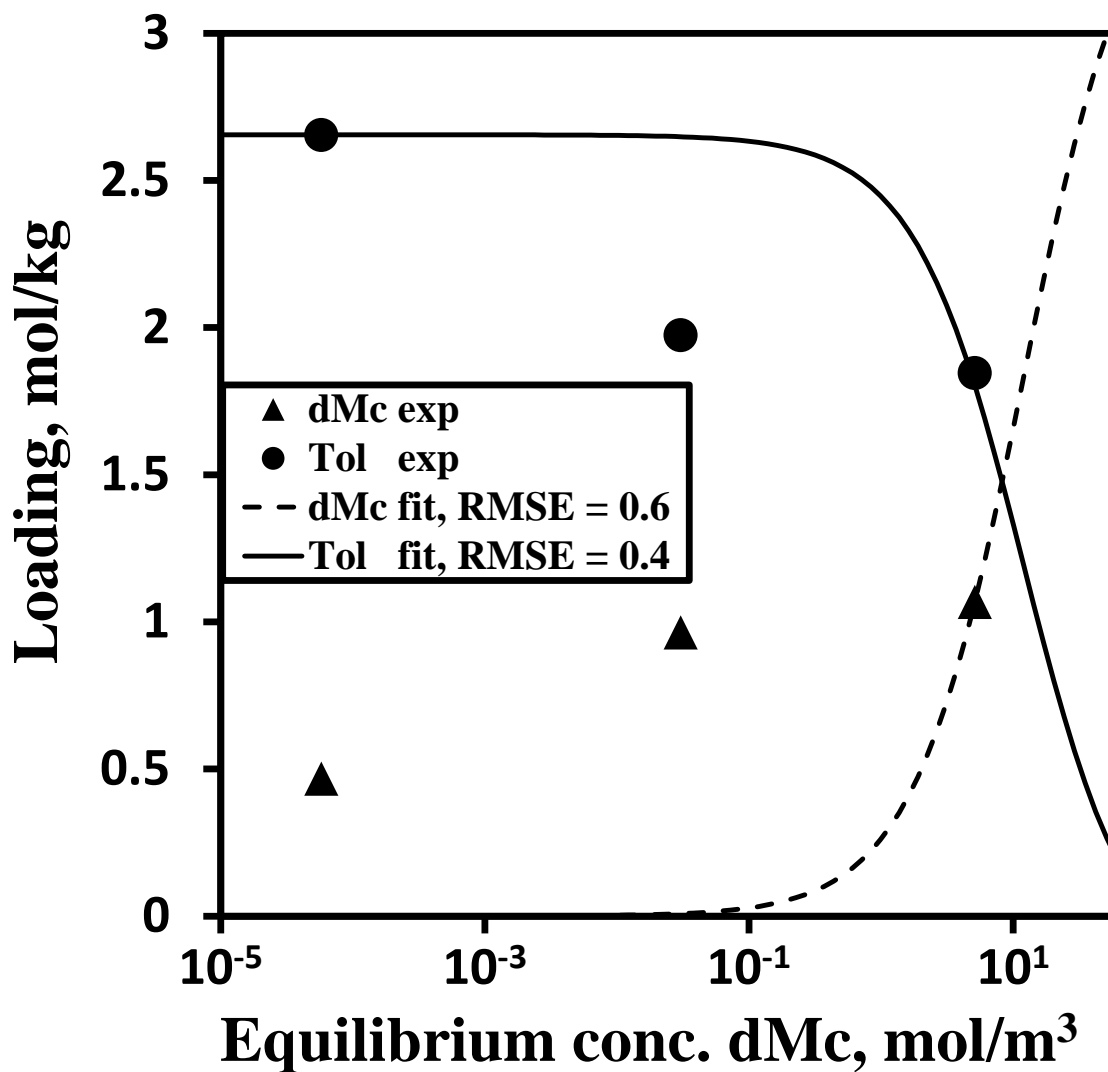


Figure C10. Binary adsorption data for the system toluene - 2,6-dimethylcyclohexanone. Circles - toluene (Tol) experimental data, triangles - 2,6-dimethylcyclohexanone (dMc) experimental data, lines - fit using the coupled IAST - dual-site Langmuir model. RMSE (mol/kg) represents the root mean square error of the fit calculated according to Eq. B4 (Appendix B). The parameters resulting from the fit are listed in Table C3.

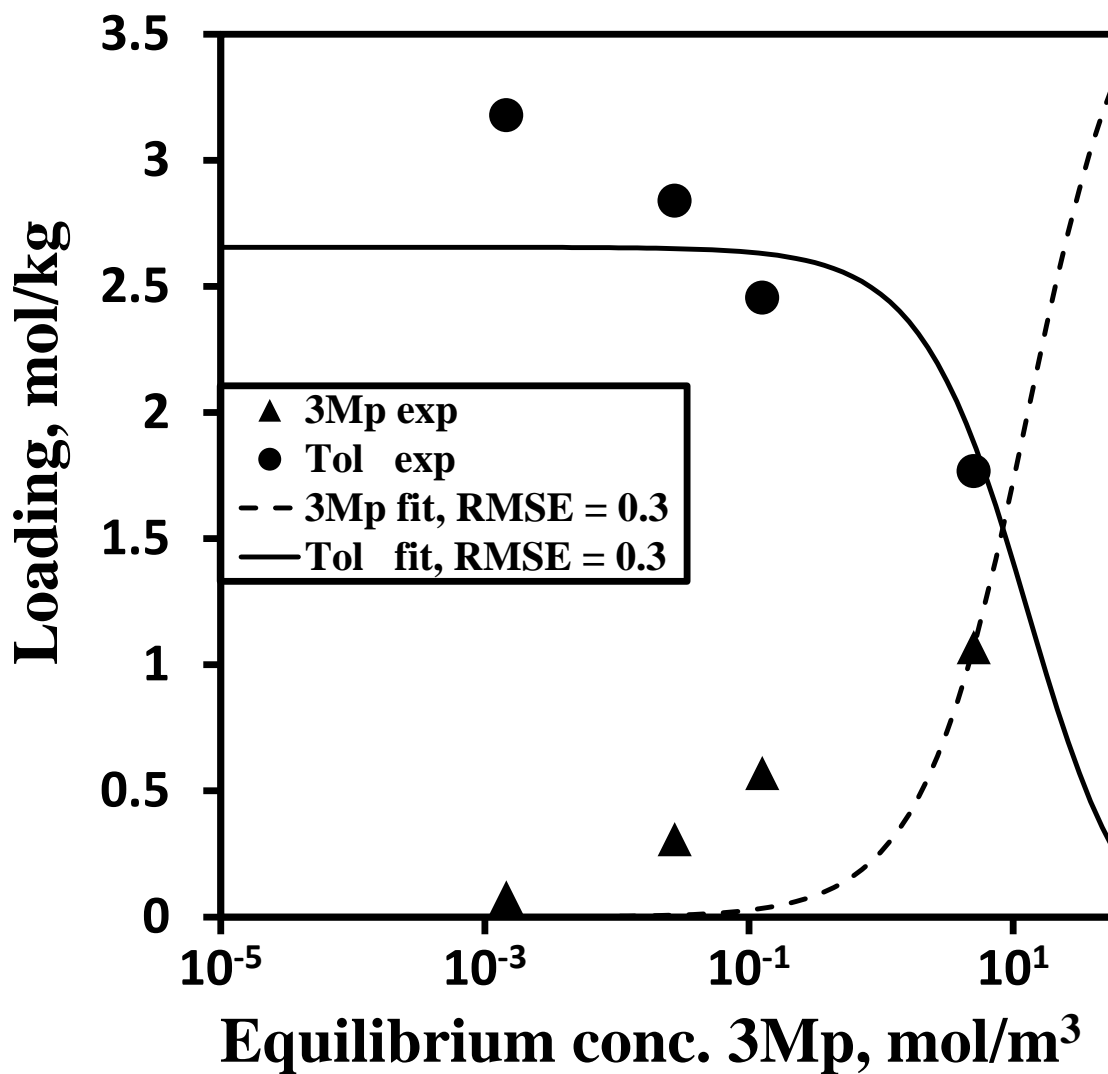


Figure C11. Binary adsorption data for the system toluene - 2,4,6-trimethylphenol. Circles - toluene (Tol) experimental data, triangles - 2,4,6-trimethylphenol (3Mp) experimental data, lines - fit using the coupled IAST - dual-site Langmuir model. RMSE (mol/kg) represents the root mean square error of the fit calculated according to Eq. B4 (Appendix B). The parameters resulting from the fit are listed in Table C3.

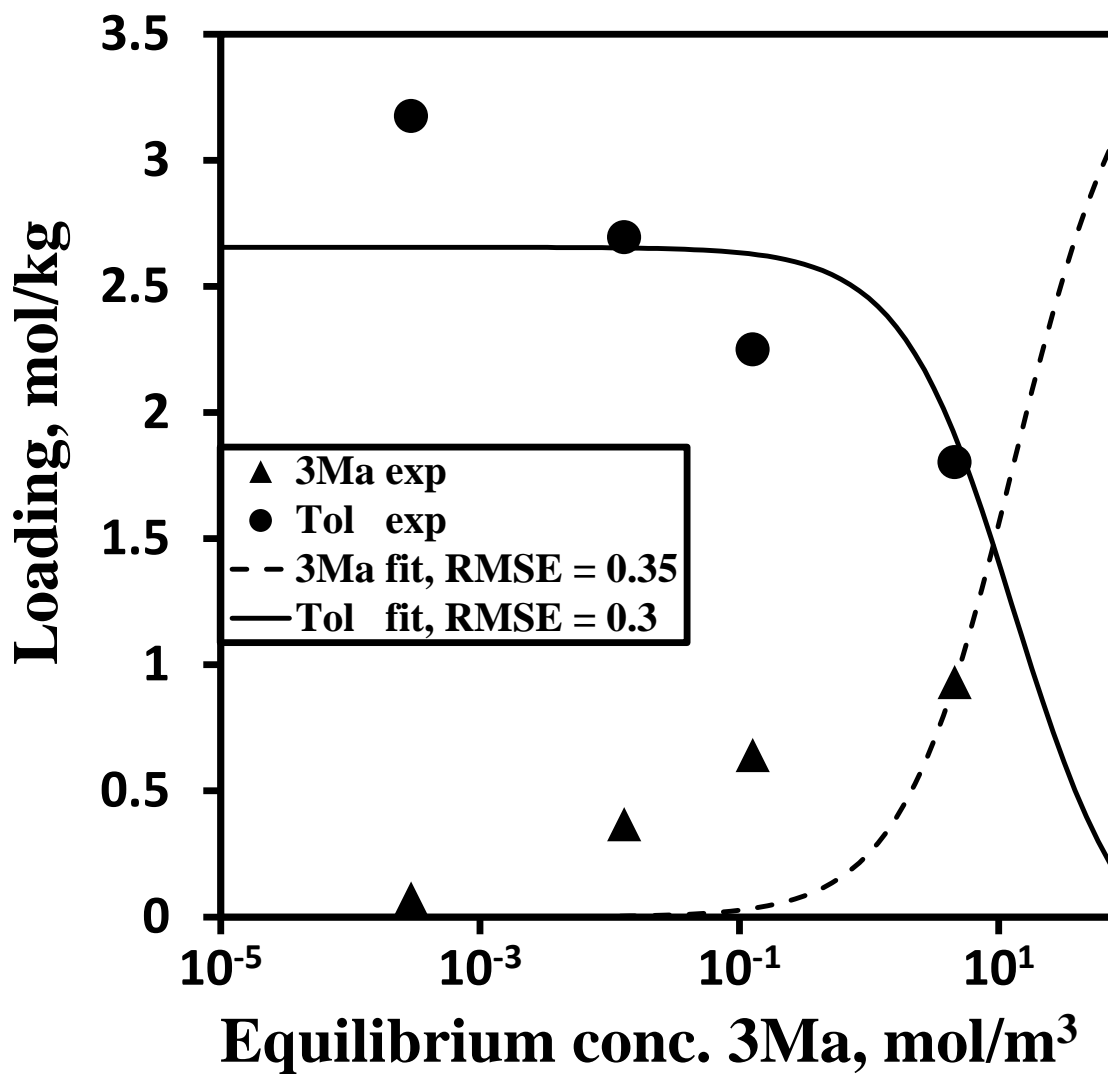


Figure C12. Binary adsorption data for the system toluene - 2,4,6-trimethylanisole. Circles - toluene (Tol) experimental data, triangles - 2,4,6-trimethylanisole (3Ma) experimental data, lines - fit using the coupled IAST - dual-site Langmuir model. RMSE (mol/kg) represents the root mean square error of the fit calculated according to Eq. B4 (Appendix B). The parameters resulting from the fit are listed in Table C3.

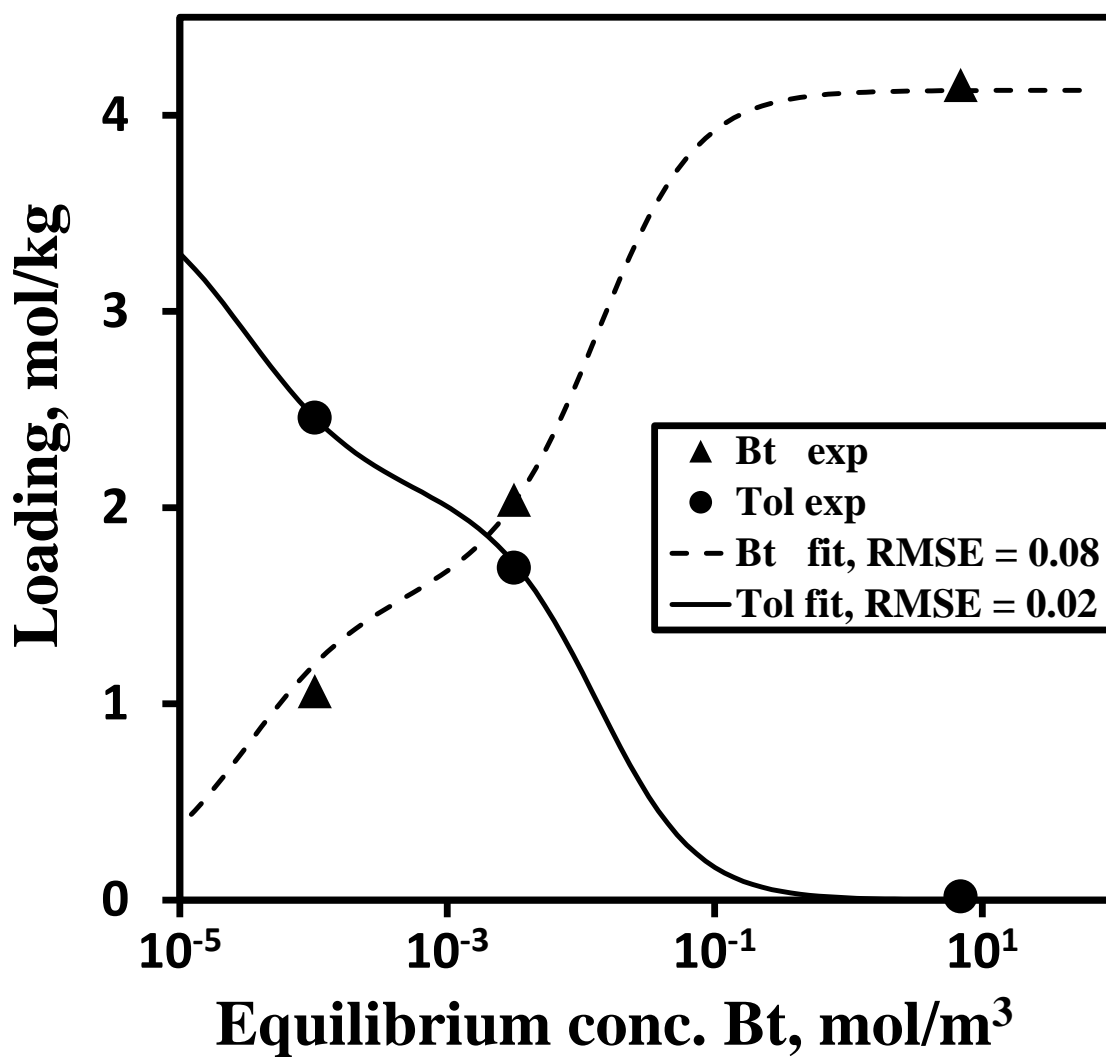


Figure C13. Binary adsorption data for the system toluene - butanal. Circles - toluene (Tol) experimental data, triangles - butanal (Bt) experimental data, lines - fit using the coupled SIAST - Langmuir model. RMSE (mol/kg) represents the root mean square error of the fit calculated according to Eq. B4 (Appendix B). The parameters resulting from the fit are listed in Table C4.

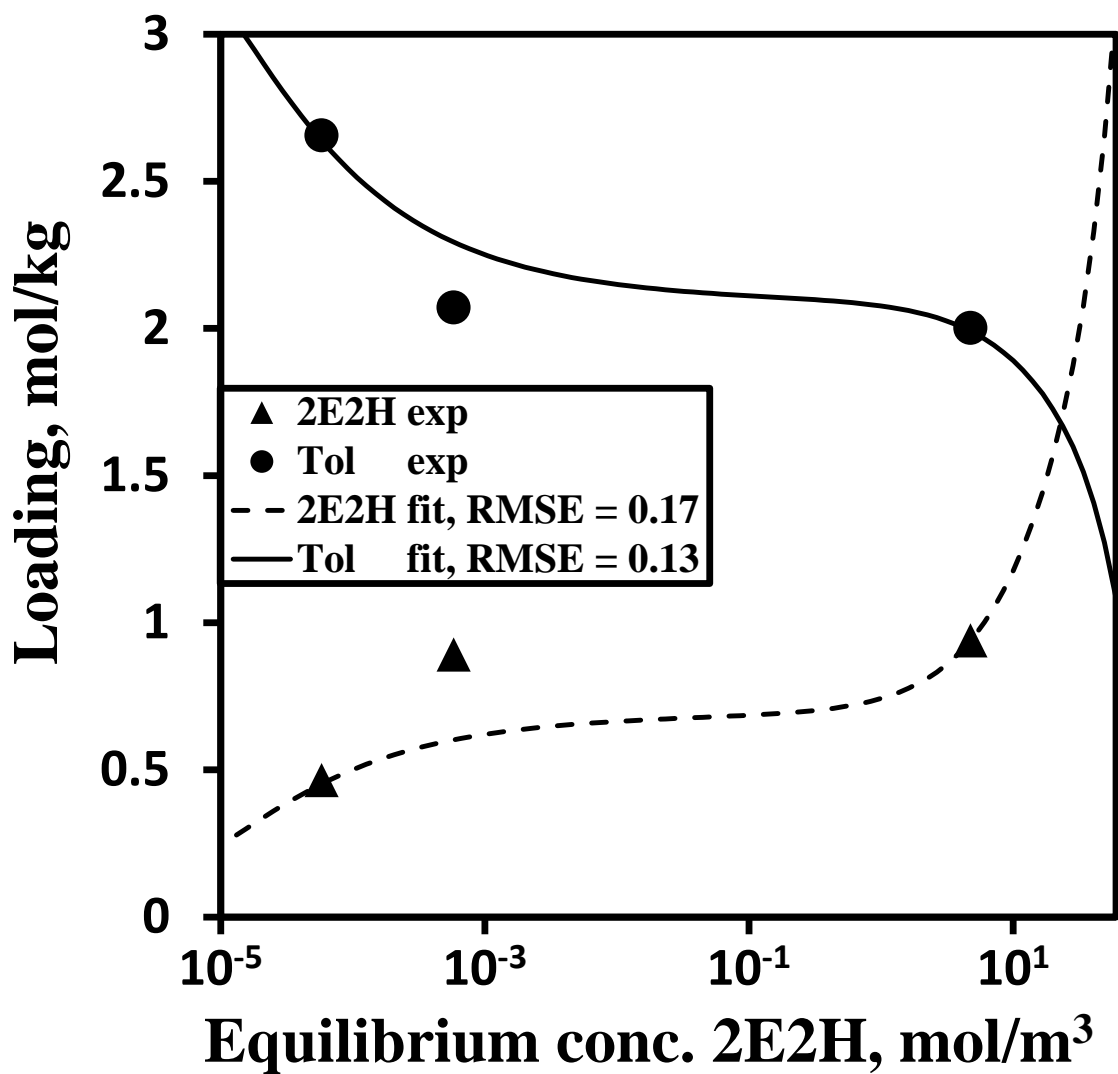


Figure C14. Binary adsorption data for the system toluene - 2-ethyl-2-hexenal. Circles - toluene (Tol) experimental data, triangles - 2-ethyl-2-hexenal (2E2H) experimental data, lines - fit using the coupled SIAST - Langmuir model. RMSE (mol/kg) represents the root mean square error of the fit calculated according to Eq. B4 (Appendix B). The parameters resulting from the fit are listed in Table C4.

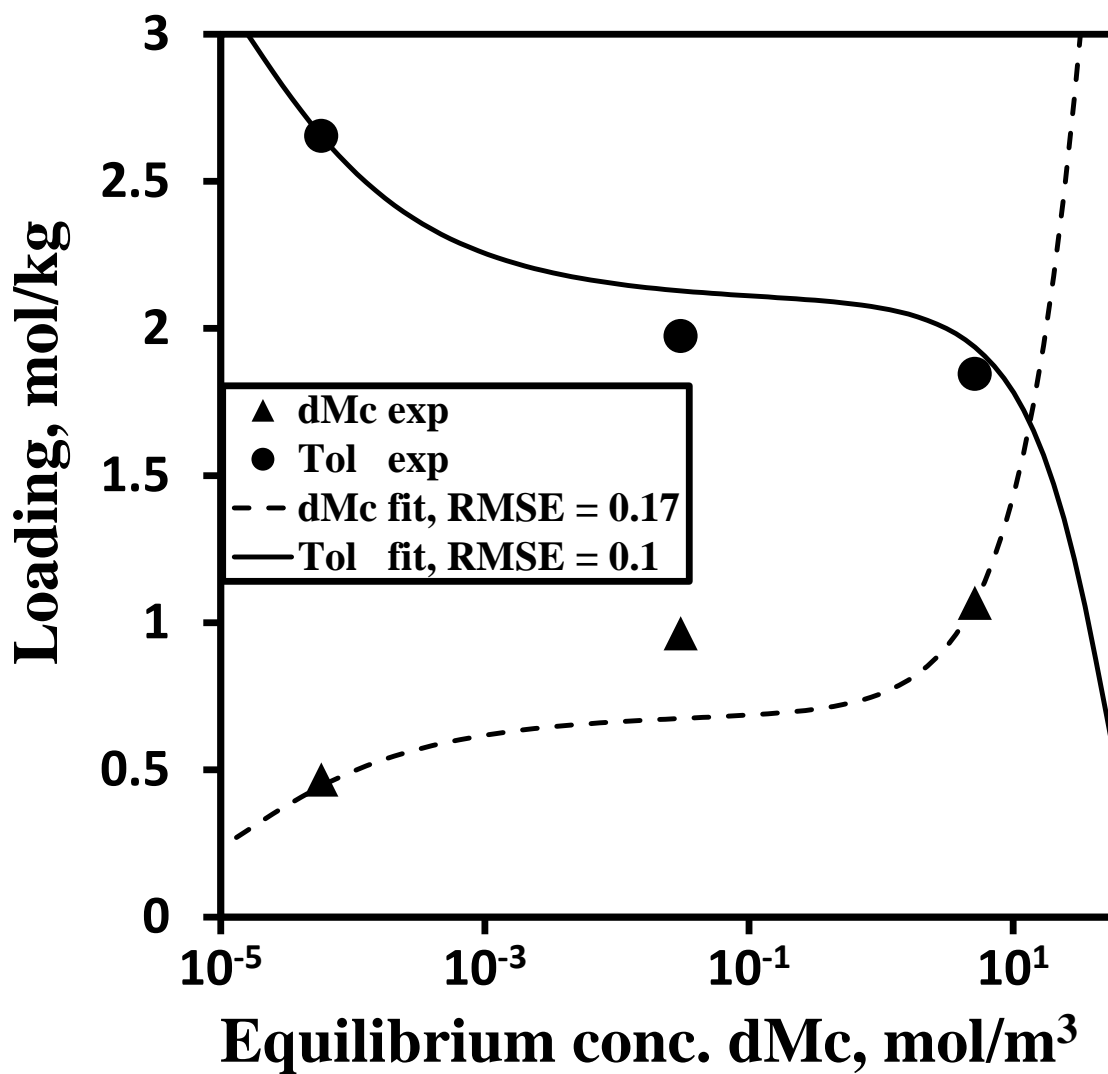


Figure C15. Binary adsorption data for the system toluene - 2,6-dimethylcyclohexanone. Circles - toluene (Tol) experimental data, triangles - 2,6-dimethylcyclohexanone (dMc) experimental data, lines - fit using the coupled SIAST - Langmuir model. RMSE (mol/kg) represents the root mean square error of the fit calculated according to Eq. B4 (Appendix B). The parameters resulting from the fit are listed in Table C4.

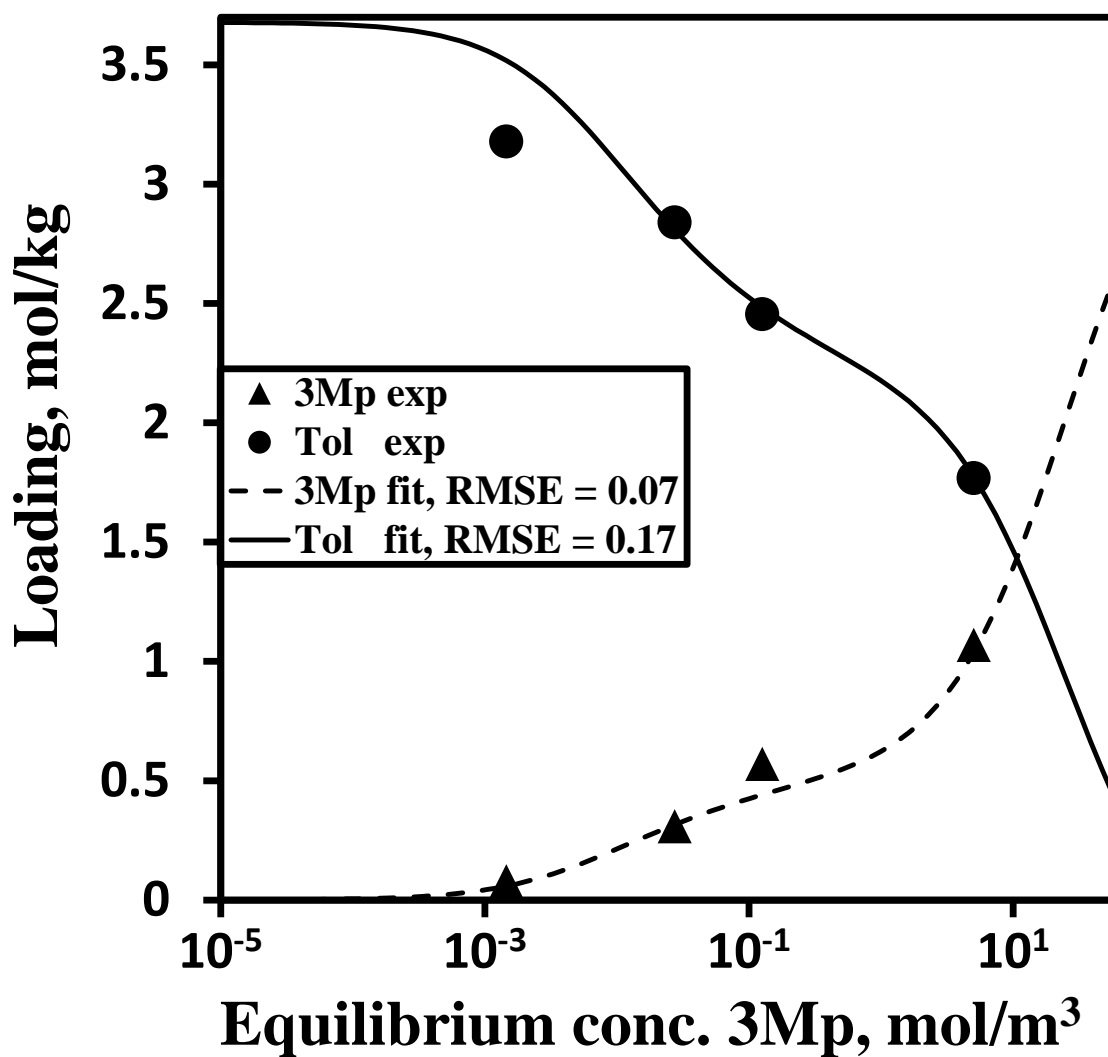


Figure C16. Binary adsorption data for the system toluene - 2,4,6-trimethylphenol. Circles - toluene (Tol) experimental data, triangles - 2,4,6-trimethylphenol (3Mp) experimental data, lines - fit using the coupled SIAST - Langmuir model. RMSE (mol/kg) represents the root mean square error of the fit calculated according to Eq. B4 (Appendix B). The parameters resulting from the fit are listed in Table C4.

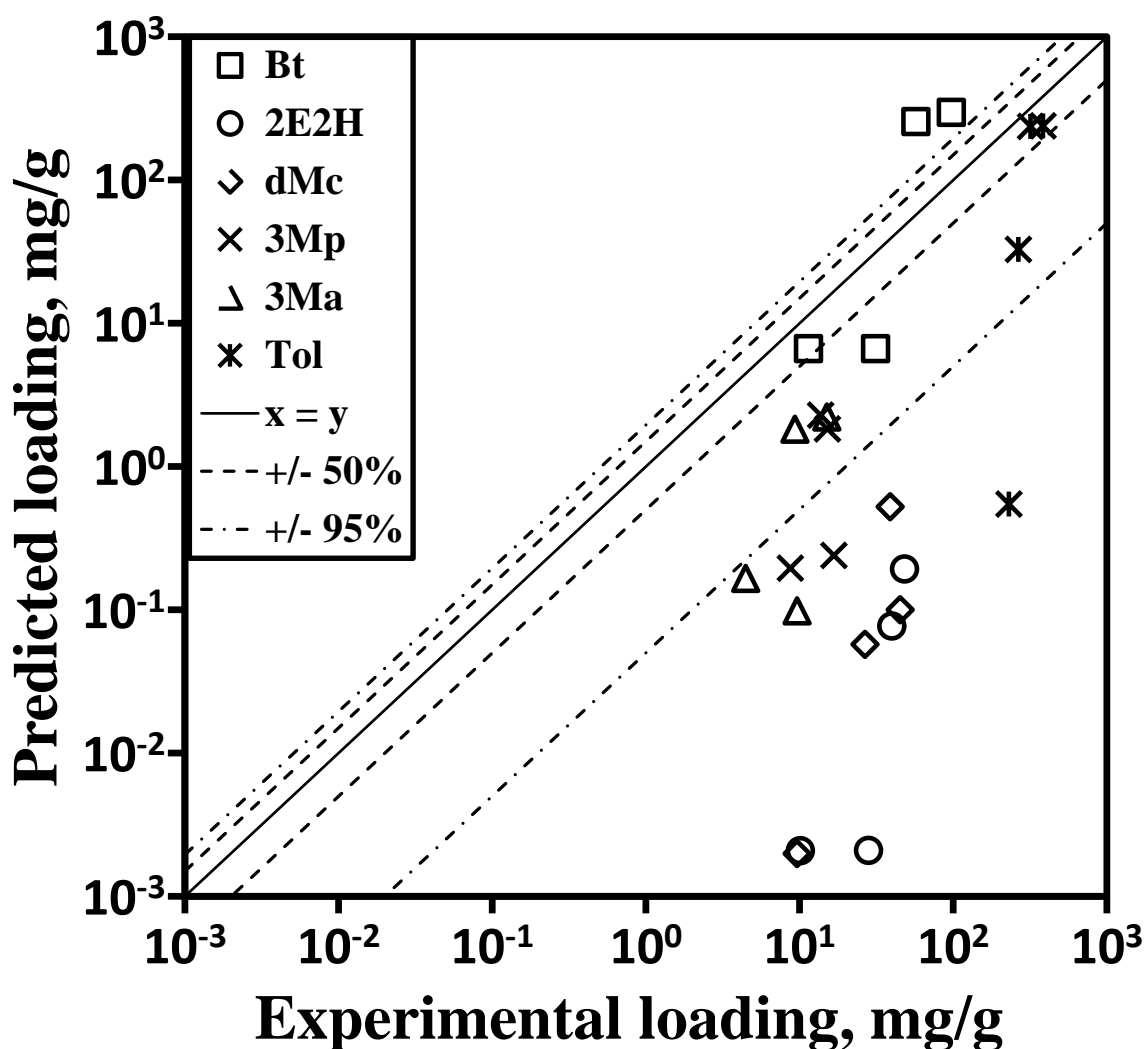


Figure C17. Experimental vs predicted multicomponent adsorption isotherms in zeolite Y for impurities in liquid toluene. The predicted data was obtained using the coupled IAST - dual-site Langmuir model. Squares - butanal, circles - 2-ethyl-2-hexenal, diamonds - 2,6-dimethylcyclohexanone, crosses - 2,4,6-trimethylphenol, triangles - 2,4,6-trimethylanisole, stars - toluene. The dashed and dotted lines represent the plus/minus 50% and respectively 90% deviation lines.

Bibliography

- [1] S. Xian, Y. Yu, J. Xiao, Z. Zhang, Q. Xia, H. Wang, Z. Li, *Competitive adsorption of water vapor with VOCs dichloroethane, ethyl acetate and benzene on MIL-101(Cr) in humid atmosphere*. Rsc Advances, 2015. 5: p. 1827-1834.
- [2] K.N. Gupta, N.J. Rao, G.K. Agarwal, *Gaseous phase adsorption of volatile organic compounds on granular activated carbon*. Chemical Engineering Communications, 2015. 202: p. 384-401.
- [3] L. Zhou, Y.L. Chen, X.H. Zhang, F.M. Tian, Z.N. Zu, *Zeolites developed from mixed alkali modified coal fly ash for adsorption of volatile organic compounds*. Materials Letters, 2014. 119: p. 140-142.
- [4] S.M. Yakout, *Removal of the hazardous, volatile, and organic compound benzene from aqueous solution using phosphoric acid activated carbon from rice husk*. Chemistry Central Journal, 2014. 8: p. 52-58.
- [5] S.M. Saqer, D.I. Kondarides, X.E. Verykios, *Catalytic oxidation of toluene over binary mixtures of copper, manganese and cerium oxides supported on g- Al_2O_3* . Appl. Catal., B, 2011. 103: p. 275-286.
- [6] P. Kolar, J.R. Kastner, *Low-temperature catalytic oxidation of aldehyde mixtures using wood fly ash: kinetics, mechanism, and effect of ozone*. Chemosphere, 2010. 78: p. 1110-1115.
- [7] A. Fullana, A.A. Carbonell-Barrachina, S. Sidhu, *Volatile aldehyde emissions from heated cooking oils*. J. Sci. Food Agric., 2004. 84: p. 2015-2021.
- [8] J.R. Kastner, K.C. Das, *Wet scrubber analysis of volatile organic compound removal in the rendering industry*. Journal of the Air & Waste Management Association, 2002. 52: p. 459-469.

- [9] M.G.D. Baumann, L.F. Lorenz, S.A. Batterman, G.Z. Zhang, *Aldehyde emissions from particleboard and medium density fiberboard products*. Forest Products Journal, 2000. 50: p. 75-82.
- [10] D.M. Ruthven, *Principles of adsorption and adsorption processes*. 1984, New-York: Wiley-Interscience. 2nd edition.
- [11] F. Rouquerol, J. Rouquerol, K. Sing, *Adsorption by powders and porous solids*. 1999, Marseille, France: Academic Press. 1st edition.
- [12] M.A. Monsalvo, A.A. Shapiro, *Modeling adsorption of binary and ternary mixtures on microporous media*. Fluid Phase Equilibria, 2007. 254: p. 91-100.
- [13] S. Bartholdy, M.G. Bjorner, E. Solbraa, A. Shapiro, G.M. Kontogeorgis, *Capabilities and limitations of predictive engineering theories for multicomponent adsorption*. Industrial & Engineering Chemistry Research, 2013. 52: p. 11552-11563.
- [14] H.O.R. Landa, D. Flockerzi, A. Seidel-Morgenstern, *A method for efficiently solving the IAST equations with an application to adsorber dynamics*. AIChE Journal, 2013. 59: p. 1263-1277.
- [15] B. Noroozi, G.A. Sorial, *Applicable models for multi-component adsorption of dyes: A review*. Journal of Environmental Sciences-China, 2013. 25: p. 419-429.
- [16] L. Hamon, N. Heymans, P.L. Llewellyn, V. Guillerm, A. Ghoufi, S. Vaesen, G. Maurin, C. Serre, G. de Weireld, G.D. Pirngruber, *Separation of CO₂-CH₄ mixtures in the mesoporous MIL-100(Cr) MOF: experimental and modelling approaches*. Dalton Transactions, 2012. 41: p. 4052-4059.
- [17] S. Qi, L. Schideman, B.J. Marinas, V.L. Snoeyink, C. Campos, *Simplification of the IAST for activated carbon adsorption of trace organic compounds from natural water*. Water Research, 2007. 41: p. 440-448.
- [18] R.T. Yang, *Adsorbents: Fundamentals and applications*. 2003. New-York: Wiley-Interscience. 1st edition.
- [19] A. Erto, A. Lancia, D. Musmarra, *A modelling analysis of PCE/TCE mixture adsorption based on Ideal Adsorbed Solution Theory*. Separation and Purification Technology, 2011. 80: p. 140-147.
- [20] O. Talu, *Needs, status, techniques and problems with binary gas adsorption experiments*. Advances in Colloid and Interface Science, 1998. 76: p. 227-269.

- [21] A.L. Myers, J.M. Prausnitz, *Thermodynamics of mixed-gas adsorption*. AIChE Journal, 1965. 11: p. 121-127.
- [22] M. Murthi, R.Q. Snurr, *Effects of molecular siting and adsorbent heterogeneity on the ideality of adsorption equilibria*. Langmuir, 2004. 20: p. 2489-2497.
- [23] F. Karavias, A.L. Myers, *Monte Carlo simulation of binary gas adsorption in zeolite cavities*. Molecular Simulation, 1991. 8: p. 51-72.
- [24] T. Vuong, P.A. Monson, *Monte Carlo simulations of adsorbed solutions in heterogeneous porous materials*. Adsorption, 1999. 5: p. 295-304.
- [25] E. Costa, J.L. Sotelo, G. Calleja, C. Marron, *Adsorption of binary and ternary hydrocarbon-gas mixtures on activated carbon - experimental-determination and theoretical prediction of the ternary equilibrium data*. AIChE Journal, 1981. 27: p. 5-12.
- [26] S. Sochard, N. Fernandes, J.M. Reneaume, *Modeling of adsorption isotherm of a binary mixture with Real Adsorbed Solution Theory and Nonrandom Two-Liquid Model*. AIChE Journal, 2010. 56: p. 3109-3119.
- [27] J.A. Swisher, L.C. Lin, J. Kim, B. Smit, *Evaluating mixture adsorption models using molecular simulation*. AIChE Journal, 2013. 59: p. 3054-3064.
- [28] V.F. Cabral, F.W. Tavares, M. Castier, *Monte Carlo simulation of adsorption using 2-D models of heterogeneous solids*. AIChE Journal, 2003. 49: p. 753-763.
- [29] P.M. Mathias, R. Kumar, J.D. Moyer, J.M. Schork, S.R. Srinivasan, S.R. Auvil, O. Talu, *Correlation of multicomponent gas adsorption by the dual-site Langmuir model. Application to nitrogen/oxygen adsorption on 5A-zeolite*. Industrial & Engineering Chemistry Research, 1996. 35: p. 2477-2483.
- [30] J. Li, C.J. Werth, *Modeling sorption isotherms of volatile organic chemical mixtures in model and natural solids*. Environ. Toxicol. Chem., 2002. 21: p. 1377-1383.
- [31] B. Noroozi, G.A. Sorial, H. Bahrami, M. Arami, *Adsorption of binary mixtures of cationic dyes*. Dyes and Pigments, 2008. 76: p. 784-791.
- [32] O. Talu, I. Zwiebel, *Spreading pressure dependent equation for adsorbate phase activity coefficients*. Reactive Polymers, 1987. 5: p. 81-91.

- [33] B. Smit, J.I. Siepmann, *Simulating the adsorption of alkanes in zeolites*. Science, 1994. 264: p. 1118-1120.
- [34] B. Smit, J.I. Siepmann, *Computer-simulations of the energetics and siting of n-alkanes in zeolites*. Journal of Physical Chemistry, 1994. 98: p. 8442-8452.
- [35] D. Frenkel, B. Smit, *Understanding molecular simulations: from algorithms to applications*. 2002, San Diego: Academic Press. 2nd edition.
- [36] A.H. Fuchs, A.K. Cheetham, *Adsorption of guest molecules in zeolitic materials: Computational aspects*. Journal of Physical Chemistry B, 2001. 105: p. 7375-7383.
- [37] B. Smit, R. Krishna, *Molecular simulations in zeolitic process design*. Chemical Engineering Science, 2003. 58: p. 557-568.
- [38] R. Krishna, B. Smit, S. Calero, *Entropy effects during sorption of alkanes in zeolites*. Chemical Society Reviews, 2002. 31: p. 185-194.
- [39] T.J.H. Vlucht, R. Krishna, B. Smit, *Molecular simulations of adsorption isotherms for linear and branched alkanes and their mixtures in silicalite*. Journal of Physical Chemistry B, 1999. 103: p. 1102-1118.
- [40] R.Q. Snurr, A.T. Bell, D.N. Theodorou, *Prediction of adsorption of aromatic-hydrocarbons in silicalite from grand-canonical Monte Carlo simulations with biased insertions*. Journal of Physical Chemistry, 1993. 97: p. 13742-13752.
- [41] S. Chempath, R.Q. Snurr, J.J. Low, *Molecular modeling of binary liquid-phase adsorption of aromatics in silicalite*. AIChE Journal, 2004. 50: p. 463-469.
- [42] D.S. Abrams, J.M. Prausnitz, *Statistical thermodynamics of liquid mixtures: A new expression for the excess Gibbs energy of partly or completely miscible systems*. AIChE Journal, 1975. 21: p. 116-128.
- [43] H. Renon, J.M. Prausnitz, *Local compositions in thermodynamic excess functions for liquid mixtures*. AIChE Journal, 1968. 14: p. 135-144.
- [44] A. Erto, A. Lancia, D. Musmarra, *A Real Adsorbed Solution Theory model for competitive multicomponent liquid adsorption onto granular activated carbon*. Microporous and Mesoporous Materials, 2012. 154: p. 45-50.
- [45] G.M. Wilson, *Vapor-liquid equilibrium XI. A new expression for excess free energy of mixing*. Journal of the American Chemical Society, 1964. 86: p. 127-130.

- [46] A. Kopatsis, A. Salinger, A.L. Myers, *Thermodynamics of solutions with solvent and solute in different pure states*. AIChE Journal, 1988. 34: p. 1275-1286.
- [47] A.J. Jadhav, V.C. Srivastava, *Adsorbed solution theory based modeling of binary adsorption of nitrobenzene, aniline and phenol onto granulated activated carbon*. Chemical Engineering Journal, 2013. 229: p. 450-459.
- [48] C.J. Radke, J.M. Prausnitz, *Thermodynamics of multi-solute adsorption from dilute liquid solutions*. AIChE Journal, 1972. 18: p. 761-768.
- [49] T. Duerinck, P. Leflaive, P. Martin, G.D. Pirngruber, J.F.M. Denayer, *A high-throughput methodology for liquid phase adsorption experimentation*. Adsorption, 2011. 17: p. 347-359.
- [50] T.R.C. van Assche, T. Remy, G. Desmet, G.V. Baron, J.F.M. Denayer, *Adsorptive separation of liquid water/acetonitrile mixtures*. Separation and Purification Technology, 2011. 82: p. 76-86.
- [51] J.P. Ryckaert, A. Bellemans, *Molecular dynamics of liquid alkanes*. Faraday Discuss., 1978. 66: p. 95-106.
- [52] J.M. Stubbs, J.J. Potoff, J.I. Siepmann, *Transferable potentials for phase equilibria. 6. United-atom description for ethers, glycols, ketones, and aldehydes*. Journal of Physical Chemistry B, 2004. 108: p. 17596-17605.
- [53] C.D. Wick, M.G. Martin, J.I. Siepmann, *Transferable potentials for phase equilibria. 4. United-atom description of linear and branched alkenes and alkylbenzenes*. Journal of Physical Chemistry B, 2000. 104: p. 8008-8016.
- [54] M.G. Martin, J.I. Siepmann, *Transferable potentials for phase equilibria. 1. United-atom description of n-alkanes*. Journal of Physical Chemistry B, 1998. 102: p. 2569-2577.
- [55] N. Rai, J.I. Siepmann, *Transferable potentials for phase equilibria. 9. Explicit hydrogen description of benzene and five-membered and six-membered heterocyclic aromatic compounds*. Journal of Physical Chemistry B, 2007. 111: p. 10790-10799.
- [56] B. Chen, J.J. Potoff, J.I. Siepmann, *Monte Carlo calculations for alcohols and their mixtures with alkanes. Transferable potentials for phase equilibria. 5. United-atom description of primary, secondary, and tertiary alcohols*. Journal of Physical Chemistry B, 2001. 105: p. 3093-3104.

- [57] D. S. Coombs, A. Alberti, T. Armbruster, G. Artioli, C. Colella, E. Galli, J. D. Grice, F. Liebau, J. A. Mandarino, H. Minato, E. H. Nickel, E. Passaglia, D. R. Peacor, S. Quartieri, R. Rinaldi, M. Ross, R. A. Sheppard, E. Tillmanns, G. Vezzalini, *Recommended nomenclature for zeolite minerals: report of the subcommittee on zeolites of the International Mineralogical Association, Commission on new minerals and mineral names*. Mineral. Mag., 1998. 62: p. 533-571.
- [58] E. García-Pérez, D. Dubbeldam, T.L.M. Maesen, S. Calero, *Influence of cation Na/Ca ratio on adsorption in LTA 5A: A systematic molecular simulation study of alkane chain length*. Journal of Physical Chemistry B, 2006. 110: p. 23968-23976.
- [59] A.G. Bezus, A.V. Kiselev, A.A. Lopatkin, P.Q. Du, *Molecular statistical calculation of the thermodynamic adsorption characteristics of zeolites using the atom-atom approximation. Part 1.-Adsorption of methane by zeolite NaX*. J. Chem. Soc., Faraday Trans. , 1978. 74: p. 367-379.
- [60] T.J.H. Vlught, M. Schenk, *Influence of framework flexibility on the adsorption properties of hydrocarbons in the zeolite silicalite*. Journal of Physical Chemistry B, 2002. 106: p. 12757-12763.
- [61] M.G. Martin, J.I. Siepmann, *Novel configurational-bias Monte Carlo method for branched molecules. Transferable potentials for phase equilibria. 2. United-atom description of branched alkanes*. Journal of Physical Chemistry B, 1999. 103: p. 4508-4517.
- [62] D. Dubbeldam, S. Calero, T.J.H. Vlught, R. Krishna, T.L.M. Maesen, B. Smit, *United atom force field for alkanes in nanoporous materials*. Journal of Physical Chemistry B, 2004. 108: p. 12301-12313.
- [63] A.V. Kiselev, A.A. Lopatkin, A.A. Shulga, *Molecular statistical calculation of gas adsorption by silicalite*. Zeolites, 1985. 5: p. 261-267.
- [64] R.L. June, A.T. Bell, D.N. Theodorou, *Prediction of low occupancy sorption of alkanes in silicalite*. Journal of Physical Chemistry, 1990. 94: p. 1508-1516.
- [65] H.A. Lorentz, Ueber die anwendung des satzes vom virial in der kinetischen theorie der gase, *Annalen Phys.*, 1881. 248: p. 127-136.
- [66] D.C.R. Berthelot, Sur le mélange des gaz, *C. R. Hebd. Séances Acad. Sci.*, 1898.126: p. 1703-1706.

- [67] A.O. Yazaydin, R.W. Thompson, *Molecular simulation of the adsorption of MTBE in Silicalite, Mordenite, and zeolite Beta*. Journal of Physical Chemistry B, 2006. 110: p. 14458-14462.
- [68] B. Liu, B. Smit, F. Rey, S. Valencia, S. Calero, *A new united atom force field for adsorption of alkenes in zeolites*. Journal of Physical Chemistry C, 2008. 112: p. 2492-2498.
- [69] T.J.H. Vlugt, E. García-Pérez, D. Dubbeldam, S. Ban, S. Calero, *Computing the heat of adsorption using molecular simulations: The effect of strong Coulombic interactions*. Journal of Chemical Theory and Computation, 2008. 4: p. 1107-1118.
- [70] C.L. Yaws, *Yaws' Handbook of Thermodynamic and Physical Properties of Chemical Compounds*. 2003, Knovel. 1st edition.
- [71] U. Weidlich, J. Gmehling, *A modified Unifac model. 1. Prediction of VLE, He, and gamma-infinity*. Industrial & Engineering Chemistry Research, 1987. 26: p. 1372-1381.
- [72] J. Gmehling, J. Li, M. Schiller, *A modified Unifac model. 2. Present parameter matrix and results for different thermodynamic properties*. Industrial & Engineering Chemistry Research, 1993. 32: p. 178-193.
- [73] J. Gmehling, P. Rasmussen, A. Fredenslund, *Vapor-liquid equilibria by UNIFAC group contribution. Revision and extension. 2*. Industrial & Engineering Chemistry Process Design and Development, 1982. 21: p. 118-127.
- [74] J. Gmehling, J. Lohmann, A. Jakob, J. Li, R. Joh, *A modified UNIFAC (Dortmund) model. 3. Revision and extension*. Industrial & Engineering Chemistry Research, 1998. 37: p. 4876-4882.
- [75] J. Gmehling, R. Wittig, J. Lohmann, R. Joh, *A modified UNIFAC (Dortmund) model. 4. Revision and extension*. Industrial & Engineering Chemistry Research, 2002. 41: p. 1678-1688.
- [76] H.K. Hansen, P. Rasmussen, A. Fredenslund, M. Schiller, J. Gmehling, *Vapor-liquid equilibria by UNIFAC group contribution. 5. Revision and extension*. Industrial & Engineering Chemistry Research, 1991. 30: p. 2352-2355.

- [77] R. Wittig, J. Lohmann, J. Gmehling, *Vapor-liquid equilibria by UNIFAC group contribution. 6. Revision and extension*. Industrial & Engineering Chemistry Research, 2002. 42: p. 183-188.
- [78] B. Silva, H. Figueiredo, O.S.G.P. Soares, M.F.R. Pereira, J.L. Figueiredo, A.E. Lewandowska, M.A. Banares, I.C. Neves, T. Tavares, *Evaluation of ion exchange-modified Y and ZSM5 zeolites in Cr(VI) biosorption and catalytic oxidation of ethyl acetate*. Appl. Catal., B 2012. 117: p. 406-413.
- [79] J.M. Castillo, D. Dubbeldam, T.J.H. Vlught, B. Smit, S. Calero, *Evaluation of various water models for simulation of adsorption in hydrophobic zeolites*. Molecular Simulation, 2009. 35: p. 1067-1076.
- [80] O. Talu, *Measurement and analysis of mixture adsorption equilibrium in porous solids*. Chemie Ingenieur Technik, 2011. 83: p. 67-82.
- [81] V.F. Cabral, C.R.A. Abreu, M. Castier, F.W. Tavares, *Monte Carlo simulations of the adsorption of chainlike molecules on two-dimensional heterogeneous surfaces*. Langmuir, 2003. 19: p. 1429-1438.
- [82] G.F. Araujo, V.F. Cabral, M. Castier, F.W. Tavares, *Monte Carlo simulation of binary mixtures adsorbed on heterogeneous surfaces*. Latin American Applied Research, 2006. 36: p. 277-282.
- [83] G. Manos, L.J. Dunne, S. Jalili, A. Furgani, T. Neville, *Monte Carlo simulation and exact statistical mechanical lattice models as a development tool for zeolite multi-component adsorption isotherm derivation*. Adsorption Science & Technology, 2012. 30: p. 503-519.
- [84] D. Dubbeldam, A. Torres-Knoop, K.S. Walton, *On the inner workings of Monte Carlo codes*. Molecular Simulation, 2013. 39: p. 1253-1292.
- [85] G.A. Mansoori, *Classical thermodynamic basis of activity coefficients: predictive and consistency rules for binary and ternary mixtures based on the relation between excess Gibbs free energies of (C)- and (C-1)-component mixtures*. Fluid Phase Equilibria, 1980. 4: p. 197-209.
- [86] P.T. Eubank, B.G. Lamonte, J.F.J. Alvarado, *Consistency tests for binary VLE data*. Journal of Chemical and Engineering Data, 2000. 45: p. 1040-1048.
- [87] H. Moon, C. Tien, *Adsorption of gas mixtures on adsorbents with heterogeneous surfaces*. Chemical Engineering Science, 1988. 43: p. 2967-2980.

- [88] J.A. Ritter, S.J. Bhadra, A.D. Ebner, *On the use of the dual-process Langmuir model for correlating unary equilibria and predicting mixed-gas adsorption equilibria*. *Langmuir*, 2011. 27: p. 4700-4712.
- [89] D.G. Lee, J.H. Kim, C.H. Lee, *Adsorption and thermal regeneration of acetone and toluene vapors in dealuminated Y-zeolite bed*. *Separation and Purification Technology*, 2011. 77: p. 312-324.
- [90] J.H. Yun, D.K. Choi, S.H. Kim, *Equilibria and dynamics for mixed vapors of BTX in an activated carbon bed*. *AIChE Journal*, 1999. 45: p. 751-760.
- [91] E. Santacesaria, M. Morbidelli, A. Servida, G. Storti, S. Carra, *Separation of xylenes on Y zeolite. 2. Breakthrough curves and their interpretation*. *Industrial & Engineering Chemistry Process Design and Development*, 1982. 21: p. 446-451.
- [92] A.L. Ahmad, M.F. Chong, S. Bhatia, *Prediction of breakthrough curves for adsorption of complex organic solutes present in palm oil mill effluent (POME) on granular activated carbon*. *Industrial & Engineering Chemistry Research*, 2006. 45: p. 6793-6802.
- [93] A.H. Sulaymon, K.W. Ahmed, *Competitive adsorption of furfural and phenolic compounds onto activated carbon in fixed bed column*. *Environmental Science & Technology*, 2008. 42: p. 392-397.
- [94] P. Jiao, J. Wu, J. Zhou, P. Yang, W. Zhuang, Y. Chen, C. Zhu, T. Guo, H. Ying, *Mathematical modeling of the competitive sorption dynamics of acetone-butanol-ethanol on KA-I resin in a fixed-bed column*. *Adsorption-Journal of the International Adsorption Society*, 2015. 21: p. 165-176.
- [95] M.S.P. Silva, J.P.B. Mota, A.E. Rodrigues, *Fixed-bed adsorption of aromatic C₈ isomers: Breakthrough experiments, modeling and simulation*. *Separation and Purification Technology*, 2012. 90: p. 246-256.
- [96] H. Masuda, K. Higashitani, H. Yashida, *Powder Technology Handbook*. 2006. 3rd edition.
- [97] M. Minceva, A.E. Rodrigues, *Adsorption of xylenes on Faujasite-type zeolite. Equilibrium and kinetics in batch adsorber*. *Chemical Engineering Research & Design*, 2004. 82: p. 667-681.

- [98] J.J. Lee, M.K. Kim, D.G. Lee, H. Ahn, M.J. Kim, C.H. Lee, *Heat-exchange pressure swing adsorption process for hydrogen separation*. *AIChE Journal*, 2008. 54: p. 2054-2064.
- [99] S.J. Lee, J.H. Jung, J.H. Moon, J.G. Jee, C.H. Lee, *Parametric study of the three-bed pressure-vacuum swing adsorption process for high purity O₂ generation from ambient air*. *Industrial & Engineering Chemistry Research*, 2007. 46: p. 3720-3728.
- [100] H. Ahn, C.H. Lee, *Adsorption dynamics of water in layered bed for air-drying TSA process*. *AIChE Journal*, 2003. 49: p. 1601-1609.
- [101] H. Ahn, C.H. Lee, *Effects of capillary condensation on adsorption and thermal desorption dynamics of water in zeolite 13X and layered beds*. *Chemical Engineering Science*, 2004. 59: p. 2727-2743.
- [102] N. Wakao, J.M. Smith, *Diffusion in catalyst pellets*. *Chemical Engineering Science*, 1962. 17: p. 825-834.
- [103] L.R. Perkins, C.J. Geankoplis, *Molecular diffusion in a ternary liquid system with diffusing component dilute*. *Chemical Engineering Science*, 1969. 24: p. 1035-1042.
- [104] B.E. Poling, J.M. Prausnitz, J.P. O'Connell, *The properties of gases and liquids*. 2007: McGraw-Hill. 5th edition.
- [105] P.L. Chueh, J.M. Prausnitz, *Vapor-liquid equilibria at high pressures . Vapor-phase fugacity coefficients in nonpolar and quantum-gas mixtures*. *Industrial & Engineering Chemistry Fundamentals*, 1967. 6: p. 492-498.
- [106] J.M. Castillo, T.J.H. Vlught, S. Calero, *Understanding water adsorption in Cu–BTC metal–organic frameworks*. *Journal of Physical Chemistry C*, 2008. 112: p. 15934-15939.
- [107] B. Smit, T.L.M. Maesen, *Towards a molecular understanding of shape selectivity*. *Nature*, 2008. 451: p. 671-678.
- [108] *CRC Handbook of Chemistry and Physics*. 2011-2012. CRC Press. 92nd edition.
- [109] K.S. Pitzer, D.Z. Lippmann, R.F. Curl, C.M. Huggins, D.E. Petersen, *The volumetric and thermodynamic properties of fluids. II. Compressibility factor, vapor pressure and entropy of vaporization*. *Journal of the American Chemical Society*, 1955. 77: p. 3433-3440.

- [110] J. Dykyj, M. Seprakova, J. Paulech, *The vapor pressure of two C₈ alcohols and two C₈ aldehydes*. Chem. Zvesti, 1961. p. 465.
- [111] H. Conroy, R.A. Firestone, *The intermediated dienone in the para-Claisen rearrangement*. Journal of the American Chemical Society, 1956. 78: p. 2290-2297.
- [112] J.M. Smith, H.C. van Ness, M.M. Abbott, *Introduction to chemical engineering thermodynamics*. 2005, New York: McGraw-Hill. 7th edition.

Summary

The aim of this thesis is to study multicomponent adsorption equilibria in the liquid phase. Most experimental data on adsorption reported in the literature are for binary systems with only a handful of studies on ternary systems. This is mainly because multicomponent adsorption data are considerably more difficult to measure than pure component data. As a consequence, theories that can predict multicomponent adsorption equilibria using only pure component data are frequently used even though they often fail even for binary systems. For screening purposes however, such theories are important. When screening for appropriate adsorbents, a minimum amount of experimental work is desirable. In chapter 2 of this thesis, we propose a methodology that allows the calculation of multicomponent adsorption equilibria using limited experimental data. A six-component system comprising traces of butanal, 2-ethyl-2-hexenal, 2,6-dimethyl-cyclohexanone, 2,4,6-trimethylphenol and 2,4,6-trimethylanisole in liquid toluene was chosen as a test system. The compounds were chosen such that they are volatile, organic, and have different molecular sizes and functional groups.

Pure component adsorption isotherms in the sodium form of zeolite Y (NaY) were computed using Monte Carlo simulations. The Ideal Adsorbed Solution Theory (IAST) was used to compute the multicomponent adsorption equilibria using the pure component data obtained from molecular simulations. To calibrate the model, three binary experimental data points were used. We show that the combined molecular simulation - IAST approach can be used for this six-component system to predict the adsorption behavior in NaY reasonably well.

To improve the accuracy predictions of IAST, activity coefficients are used to describe the non-ideal behavior of the adsorbed phase. This approach is called the Real Adsorbed Solution Theory (RAST). However, to this date, there are no predictive models available to describe the activity coefficients for the adsorbed phase. As an approximation, models taken from the gas-liquid phase equilibria are used. Models for activity coefficients such as Wilson and NRTL are commonly used to describe the adsorbed phase activity coefficients. These activity coefficient models depend on temperature and composition, while the pressure dependence is usually neglected. The adsorbed phase activity coefficients are dependent on temperature, composition and a third thermodynamic variable called the spreading pressure. To

account for this difference, either the spreading pressure is considered constant or further approximations are used.

In chapter 3 of this thesis, molecular simulations are used to study a 2D-lattice model to generate activity coefficient data at constant spreading pressure. The obtained data is used to check the accuracy of the Wilson and NRTL models for evaluating adsorbed phase activity coefficient data. We show that the Wilson and NRTL models cannot describe the adsorbed phase activity coefficients for slightly non-ideal to strong non-ideal mixtures. A new methodology is introduced for predicting adsorption of mixtures based on a simple 2D-lattice model coupled with the segregated sites approach. The segregated model assumes that the competition for adsorption occurs at isolated adsorption sites. Molecules from different adsorption sites cannot interact with each other and both adsorption sites are in contact with the bulk phase. The segregated 2D-lattice model provides accurate predictions for the system $\text{CO}_2\text{-N}_2$ in the hypothetical zeolite PCOD8200029, but fails in predicting the adsorption behavior of $\text{CO}_2\text{-C}_3\text{H}_8$ in all-silica MOR-type zeolite. The predictions of the segregated IAST model are superior to those of the 2D-lattice model.

The multicomponent Langmuir model, the multicomponent dual-site Langmuir model, IAST, and segregated IAST models are commonly used in dynamic models for adsorption processes, even though they usually fail in predicting the behavior of multicomponent adsorption systems. In chapter 4, we investigate the accuracy of these models in predicting the adsorption behavior of a six-component mixture comprising butanal, 2-ethyl-2-hexenal, 2,6-dimethylcyclohexanone, 2,4,6-trimethylphenol, 2,4,6-trimethylanisole and toluene in the ammonium form of Y zeolite. The multicomponent dual-site Langmuir model and the segregated IAST model work best for this system and are further used in a multicomponent breakthrough model. We show that the breakthrough model, together with the multicomponent dual-site Langmuir model (used to calculate the equilibrium isotherms), can provide a rough qualitative estimation of the breakthrough behavior for this system.

The system used as case study in this thesis comprised molecules of different size, shape, functional groups and polarity. Most pure component data required for describing the multicomponent adsorption behavior of this system were estimated. Despite these challenges, the force field developed in chapter 2 was used, together with IAST, to predict the adsorption behavior of the multicomponent system with sufficient accuracy for screening purposes. In chapter 3, we showed that the commonly used activity coefficient models taken from the gas-liquid theory cannot describe non-idealities in the adsorbed phase. In chapter 4, we introduced a simple breakthrough model and investigate several equilibrium models for predicting the adsorption of the six-component mixture in the ammonium form of Y zeolite. For this

system, the multicomponent dual-site Langmuir model works best. The simple breakthrough model, together with the multicomponent dual-site Langmuir model, can only provide a rough estimate of the multicomponent breakthrough curves.

Samenvatting

Het doel van dit proefschrift is om vloeistof adsorptie evenwichten in systemen met meerdere componenten te bestuderen. De meeste experimentele gegevens van adsorptie uit de literatuur betreffen binaire systemen. Slechts een handvol studies heeft betrekking op ternaire systemen. Dit komt vooral omdat adsorptie data van systemen met meerdere componenten aanzienlijk moeilijker te meten zijn dan die van pure componenten. Bijgevolg worden voor het voorspellen van het gedrag van systemen met meerdere componenten in de praktijk vaak theorieën gebruikt die alleen zijn gebaseerd op data van de zuivere componenten, hoewel ze vaak falen zelfs voor binaire systemen. Voor screeningsdoeleinden zijn dergelijke theorieën echter belangrijk. Bij het screenen van geschikte adsorptiemiddelen, is een minimale hoeveelheid experimenteel werk wenselijk. In hoofdstuk 2 van dit proefschrift, stellen we een methodologie voor die, de berekening van de adsorptie evenwichten voor systemen met meerdere componenten met beperkte hoeveelheid experimentele data mogelijk maakt. Een zes-componenten systeem met lage concentraties butanal, 2-ethyl-2-hexenal, 2,6-dimethyl-cyclohexanon, 2,4,6-trimethylfenol en 2,4,6-trimethyl-anisole in vloeibare toluen werd gekozen als een testsysteem. De verbindingen werden zodanig gekozen dat ze vluchtig en organisch zijn en onderscheidende moleculaire afmetingen en functionele groepen hebben.

Adsorptie isothermen van zuivere componenten werden berekend voor de natriumvorm van zeoliet Y (NaY) met behulp van Monte Carlo simulaties. De “Ideal Adsorbed Solution Theory” (IAST) werd gebruikt om de adsorptie evenwichten te berekenen van een systeem met meerdere componenten gebruik makend van gegevens van de zuivere componenten die werd verkregen uit de moleculaire simulaties. Om het model te kalibreren, werden drie binaire experimentele datapunten gebruikt. We laten zien dat de gecombineerde moleculaire simulatie - IAST benadering gebruikt voor dit zes-componentensysteem het adsorptiegedrag in NaY redelijk kan voorspellen.

Om de nauwkeurigheid van de voorspellingen van IAST te verbeteren zijn activiteitscoëfficiënten gebruikt voor de beschrijving van het niet-ideale gedrag van de geadsorbeerde fase. Deze benadering is al bekend en wordt de “Real Adsorption Solution Theory”, (RAST) genoemd. Tot op heden zijn er echter geen voorspellende modellen, die de activiteitscoëfficiënten van de geadsorbeerde fase kunnen beschrijven. Als benadering worden modellen afkomstig uit gas-vloeistof fase-evenwichten gebruikt. Modellen zoals het Wilson en het NRTL model worden gewoonlijk gebruikt voor de beschrijving van de activiteitscoëfficiënten in de geadsorbeerde fase. Deze activiteitscoëfficiënt modellen zijn afhankelijk van temperatuur en samenstelling, terwijl de drukafhankelijkheid meestal verwaarloosd kan worden. De activiteitscoëfficiënten van de geadsorbeerde fase zijn afhankelijk van de temperatuur, samenstelling en een derde thermodynamische variabele genaamd de “spreading pressure”. Om rekening te houden met dit verschil, wordt ofwel deze “spreading pressure” als constant beschouwd of worden verdere benaderingen gebruikt.

In hoofdstuk 3 van dit proefschrift worden moleculaire simulaties gebruikt voor de bestudering van een 2D-rooster model om de data te genereren voor de activiteitscoëfficiënten bij constante “spreading pressure”. De verkregen gegevens worden gebruikt om de nauwkeurigheid te testen van de Wilson en NRTL modellen voor de evaluatie van de activiteitscoëfficiënt data in de geadsorbeerde fase. We laten zien dat de Wilson en NRTL modellen niet in staat zijn de activiteitscoëfficiënten in de geadsorbeerde fase voor zwak tot sterk niet-ideale mengsels te beschrijven. Een nieuwe methode is ingevoerd voor het voorspellen van de adsorptie van mengsels gebaseerd op een eenvoudige 2D-roostermodel gecombineerd met een gescheiden locatie benadering. Het gescheiden locatie model gaat ervan uit dat de competitie voor adsorptie plaatsvindt op geïsoleerde adsorptie sites. Moleculen van verschillende adsorptieplaatsen hebben geen interactie met elkaar en beide adsorptieplaatsen staan in contact met de bulkfase. Het gescheiden 2D-rooster model biedt nauwkeurige voorspellingen voor het systeem van CO₂-N₂ in het hypothetische zeoliet PCOD8200029, maar slaagt er niet in het adsorptie gedrag van CO₂-C₃H₈ in all-silica MOR-type zeoliet te voorspellen. De voorspellingen van de gescheiden IAST model zijn superieur zijn aan die van de 2D-roostermodel.

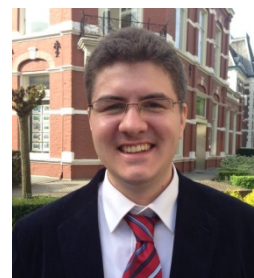
Het multicomponent Langmuir, het multicomponent twee locatie Langmuir, het IAST en het afzonderlijke locatie IAST model worden vaak gebruikt in dynamische modellen voor adsorptie processen, hoewel ze er gewoonlijk niet in slagen om het gedrag van multicomponent adsorptie systemen te voorspellen. In hoofdstuk 4 onderzoeken we de nauwkeurigheid van deze modellen in het voorspellen van het adsorptie gedrag van een zes-component mengsel bestaande uit butanal, 2-ethyl-2-hexenal, 2,6-dimethylcyclohexanon, 2,4,6-trimethylfenol, 2,4,6-trimethylanisole en toluen in de ammoniumvorm van de Y zeoliet. Het twee locatie Langmuir model en het gescheiden locatie IAST model werken het beste voor dit systeem en worden verder gebruikt in een multi-component doorbraak model. We zien dat het doorbraak model, alsmede het meerdere-component, twee locatie, Langmuir model (gebruikt om de evenwicht isothermen berekening), een ruwe schatting van de kwalitatieve doorbraak gedrag van het systeem kan geven.

Het systeem gebruikt als casus in dit proefschrift bestaat uit moleculen van verschillende grootte, vorm, functionele groepen en polariteit. De meeste zuivere component gegevens die nodig zijn voor het beschrijven adsorptie gedrag van dit multi-component systeem werden geschat. Ondanks deze uitdagingen, bleek het krachtveld ontwikkeld in hoofdstuk 2 samen met IAST, geschikt om het adsorptie gedrag van het multi-component systeem met voldoende nauwkeurigheid te voorspellen voor screening doeleinden. In hoofdstuk 3 hebben we laten zien dat de meest gebruikte activiteitscoëfficiënt modellen afkomstig uit de gas-vloeistof theorie het niet-ideaal gedrag in de geadsorbeerde fase niet adequaat kunnen beschrijven. In hoofdstuk 4 hebben we een eenvoudige doorbraak model geïntroduceerd en hebben verschillende evenwicht modellen onderzocht voor het voorspellen van de adsorptie van het zes-component mengsel in de ammonium vorm van de Y-zeoliet. Voor dit systeem werkt het multicomponent twee locatie Langmuir model het beste. Het eenvoudige doorbraak model, alsmede het multi-component twee locatie Langmuir

model, kan slechts een ruwe schatting geven van de multi-component doorbraak profielen.

Curriculum Vitae

Cristian Constantin Brunchi was born in Bucharest, Romania on 16th of December 1984. He received a Master of Science degree in chemical engineering at the University Politehnica of Bucharest in 2008. For the Msc. graduation he worked on experiments and calculation of chemical equilibrium for the etherification reactions of glycerol with olefins (for the production of biodiesel additives) as well as the design of a chemical reactor for methanol synthesis.



After completing the university studies in Romania, he obtained a PhD candidate position in trace removal by crystallization at the Process & Energy Department of the Delft University of Technology. After 1 year, he changed the topic of his PhD to adsorption. In March 2013, he obtained a post-doctoral researcher position in the same department. Since January 2014 he worked as a guest researcher on finishing his PhD thesis.

Published Work

Journal Papers

Brunchi, C. C.; Castillo Sanchez, J. M.; Stankiewicz, A. I.; Kramer, H. J. M.; Vlugt, T. J. H., Adsorption of volatile organic compounds. Experimental and theoretical study, *Ind Eng Chem Res*, 51, 2012, 16697-16708.

Brunchi, C. C.; Englebienne, P.; Kramer, H. J. M.; Schnell, S.K.; Vlugt, T. J. H., Evaluating adsorbed-phase activity coefficient models using a 2D-lattice model, *Molecular Simulation*, 2015, in press, DOI: 10.1080/08927022.2014.972394.

Selected conference proceedings

Brunchi, C. C.; Castillo Snachez, J. M.; Vlugt, T. J. H.; Kramer, H. J. M., Prediction of adsorption of odor compounds in zeolites by molecular modelling studies, *In proceedings of 5th International FEZA Conference (FEZA 2011)*, 2011, 637-638

Bildea, C. S.; Brunchi, C. C.; Bozga, G., Analysis of chemical routes and processes for production of glycerol ethers, *19th European Symposium on Computer Aided Process Engineering, Computer Aided Chemical Engineering*, 26, 2009, 99-104.

Selected oral presentations

Prediction of adsorption of odor compounds in zeolites by molecular modelling studies, 4th International Symposium Advanced Micro and Mesoporous Materials (MICRO 2011), 6 - 9 September, Riviera Resort, Bulgaria.

Developing a predictive tool for adsorption in zeolites, NPS11, 2011, 24 - 26 October, Arnhem, Netherlands.

Removal of Oxygenated Species From Liquid Toluene by Adsorption, American Institute of Chemical Engineers (AIChE) Annual Meeting 2012, 28 October - 2 November, Pittsburgh, PA, USA.

Acknowledgements

The completion of this booklet would not have been possible without the help and support of many people. While I would like to thank everyone, I will without doubt, forget to mention some of you. I apologize to those that I might forget.

I would like to start by thanking my daily supervisor and co-promotor, Herman Kramer, for his constant support throughout the years. His door was always opened when I needed to discuss scientific challenges. I will always remember his sense of humor and the smile on his face when entering my office. Many thanks go towards Andrzej Stankiewicz for his patient guidance and enthusiastic encouragement during my time spent at TU Delft. Without Herman and Andrzej, who accepted me for this PhD position, I wouldn't be where I am today. Much appreciation goes towards my promoter and supervisor, Thijs Vlugt. He always found the right words to explain even the most abstract theory. Although he was exigent when correcting my manuscripts, he always praised my efforts and I knew that once a manuscript was finished, the reviewers would have few comments. His wisdom and guidance were invaluable for my development. I always knew how to approach my challenges after meeting with Thijs.

I will never forget the people that guided me through my master study at the university Politehnica of Bucharest, Prof. Sorin Bildea and Prof. Grigore Bozga. They had a big influence in creating the engineer I am today and provided the recommendations that granted me the position at TU Delft.

Throughout the years, I received help in the laboratory with my experiments/experimental setup and I would like to thank the people that were constantly involved in my work: Michel van den Brink, Eugene Straver, Andre van den Bosch, Stefan ten Hagen, Daniel van Baarle, Martijn Karsten and Gerard van de Sande.

Life at TU Delft would have been an inferno without the constant help of the four management assistant ladies: Leslie, Ilona, Helma and Eveline. Thank you for always helping me with all the nasty but necessary paperwork!

The coffee breaks and interaction with my former colleagues is what kept me going as a PhD student. Somnath, Richard, Ryuta, Widya, Ernesto, Jelani, Alondra, Albert,

Marta, Magda, Tomek, Masha, Dennis, Lalit, Samir, Stevia, Sara, Sergio, Michel, Ali, Antonella, Aylin, Christian, Erin, Mahinder, Norbert, Zuopeng, Jie, Xin, Xiaohua, David, Sayee, Sondre, Juan, Pablo, Sander, Stephanie, Maryam, Alvaro, Fatima, Almudena, Iza... I could probably fill this entire page with names, if only I could remember you all... thank you all for making the coffee breaks more enjoyable.

Thank you Shohreh and Joyce for doing your master graduation project with me. I hope you enjoyed our collaboration as much as I did.

Whenever I think about remarkable moments from my past at TU Delft, and I mean the type of memory that always brings a smile on my face, there are a few people that stand out. These people deserve special thanks. You will always have a place in my memory and my heart. George, Javi, Rohit, Gerasimos, Guido, Daniel and Marloeus, thank you for being my friends!

To my Romanian friends in Netherlands, thank you for your support, all the great time we had together and the nice barbeques we shared. Thanks goes to Daniela & Cristi & Alex, Catalina & Alex, Raluca & Alex, Le Guțanu', Petre, Razvan and Daniel.

I didn't forget Georgiana, Mihai and Tudor, I just saved family for last. Thank you for always being there and for becoming our godparents. Thanks go to my parents in law for the constant support and guidance. Thank you mom and dad for raising the man I am today; you always encouraged me to follow my dreams. Thank you Roxi for making me a proud uncle.

My dearest Ana, thank you for loving me the way I am, for sharing your life with me and for making me a better man. You are my only constant, my love, my everything.

Cristian,

Deventer, August 2015

